

Review

Mesoporous Silica Particles as Drug Delivery Systems—The State of the Art in Loading Methods and the Recent Progress in Analytical Techniques for Monitoring These Processes

Katarzyna Trzeciak, Agata Chotera-Ouda , Irena I. Bak-Sypien and Marek J. Potrzebowski *

Centre of Molecular and Macromolecular Studies, Polish Academy of Sciences, Sienkiewicza 112, 90-363 Lodz, Poland; ktrzecik@cbmm.lodz.pl (K.T.); achotera@cbmm.lodz.pl (A.C.-O.); sypieni@cbmm.lodz.pl (I.I.B.-S.)

* Correspondence: marekpot@cbmm.lodz.pl; Tel.: +48-42-68-03-240



Citation: Trzeciak, K.; Chotera-Ouda, A.; Bak-Sypien, I.I.; Potrzebowski, M.J. Mesoporous Silica Particles as Drug Delivery Systems—The State of the Art in Loading Methods and the Recent Progress in Analytical Techniques for Monitoring These Processes. *Pharmaceutics* **2021**, *13*, 950. <https://doi.org/10.3390/pharmaceutics13070950>

Academic Editors: Samantha Meenach and Jie Shen

Received: 1 June 2021
Accepted: 21 June 2021
Published: 24 June 2021

Publisher's Note: MDPI stays neutral with regard to jurisdictional claims in published maps and institutional affiliations.



Copyright: © 2021 by the authors. Licensee MDPI, Basel, Switzerland. This article is an open access article distributed under the terms and conditions of the Creative Commons Attribution (CC BY) license (<https://creativecommons.org/licenses/by/4.0/>).

Abstract: Conventional administration of drugs is limited by poor water solubility, low permeability, and mediocre targeting. Safe and effective delivery of drugs and therapeutic agents remains a challenge, especially for complex therapies, such as cancer treatment, pain management, heart failure medication, among several others. Thus, delivery systems designed to improve the pharmacokinetics of loaded molecules, and allowing controlled release and target specific delivery, have received considerable attention in recent years. The last two decades have seen a growing interest among scientists and the pharmaceutical industry in mesoporous silica nanoparticles (MSNs) as drug delivery systems (DDS). This interest is due to the unique physicochemical properties, including high loading capacity, excellent biocompatibility, and easy functionalization. In this review, we discuss the current state of the art related to the preparation of drug-loaded MSNs and their analysis, focusing on the newest advancements, and highlighting the advantages and disadvantages of different methods. Finally, we provide a concise outlook for the remaining challenges in the field.

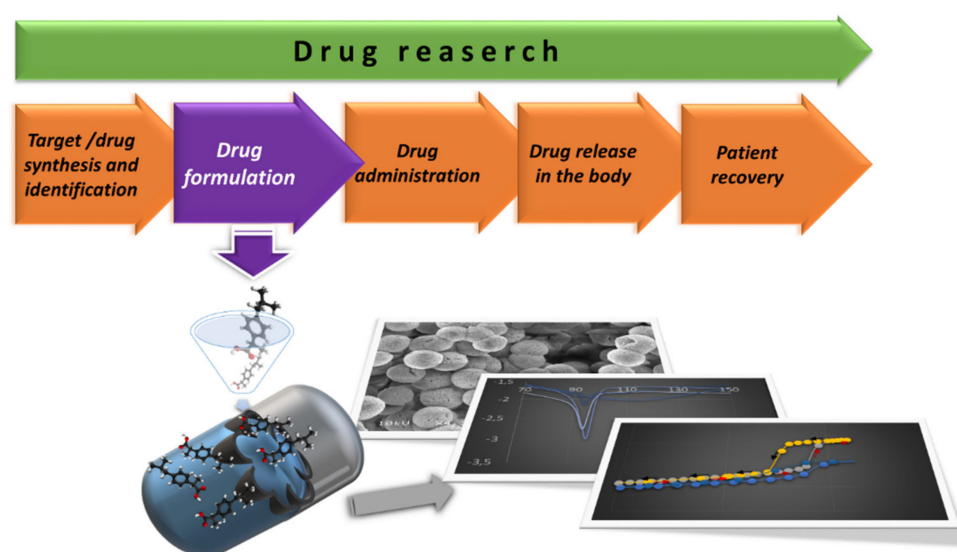
Keywords: mesoporous silica nanoparticles; drug delivery systems; drug loading methods; solid-state NMR; thermal analysis; gas sorption; vibrational spectroscopy; mass spectrometry; electron microscopy; PXRD

1. Introduction

Drug nanoformulations have been a challenge for scientists for many years. It remains very difficult to create non-toxic, body friendly systems that would deliver the desired drug concentration to the target site overcoming all barriers in vivo. One of the attractive options that can help solve this problem is the use of smart, intelligent drug delivery systems (DDS). Mesoporous silica is a promising material in this respect. Discovered in the early 1990s, mesoporous silica nanoparticles (MSNs) have found numerous applications in industry and many fields of science, including heterogeneous catalysis, electrochemistry, analytical chemistry, molecular biology, and others. The first application of these nano-structured materials in pharmacy dates back to 2001 when Vallet-Regi described the use of MCM-41 silica in the ibuprofen release process [1]. This seminal work initiated the dynamic development of research focused on the application of mesoporous particles as carriers in drug delivery systems. Silica has been approved by the FDA (The US Food and Drug Administration) as “Generally Recognized as Safe” (GRAS) and can also be used in cosmetics and as a food additive [2]. Studies in a simulated body fluid have shown that mesoporous silica nanoparticles undergo a three-stage degradation after administration, which seems to be beneficial for the drug release process. Moreover, in vivo absorption, distribution, and excretion studies in mice following administration of MSN by various routes indicate good tissue biocompatibility for oral and intravenous injection. In contrast, MSNs were difficult to absorb after intramuscular and subcutaneous administration.

In vivo mortality, clinical, pathological, and blood chemistry studies showed low toxicity of MSN in mice. The silica nanoparticles accumulated mainly in the liver cells, from where they were removed within about four weeks, although liver damage has been seen at higher doses and longer use [3–6].

The treatment of a patient with synthetic drugs or natural products is a multi-stage procedure in which we can distinguish several key steps, starting from the synthesis or isolation of a chemical compound, its full characterization, approval by the FDA and/or EMA (The European Medicines Agency), and ending with the full recovery of the patient. The complexity of this process in graphical form is shown in Scheme 1. Our review focuses on the issues described in Panel 2, “Drug formulation”, and summarizes the latest developments in research into mesoporous silica particles used as drug transporters. Particularly, we will describe loading procedures and physicochemical methods utilized to understand the molecular state of the drug in mesoporous silica and its location in the pores.

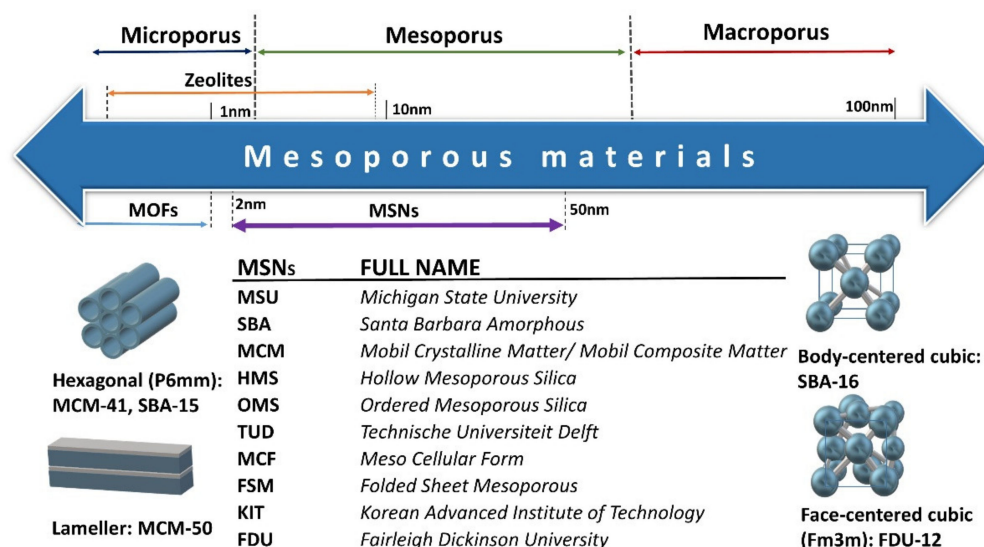


Scheme 1. A multi-step pathway in the drug research—from synthesis of Active Pharmaceutical Ingredient (API) to patient recovery.

2. Drug Loading Methods

Today the porous silica matrices are commonly used as carriers for active substances. For pharmaceutical applications, the most prevalent is the amorphous silica, due to its lower toxicity in comparison to the crystalline form. Therefore, various types of it have been investigated thoroughly [7–12], including porous and non-porous silica, fumed silica, silica gels, etc. The properties of porous silica materials can be improved further by the tailored control of pore structural features, resulting in ordered mesoporous particles, currently the most commonly used type, as demonstrated by the extensive literature display [10,13]. Due to the orderly porous structure (mostly channels without interconnection), large surface area (more than $700 \text{ m}^2/\text{g}$), and high pore volume (above $1 \text{ cm}^3/\text{g}$), they offer precise load control and drug release kinetics [14].

MSNs have two functional surfaces: an inner cylindrical formed by pores and an outer surface. Both surfaces can be selectively functionalized to improve loading and release properties. The outer surface can also be functionalized to increase the efficiency of delivering a drug to a specific target in the body [15,16]. The greatest advantage from the pharmaceutical point of view is the improvement of the solubility of the API (active pharmaceutical ingredient) loaded into the mesoporous silica and the formation of the drug-carrier dispersion systems [17]. Scheme 2 shows the most commonly used MSNs in the formulation of drug substances.



Scheme 2. Schematic representation of various mesoporous materials used as Drug Delivery Systems (DDS).

The loading of drugs into the pores of mesoporous silica can be accomplished in many different ways (Figure 1). Generally, they have been divided into two main approaches: solvent-free methods and solvent-based methods (so-called wet methods) [17,18].

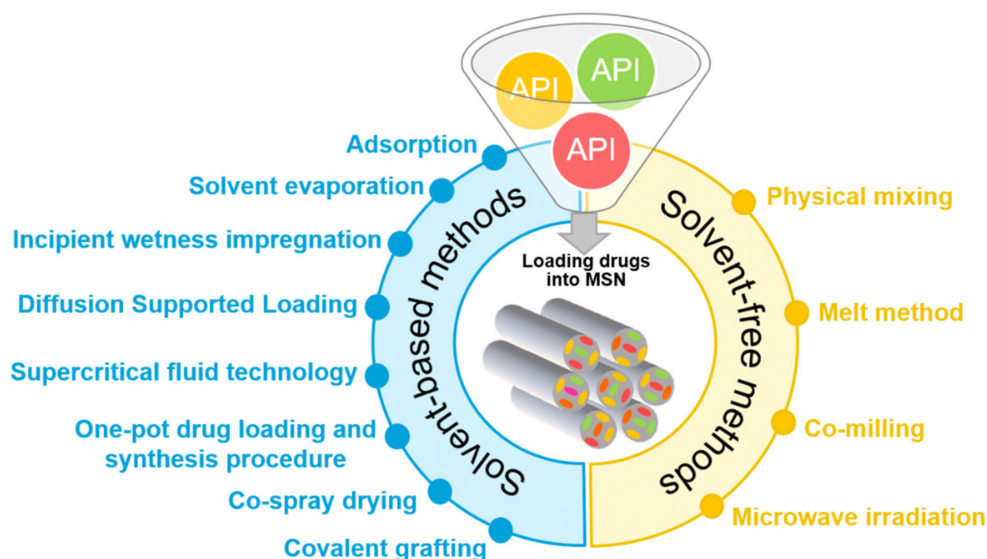


Figure 1. Schematic breakdown of the different methods used to load drugs into MSN.

According to the literature search, the solvent-based methods such as solvent evaporation, adsorption, and incipient wetness impregnation, which encapsulate various types of drugs are commonly employed. Among the solvent-free methods, melting and co-milling are particularly preferred to load the drug into MSNs pores (Table 1). The drug encapsulation process involves adsorption of the drug molecules to the mesoporous silica inner/outer surface under conditions that favor drug-carrier interactions like van der Waals interactions, hydrogen bonding, electrostatic binding, or covalent bonding [19]. The ideal drug loading process should quickly load a large amount of the drug and then unload it with the desired release profile [18]. It is also desirable to minimize the fraction of the drug adsorbed on the external particle surface to avoid the possibility of its crystallization due to the lack of (pores) entrapment effects [20]. The extent of drug loading depends on several parameters. The most significant is the surface area and the affinity of the drug to the silica

substrate [21,22]. In the wet methods, the internal pore volume of the silica, polarity of the solvent, and the concentration of the drug in the solution are also important [23]. The choice of drug loading method affects the degree of drug loading, the distribution of the drug in silica, and the physicochemical properties of the loaded drug [9].

Table 1. Review of drug loading methods used, drug type, and mesoporous silicas in published papers.

Drug	BCS Class	MSP	Loading Method	Reference
Aceclofenac	II	MCM-41	Solvent evaporation	[24]
Atenolol	III	SBA-16	Adsorption	[25]
Atorvastatin	II	SBA-15	Solvent evaporation	[26]
Carbamazepine	II	SBA-16	Adsorption	[27]
		MCM-41	Adsorption	[28]
		SBA-15	Incipient wetness	[29]
		SBA-15	Solvent evaporation	[30]
		OMS	Liquid solid technique	[31]
Carvedilol	II	MCM-41 SBA-16	Solvent evaporation	[32]
Celecoxib	II	MCM-41	Adsorption	[33]
		SBA-15		[34]
Cilostazol	II	SNT	Solvent evaporation	[35]
Cinnarizine	II	SBA-15	Incipient wetness	[29]
Clofazimine	II	MSN	Chaperone assistance	[36]
Danazol	II	SBA-15	Incipient wetness	[29]
Dasatinib	II	SBA-15	Solvent evaporation	[37]
Diazepam	II	SBA-15	Incipient wetness	[29]
Econazole	II	MCM-41	Melting	[38]
Ezetimibe	II	OMS	Incipient wetness	[39]
Felodipine	II	MSN	Solvent evaporation	[40]
Fenofibrate	II	SBA-15	Supercritical CO ₂	[41]
			Incipient wetness	[42]
			Physical mixing	[43]
		MCM-41	Incipient wetness	[44]
			Co-spray drying	[44]
OMS	Supercritical CO ₂	[45]		
Flurbiprofen	II	COK-12	The one-pot drug loading and synthesis	[46]
		MCM-41	Diffusion Supported Loading	[47]
Furosemide	IV	MCM-41	Solvent evaporation	[48]
		SBA-15		[49]
Glibenclamide	II	SBA-15	Incipient wetness	[50]
Griseofulvin	II	MCM-41	Solvent evaporation	[51]
Ibuprofen	II	MCM-41	Diffusion Supported Loading	[47]
			Liquid CO ₂	[52]
			Co-spray drying	[53]
			Incipient wetness	[54]
			Adsorption	[54]
		SBA-15	Covalent grafting	[55]
			Adsorption	[56]
			Incipient wetness	[57]
			Solvent evaporation	[57]
Melting	[57]			
Co-spray drying	[58]			
Co-milling	[59]			

Table 1. Cont.

Drug	BCS Class	MSP	Loading Method	Reference
Indomethacin	II	SBA-16	Solvent evaporation	[60]
		MCM-41	Solvent evaporation	[61]
			Adsorption	[62]
		SBA-15	Incipient wetness	[50]
			Solvent evaporation	[61]
Itraconazole	II	SBA-15	Solvent evaporation	[57]
			Incipient wetness	[57,63]
			Melting	[57]
		MCM-41	Incipient wetness	[63]
		KIT-6		[63]
FDU-12	[63]			
		COK-12	[64]	
Ketoconazole	II	SBA-15	Incipient wetness	[29]
Ketoprofen	II	MCM-41	Diffusion Supported Loading	[47]
			Solvent evaporation	[65]
			Incipient wetness	[65]
			Adsorption	[65]
Methotrexate	III	MCM-41	Adsorption	[66]
Naproxen	II	MCM-41	Adsorption	[67]
		SBA-15		[67]
Nifedipine	II	SBA-15	Incipient wetness	[29]
Paclitaxel	IV	MSN	Adsorption	[68]
			Covalent grafting	[69]
Phenylbutazone	II	SBA-15	Incipient wetness	[29]
Piroxicam	II	SBA-15	Adsorption	[70]
		MCM-41		[71]
Prednisolone	I	SBA-15	Adsorption	[72]
		SBA-3		[72]
		FDU-12		[72]
Resveratrol	II	MSM	Incipient wetness	[73]
Rufinamide	II	SBA-16	Adsorption	[27]
Telmisartan	II	MSN	Solvent evaporation	[74]

The table is a compilation and extension of data published by Maleki et al. [20]; BCS—Biopharmaceutics Classification System; COK—Center for Research Chemistry and Catalysis; MSM—mesoporous silica materials; SNT—mesoporous silica nanotubes.

Successful commercialization of any DDS requires an easy, cost-effective, and reproducible method of large-scale production. Since API encapsulation is the most critical step in mesoporous silica based delivery system applications, there is a great need to develop suitable large-scale drug loading techniques. Many of the methods listed in Table 1 do not offer optimal and universal solutions that would make them indisputably used on a larger scale than in the laboratory. These restrictions significantly affect the strategy and decisions of the pharmaceutical industry, which expects simple, cheap, and repeatable solutions that meet economic and ecological criteria. The most common methods of drug loading will be characterized below, taking into account their advantages and disadvantages.

2.1. Solvent-Based Methods

There are several solvent-based approaches for loading a drug into mesoporous silica. All of them improve drug release through the amorphous state of API in MSN. The most popular are described below. In the wet methods, regardless of the used procedure, it is necessary to remove the solvent to the acceptable levels specified in the guidelines of the International Conference on Harmonization (ICH) Q3 (R5) [75]. It is worth mentioning that

some residual solvents used may remain in MSN despite its disposal. As demonstrated by Eren et al. the hexane used in the synthesis of SBA-15, although later evaporated, reduced the viability of the HLA-116 and HT-29 cells incubated with these particles [34]. Therefore, using less toxic and safe solvents, e.g., ethanol or supercritical or near-critical CO₂, as an alternative to organic solvents in the drug loading process is recommended, if possible, for human pharmaceutical applications [34,52,76]. The loading procedures using solvent methods are challenging because it often requires multi-stage and long-lasting processes, uses large amounts of solvents, and it is also difficult to control the filling factor. Another, equally important issue is the concentration of the drug used and the selection of an appropriate solvent.

The adsorption method is a simple and widely used technique for loading drugs into the pores of MSNs. In adsorption from the organic solution, the mesoporous silica is immersed in the concentrated drug solution. After this time, the drug molecules are adsorbed on the pore walls. The drug-loaded MSNs are then separated from the solution by filtration or centrifugation. Finally, the particles are dried to remove the residual solvent. However, sometimes this step is omitted [77]. The adsorption method can be used for both hydrophilic [78] and hydrophobic [79] drugs. The process does not require high temperatures, so it is suitable for loading thermally sensitive substances. However, in most cases this process is inefficient, therefore a high concentration of drug solutions is required to achieve a high degree of drug loading. This can be problematic, especially for drugs with poor solubility [77]. If the concentration is too high, the drug molecules will quickly adsorb onto the surface and block the mesopores, reducing the potentially available surface area for drug loading [80]. The main disadvantage of the adsorption method is time-consuming. It is also difficult to predict what degree of drug loading will be achieved. Moreover, a large proportion of the drug is wasted in the filtration/centrifugation process [81]. The choice of a solvent has a significant influence on the process of loading drugs into MSN. The solvent with the highest API solubility is not necessarily the best candidate for obtaining a high filling factor. For example, valsartan dissolved in dichloromethane can be incorporated into MSN with a twice higher degree of loading than methanol, although the concentration of valsartan in methanol was higher than in dichloromethane. Similarly, the aprepitant loaded into MSN using chloroform as a solvent obtained over three times higher filling factor than at using methanol, even though its concentration in chloroform was approximately three times higher compared to methanol [82]. Charnay et al. showed that the use of polar solvents such as dimethyl sulfoxide, dimethylformamide, and dimethylacetamide causes a low degree of ibuprofen loading into MCM-41 [54]. In contrast, ethanol and hexane (non-polar solvents) gave relatively high filling factors. The hexane loading capacity was up to 37 wt %. This is because polar solvents can form competitive adsorption with drug molecules, causing a low degree of drug loading [54]. If the affinity of solvent (often associated with the formation of hydrogen bonds) to MSN is higher compared to the drug, the pores of the silica are filled by solvents and there is not enough space for API [83]. This is one of the limitations of the applicability of this method.

The incipient wetness impregnation method is the most commonly used for the preparation of catalysts [84,85] but is also suitable for loading drugs into mesoporous materials [29,54,57]. In this method, a known volume of concentrated drug solution approximately equal to the pore volume of the MSN used is added dropwise to the silica. Next, the wet powder in which the drug diffuses into the pores by capillarity is dried and quickly washed on a filter with a small amount of used solvent to remove the excess drug coating the external surface of silica [54]. Finally, the powder is dried using air for 24 h and placed under a vacuum for 48 h at a temperature of 40 °C [57]. The washing step for eliminating APIs outside the pores has a significant impact on drug loading efficiency. Charnay et al. observed reducing the amount of ibuprofen encapsulated onto MCM-41 after washing the silica with ethanol from 1350 to 500 mg/g [54]. They also proved that successive impregnations enable to achieve a complete pore filling and significantly improve the concentration of ibuprofen. Their research has shown that the incipient wetness impregnation method is

more efficient than the traditional solvent immersion process. Ibuprofen in the pores was in an amorphous state and the dissolution rates were increased compared to the crystalline drug [54]. The main advantage of the impregnation method is that it exploits the large pore volume of the mesoporous silica and can easily determine the amount of drug-loaded into the carrier [57]. Furthermore, the drug is efficiently loaded and thus the method is suitable for expensive drug molecules. However, to obtain a high degree of drug loading, typically in the range of 5–40% *w/w*, the high concentrated drug solution and repeated impregnations are required, which significantly extend the process of loading the drug into the MSN [81]. The uniformity of drug distribution is difficult to control. There is also a high risk of drug crystallization on the outer silica surface and plugging the mesopores [20].

The solvent evaporation method is another often used drug loading approach that involves a combination of adsorption and subsequent rapid solvent evaporation [86]. In this method, the silica is dispersed in a drug volatile organic solution (e.g., ethanol, dichloromethane) and dried by fast solvent evaporation using a rotary evaporator [65] or heating [49] for obtaining drug-loaded MSNs [20,87]. In the adsorption method, the solvent is removed by filtration, which can result in partial loss of the drug. In contrast, solvent evaporation may affect the physical state of the drug, its localization in the MSN, and the rate of release from the carrier [57,86]. Mellaerts et al. used the solvent evaporation method and incipient wetness impregnation to load itraconazole and ibuprofen into SBA-15 silica [57]. In both methods, the samples were dried at 35 °C and then placed under reduced pressure (1 hPa) at 40 °C for 48 h. The ibuprofen location in SBA-15 was the same regardless of the technique used. Ibuprofen preferably was positioned inside the micropores. It was observed that itraconazole molecules were located on the walls of the mesopores during the adsorption process from dichloromethane, while the incipient wetness impregnation method favored the positioning of itraconazole in the micropores (Figure 2). The authors suggested that the localization of itraconazole in the mesopores was related to the slow introduction of the drug requiring diffusion of itraconazole molecules from an external dichloromethane solution into the SBA-15 particles. Thus, the solvent evaporation method gives the drug molecules enough time to rearrange and aggregate inside the mesopores. In the incipient wetness impregnation method, all the itraconazole molecules were incorporated at once into the pores, followed immediately by solvent removal. Samples prepared via the solvent evaporation method showed the fastest release kinetics [57].

Diffusion supported loading (DiSupLo) is the new extremely easy and efficient method of loading APIs into the pores of mesoporous silica developed by Potrzebowski and co-workers [47]. In this approach the starting material, pre-homogenized physical mixture of API and MSN with the desired proportion of both or more components is transferred to an opened weighing vessel as a solid matter and then placed in a closed vessel containing ethanol for 3 h at room temperature (Figure 3).

The drug loading time was established experimentally using NMR measurements at 30 min. intervals. The layer thickness of the physical mixture should be small and experimentally optimized. Finally, the ethanol was thermally removed from the drug-loaded samples. The mechanism of drug encapsulation in the DiSupLo method is as follows. In the first stage of the process, there is no direct contact between the solid sample and the liquid solvent, the only one between the diffusing ethanol vapors and the solid mixture. In the second step, the vapors penetrate the solid-state mixture in the whole volume, locally condense and dissolve the drug. At this stage API dissolved in the minimum volume of solvent is transported into the pores of MSN [47]. The applicability of the DiSupLo method has been proven by testing the loading of selected non-steroidal anti-inflammatory drugs such as ibuprofen, flurbiprofen, ketoprofen, and their mixtures to the pores of MCM-41 as the drug carrier. Studies have shown the introduction of all drugs with weight ratios API/MCM-41 of 1:3 into the pores of the silica with a filling factor of 33% and 50%, respectively. For a 1:1 ratio, it has been observed that some API was inside the pores with nearly 60% filling factor while part remained on the outer wall of MCM-41. It has been proven that the DiSupLo method, apart from one API, also allows the loading of

two and three drugs simultaneously with a weight ratio of API to MCM-41 of 1:3. DiSupLo uses and enhances the advantages of wet methods and eliminates their drawbacks. It is a fast process requiring a minimum amount of solvent, so it is environmentally friendly and economically justified. It is the easiest method for loading API into MSN pores described so far in the literature, since it does not require any special equipment and/or demanding experimental conditions (high temperature, high pressure, stirring, grinding, etc.) for carrying out the process. The DiSupLo method allows to achieve a high drug loading degree and encapsulate the whole API if the weight ratio of the starting API/MSN mixture is not higher than the maximal filling factor. The unique advantage of this technique is the ability to quantitatively load two or more components with the desired API composition, which significantly extends the applicability of MSN as carriers for multi-component systems [47]. Most studies using MSN as drug delivery systems focus on loading only one drug into the pores. Attempts to introduce more complex, binary, or ternary systems are rare [88,89]. Controlled-release drug synergism can be a useful therapeutic tool, especially in cancer therapies.

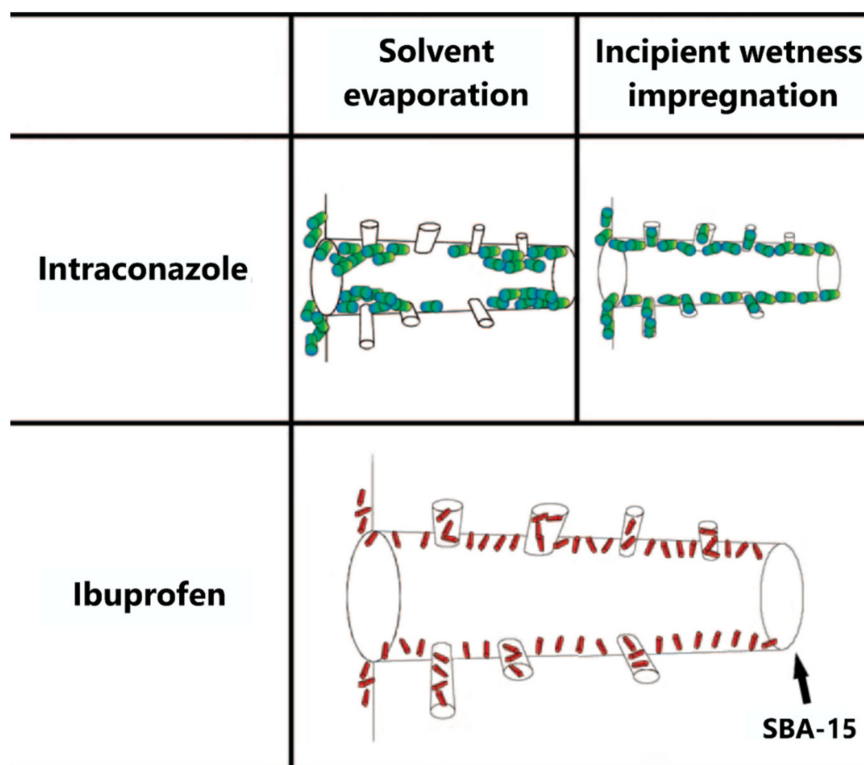


Figure 2. Physical state of itraconazole and ibuprofen upon association with SBA-15 loaded according to the solvent evaporation method and incipient wetness impregnation method. Adapted with permission from [57], Copyright 2008 American Chemical Society.

Supercritical fluid technology (SCF) commercially used in the food and chromatography industries is also a method for drug loading into mesoporous silicas [41,45,90]. The use of supercritical fluids in this technique has many advantages compared to traditional organic solvents. Their specific properties, including liquid-like density, gas-like viscosity, a diffusivity higher than that of liquids, and a very low interfacial tension allow them to be employed as impregnating agents [91]. Then, the transport of the solubilized substance in the supercritical phase is facilitated to the solid matrix, which is impregnated evenly and with a shorter processing time than in the liquid phase [45]. Carbon dioxide (CO₂) is the most commonly used in SCF technology as it has mild critical conditions (31.2 °C, 7.4 MPa). Besides, supercritical CO₂ (SCCO₂) is inert, non-flammable, non-toxic, and inexpensive, making it an excellent solvent [91,92]. Another advantage of the SCF technology is that the

final product after fluid evacuation is free of the residual solvent when the drug loading process is performed without the addition of a cosolvent. Li-hong et al., used an adsorption method and SCCO₂ technology to load ibuprofen into the pores of MCM-41 [93]. It was shown that the amount and depth of ibuprofen penetrated the pores of mesoporous silica by the SCF method were larger than those using adsorption from ethanol. The authors also studied the ibuprofen release profile and found that the sustained-release effect of the drug in the samples made with the SCF technique was 50% in 15 min and 90% in 60 min, which was longer than the one prepared by the adsorption method [93]. A similar study was carried out with fenofibrate using incipient wetness and SCCO₂ methods [45]. Both impregnation processes were compared in terms of yield, duration, and physical characteristics of the drug. Studies have shown that the incipient wetness method to load fenofibrate up to 300 mg drug/g silica in 48 h, while the SCCO₂ method resulted in loading up to 485 mg drug/g silica in 120 min, with a low degree of crystallinity (about 1%) comparable to crystallinity observed for the classical solvent method. SCF technology, therefore, provides an alternative and environmentally friendly way to load a drug onto silica support with the advantage of reduced processing time that can be achieved in 2 h [41,45,93]. Stam et al. demonstrated that the very low concentration of ibuprofen in a nonpolar liquid CO₂ was enough to achieve maximum loading of this drug in the pores of MCM-41 [94]. These studies have shown that liquid CO₂, cheaper than SCCO₂, can be an effective “green solvent” to incorporate drugs into mesoporous silica. Ahern et al. compared the use of supercritical and liquid CO₂ technology with other drug loading methods such as physical mixing, melting, and solvent evaporation [43]. Fenofibrate and SBA-15 silica were used in the research. All methods, except physical mixing, loaded the drug into the mesopores in a non-crystalline form. The release of fenofibrate from all samples was faster than that of the crystalline drug. Interestingly, the drug release from the sample prepared by the physical mixing method was improved but had a slower rate and a lower drug release rate than all other methods. Furthermore, the release of fenofibrate from the melted sample was slower compared to the solvent methods due to the negative effect of the drug’s molten viscosity on mesopore blocking [43]. Despite the many advantages of using SCF technology to impregnate BCS II molecules within the pores of MSN, studies showed that a lot of drugs exhibit poor solubility in SCCO₂ [95–97]. Therefore, lest this issue obscure the potential of this method, it has been suggested that other properties of compressed carbon dioxide may be beneficial, such as its ability to lower the melting point of the compound and reduce the viscosity of the molten products [98].

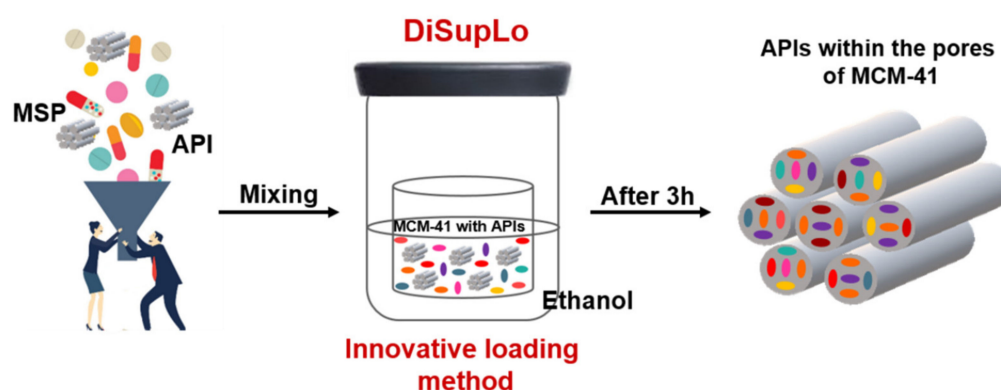


Figure 3. Schematic illustration of loading APIs into the pores of MSN using the DiSupLo method. Adapted with permission from [47]. Copyright 2020 Elsevier.

The one-pot drug loading and synthesis procedure is a new approach to drug encapsulation in which API is loaded into the mesoporous carrier during its synthesis [46]. The main route of MSN production is gel-sol synthesis using inert surfactant micelles as a template, which is finally removed through calcination or extraction [19]. The obtained MSNs are loaded

with a targeted drug by one of the available methods [18,20,46]. This traditional method is multi-step, time-consuming, and results in low drug uptake and its burst release, which is inadequate for most applications [99]. The new method combining MSNs synthesis and drug loading process overcomes these limitations and seems very promising for the design of novel drug delivery systems. Dementeva et al. presented the possibility of using the micelles of the bactericidal drug myramistin as a template in the sol-gel synthesis of mesoporous silica nanocontainers [100]. The synthesized nanocontainers were characterized by a very high drug content (≥ 1 g/g of SiO₂) and were also pH-sensitive. It should be noted that this method can be extended to other amphiphilic drugs (e.g., anti-cancer, anti-inflammatory, or bactericidal) as templating agents [46,101–103]. Interesting research was presented by Wan et al. using the one-pot synthesis method by evaporation-induced self-assembly, they introduced two drugs into mesoporous silica: hydrophilic heparin and hydrophobic ibuprofen [104]. It was shown that in situ drug loading realized through evaporation-induced self-assembly (EISA) had several advantages. The first merit was the time reduction of the delivery system preparation from about 74 h to 10 h. The second merit of in situ loading was the dramatically increased amount of heparin and ibuprofen in SBA-15 compared to the traditional solvent impregnation method. Sustained drug release over 30 days has also been achieved. Finally, the one-pot technique was environmentally friendly because the whole procedure was performed at ambient temperatures, with no calcination process, and without using toxic organic solvents, which is extremely desirable from a pharmaceutical point of view. Tourne-Peteilh et al. showed the drawback of this method may still be time-consuming and low drug loading [105]. They presented the use of sol-gel one-pot synthesis for ibuprofen encapsulation. Tween 80, a widely used surfactant in food and pharmaceutical formulations, has been chosen as a template for silica and also as a solubilizing agent for ibuprofen. In vitro studies in simulated physiological media showed a significant increase in the dissolution rate of ibuprofen compared to pure drug crystals. However, they achieved a low drug loading (<4%). Although the procedure also involved the synthesis of silica particles, it took several days to complete. Undoubtedly, in the one-pot method, selecting the appropriate surfactant will be the key to fine-tuning the drug loading, release, and interaction with the silica walls.

Covalent grafting is another possibility for loading drug molecules into the mesoporous silica [89,106,107]. Covalent linking of the drug to functional groups present on the pore walls of a mesoporous silica carrier is an attractive alternative to physical adsorption as it prevents undesirable leaching of the drug before it reaches its target site, drug release is more controlled and can occur after breakage of the covalent bond. Commonly employed bonds for covalent attachment of drugs are amide, disulfide, ester, thiol, and carbamate bonds. The targeting and release of the drug from such systems can be achieved by hydrolysis, enzymatic degradation, exchange reaction, or redox reaction [108]. This release mechanism is often called linker cleavage and has been summarized in several excellent reviews [109,110]. The covalent linking of ibuprofen to the surface of MCM-41 functionalized with amine groups has been demonstrated [111]. The stronger amide bond between the drug and the mesoporous silica surface led to an increase in ibuprofen loading, slower and more controlled drug release compared to the adsorption method. In the case of ibuprofen adsorbed into non-modified MCM-41, the weak interaction derived from the carboxylic acid groups of the drug and the silanol groups of the silica resulted in ibuprofen was easily desorbed [111]. Other exemplary studies have reported the use of the covalent linking to load cysteine, a sulfasalazine prodrug, and paclitaxel [69,112,113]. Rosenholm et al. presented the covalent attachment of the chemotherapeutic agent methotrexate (MTX) to poly (ethyleneimine)-functionalized MSNs [114]. The covalent linking of MTX to silica by using standard EDC coupling linking the carboxylic acid group present in the drug to the amino groups of silica prevented MTX premature release, and its intracellular detachment from the carrier in vitro was due to enzymatic degradation of the amide bond in lysosomes [114]. Loading of MTX to the mesoporous carrier was preferred over physical adsorption. Previously, it was shown that MTX does not adsorb to silica, only after alumina

was introduced into the silica framework the adsorption was observed [115]. Moreover, the attachment of MTX mainly to the particle surface enables the loading of additional drugs into the pore network for drug combination therapies [114]. Despite the advantages of covalent bonding over physical encapsulation, such as slow drug release, improved biodistribution, therapeutic efficacy, and reduced systemic toxicity [107], this approach has some drawbacks. The chemical bonding of the drug to the surface of MSNs can convert API to an inactive form, so it is important to perform a test confirming the original molecular structure of the drug is preserved. The presence of sufficient functional groups on the carrier surface is not always possible as they influence the colloidal stability of the carrier and its surface charge. Moreover, the steric hindrance of the drug molecules crowded on the silica surface may negatively influence the formation and breaking of chemical bonds [69,77,106].

2.2. Solvent-Free Methods

Compared to wet methods, solvent-free methods are less time-consuming and can achieve a high degree of drug loading. Moreover, the drug concentration in the mesoporous material used is easy to predict as it is directly influenced by the ratio between API and MSN. Undoubtedly, they are environmentally friendly techniques, as they do not require checking the residual solvent in drug products, and they are located in the stream of “zero waste” chemistry.

The melt method involves heating a physical mixture of the drug and mesoporous silica above the melting point of API [9,116]. This approach is very efficient and significantly reduces the time of drug incorporation into the mesoporous silica. Potrzebowski et al. showed that the melt method (which they called Thermal Solvent Free) is a much more efficient technique of confining ibuprofen in the pores of MCM-41 compared to incipient wetness [83]. From the analysis of the proton NMR spectra recorded at the very fast rotation of the sample, they have established the percentage of mesopores filled. The filling factor defined as a weight to weight ratio of ibuprofen to MCM-41 was approximately 60% [83]. Despite the advantages, the melting method has some limitations. It can be suitable only for thermally stable drugs characterized by a low viscosity after melting. Some studies emphasize the high relationship between the molten viscosity of the drug and the mesopore penetration [57,117]. Mellaerts et al. showed that itraconazole was not successfully loaded into the pores of SBA-15 due to its high viscosity in a molten state which prevented homogeneous drug distribution in the mesopores [57]. Glassy itraconazole particles accumulated on the surface of SBA-15, whereas ibuprofen has a lower molten viscosity and was loaded into the pores of SBA-15 in a non-crystalline state, achieving a rapid in vitro release [57].

Microwave irradiation is another method to load drugs into silica materials. In this technique, the sample is heated using a feedback system that controls the temperature during the loading process of the API into the silica nanoparticles and protects the drug from degradation [118]. Waters et al., used this method to load fenofibrate into a variety of silicas including SBA-15 and compared them to samples loaded by more traditional heating methods [119]. Moreover, all experiments were performed both in the presence and absence of water, used as the fluidization medium to aid drug-carrier interaction. It was investigated that samples prepared using microwave radiation without the presence of water as a solvent showed an increased rate and extent of fenofibrate release compared to pure drug and samples prepared by other techniques. This can be explained by the fact that the crystalline fenofibrate has changed to an amorphous state and the formulation provides enhanced drug release. Furthermore, the optimal drug: carrier ratio for this method was found to be 1:3 [119].

Co-milling is a commonly used technique to produce sub micrometric particles [120] as well as for solid-state amorphization [121]. Recent studies have shown that milling using a planetary ball mill is an effective solvent-free method for introducing organic compounds such as benzoic acid and 4-fluoro benzoic acid into the pores of MCM-41 [122]. This study

also appeared that the guest-loading process is fully controlled and dependent on the ratio of the loaded substance and silica. The maximum capacity of loading was over 50% at a 1:1 ratio. Moreover, it has been proven that using this technique, guest molecules are located in different zones of MCM-41 particles (Figure 4) [122]. Hedous et al. demonstrated that the co-milling of SBA-15 with ibuprofen made it possible to load the drug into the porous matrix, enhancing thereby the filling degree to almost 40 wt% [59]. This shows that milling can be considered as an alternative to solvent-based drug loading methods. The co-milling technique is simple, does not require time-consuming steps, and can be applied on an industrial scale. This is extremely important in practical applications. The problem to consider during ball milling processes is the resistance of the nanocarriers to mechanical stress. This issue was well recognized for MCM-41. Abu-Zied et al. investigated the effect of ball milling on the structure, texture, and morphological properties of mesoporous MCM-41 material [123]. Their results showed that by increasing the milling time, the amorphization process of mesoporous MCM-41 material accelerates. MCM-41 retains its initial crystallinity until 30 min of milling time. A serious loss of MCM crystallinity occurs after 1–2 h of milling, while the complete loss of crystallinity of this material is noticeable after four hours of ball milling [123].

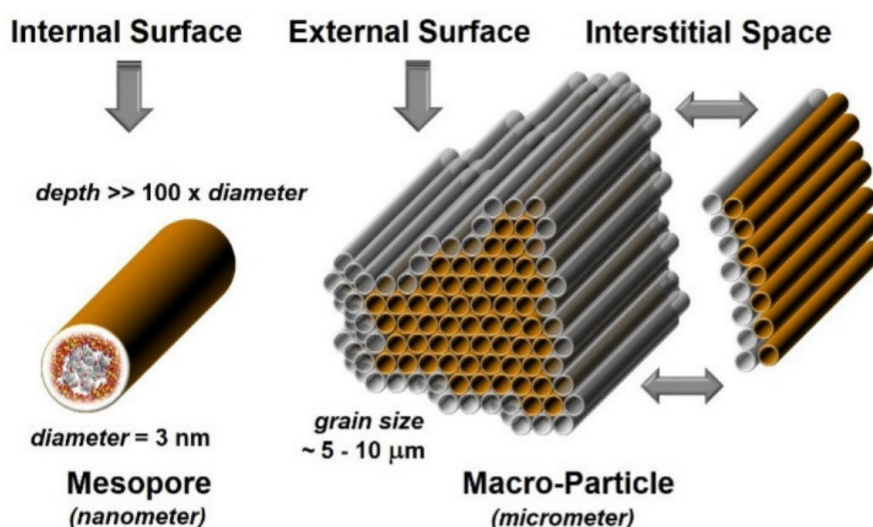


Figure 4. Illustration of internal and outer-space accessible to guest molecules in the powder samples of MCM-41 silica according to concept proposed by Torres-Barthelemy et al. [124] A single pore, with a diameter of ca. 3 nm and a depth much greater than 100 nm, give rise to a large internal volume (left). These pores are ordered in a regular honeycomb manner (middle), resulting in a non-negligible external surface (the gray area marked with the vertical arrow). The external surface gives rise to interstitial space (right) formed between the randomly ordered crystallites (see the horizontal arrows). Adapted with permission from [122], Copyright 2021 American Chemical Society.

3. Analytical Techniques

With the growing interest in the use of MSNs materials as drug delivery agents, there is an obvious need to develop adequate analytical tools to study their size and morphology, as well as loading and release processes. Knowledge about the physicochemical properties of nanoparticles is a critical step in the construction of novel delivery systems and understanding the mechanism of host-guest interactions. Many convenient and accurate tools from a wide palette of conventional analytical methods have already been used in the structural and spectroscopic studies of API/MSN systems. (Figure 5). The most common ones are thermo-analytical methods (DSC and TGA), various types of spectroscopy (NMR, IR, Raman), gas sorption, microscopy (TEM, SEM, and AFM), and powder X-ray Diffraction (PXRD). Other methods, such as chromatography, mass spectrometry (MS) have also been applied. Since different techniques analyze different properties, none of them provides

full characterization but rather only a piece of partial information, therefore only their combination represents the portrayal of the complete system.

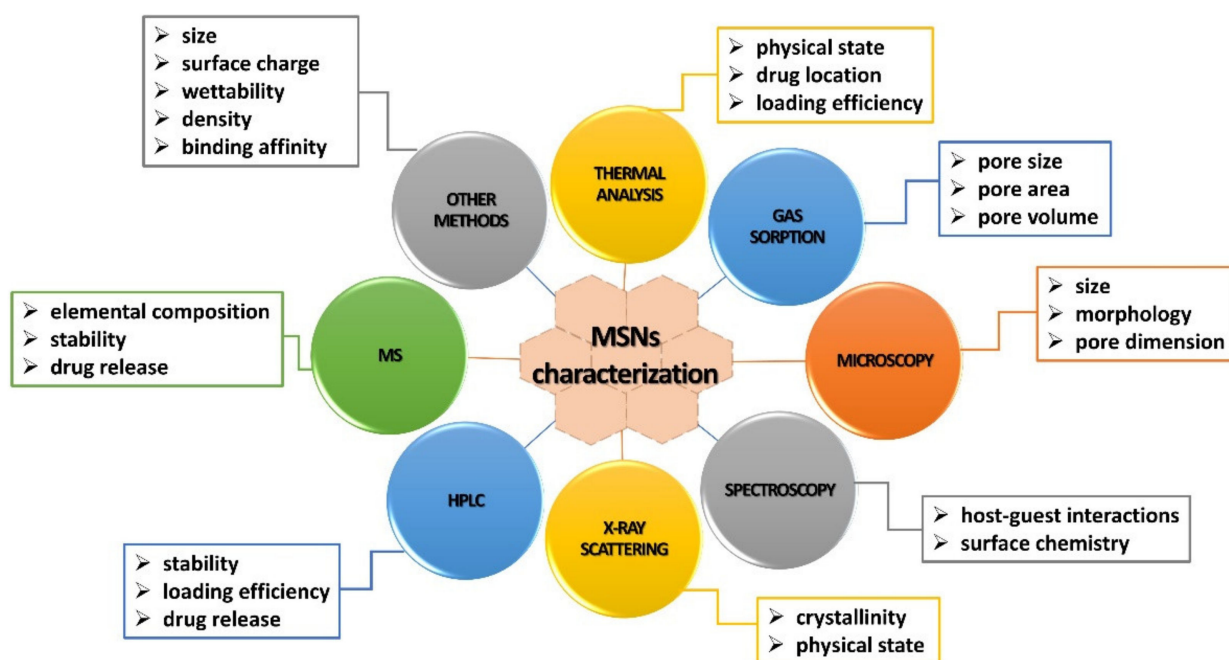


Figure 5. Different groups of analytical techniques used for MSNs characterization.

3.1. Thermal Analysis

Thermal analysis is a group of calorimetry techniques in which the properties of a sample are monitored against time or temperature while the temperature of the sample within a specific atmosphere is programmed [125]. Combined data from thermo-analytical methods such as differential scanning calorimetry (DSC) and thermogravimetry (TGA) allow quantification and characterization of the physicochemical nature of the drug introduced into the pores of silica. Differential scanning calorimetry (DSC) is used to characterize the physical state and location of API in a material by observing of its melting point. It has been noticed that when the drug is confined in the pores of mesoporous silica, its melting point data and glass transition state is lower than that of the crystalline state, and the melting is observed over a wider range. While the concentration of the drug in the MSN increases, the peak of the endothermic heat of fusion decreases. When all the drug is loaded into the porous silica structure, the melting point peak of the drug does not exist, meaning that the MSN prevents the API from recrystallizing and the incorporated substance is in an amorphous form. On the other hand, the drug on the outer surfaces of the pores is considered to be a bulk material and does not show a glass transition. Therefore, DSC analysis distinguish the compound on the surface of mesoporous silica from the one contained therein (Figure 6).

With the help of DSC measurements, it is also possible to determine the pore size distribution. The method is based on the observation of the solid-liquid phase transformation inside the pores, i.e., the melting/freezing point and the melting/freezing enthalpy. The melting point/freezing point depends on the pore size and the transformation enthalpy depends on the pore volume. The method also provides information about the interaction that takes place between the porous material and the liquid [126]. Knopp et al. used DSC to quantify monomolecular loading capacity by solvent-free melting during the heat-cool-heat cycle of ibuprofen with good glass-forming ability. The overloaded drug-silica systems were analyzed at various weight ratios. When quantifying excess API, the ibuprofen that is heated for the first time fuses into the pores of the mesoporous silica. After cooling, the unadsorbed part of the drug was amorphized. In the case of easily glass-forming sub-

stances, no crystallization occurs after cooling. The particles are adsorbed and immobilized on the silica surface and do not cause another glass transition in the DSC. As a result, their quantity can be determined after the silica is fully loaded by examining the change in heat capacity [127,128]. The same authors, using the thermo-analytical method, have demonstrated experimentally and theoretically the existence of a relationship between the pore volume and the surface of mesoporous silica, which will allow the determination of the maximum carrying capacity of the drug. By using this methodological combination, optimal textural properties of the silicone carriers can be designed for each drug [129]. In five types of mesoporous silica with the same chemical composition but the different surface area, diameter, and pore volume, the loading capacity of three model drugs: paracetamol, celecoxib, and cinnarizine was determined. Based on the heat-cool-heat DSC method load capacity was compared with the theoretical load capacity calculated from the surface area and amorphous density of drugs as well as the surface area and pore volume of silica. It was concluded that monomolecular loading ability increases with increasing surface area and decreasing pore volume.

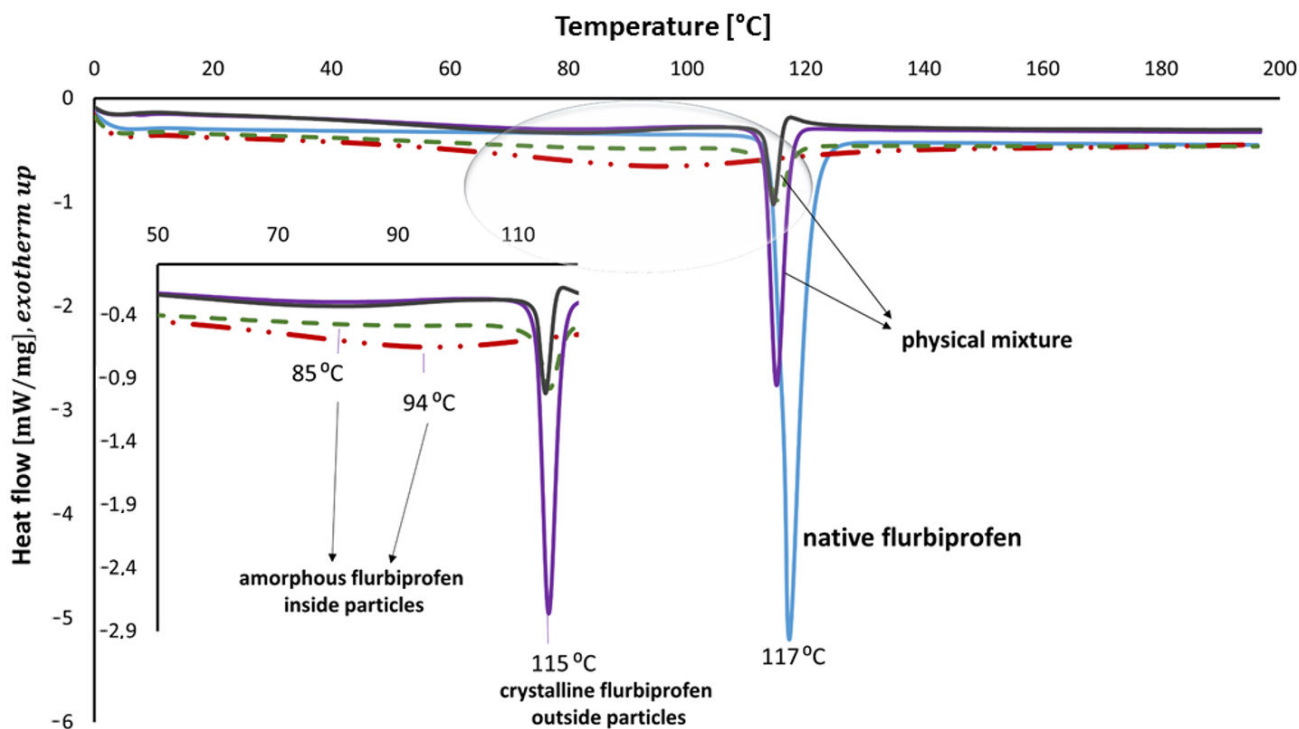


Figure 6. Illustration of DSC thermogram of native flurbiprofen (shows a sharp melting endothermic peak—blue line), flurbiprofen as a physical mixture with MCM-41 in 1:1 (violet line) and 3:1 (grey line) range and flurbiprofen loaded into MCM-41 1:1 (green line) and 3:1 (red line); flurbiprofen in the pores of carrier melt lower and the melting is observed in a wider temperature range to the native form. Data provided courtesy of Katarzyna Trzeciak.

Since the inorganic carrier is more thermally stable than the organic guest molecule, weight loss from the drug degradation followed by desorption of volatile components by gradually increasing the sample temperature using TGA can be observed. Weight loss is proportional to the total drug content. Figure 7 shows a comparative analysis of two methods of ketoprofen loading into MCM-41. MCM-41: the ketoprofen composite had two distinct weight loss regions; in the region below 100 °C (approx. 5%), typical for the water evaporation, and the range from 275 to 600 °C, typical for the degradation of ketoprofen. As a result of measuring TG, the total ketoprofen content in MCM-41 was 26.9% and 32.8% for the 3:1 combinations obtained by DiSupLo and milling, respectively. To determine the ketoprofen content in the remaining cases, one should take into account the population mass loss of two ketoprofen populations: (a) bulk-like molecules and

(b) ketoprofen molecules interacting with the pore walls. For the pure drug, the sharp decline in the TGA curve started at 175 °C and ended at 275 °C, indicating a one-step degradation of ketoprofen over a range of 252 °C, resulting in 99.98% weight loss. The amount of solvent remaining in the pores after loading can also be determined by the same principle. However, the thermogravimetric analysis may give erroneous results in determining whether all loaded material has left the carrier when thermostable compounds or the drug itself form strong connections to MSN [130].

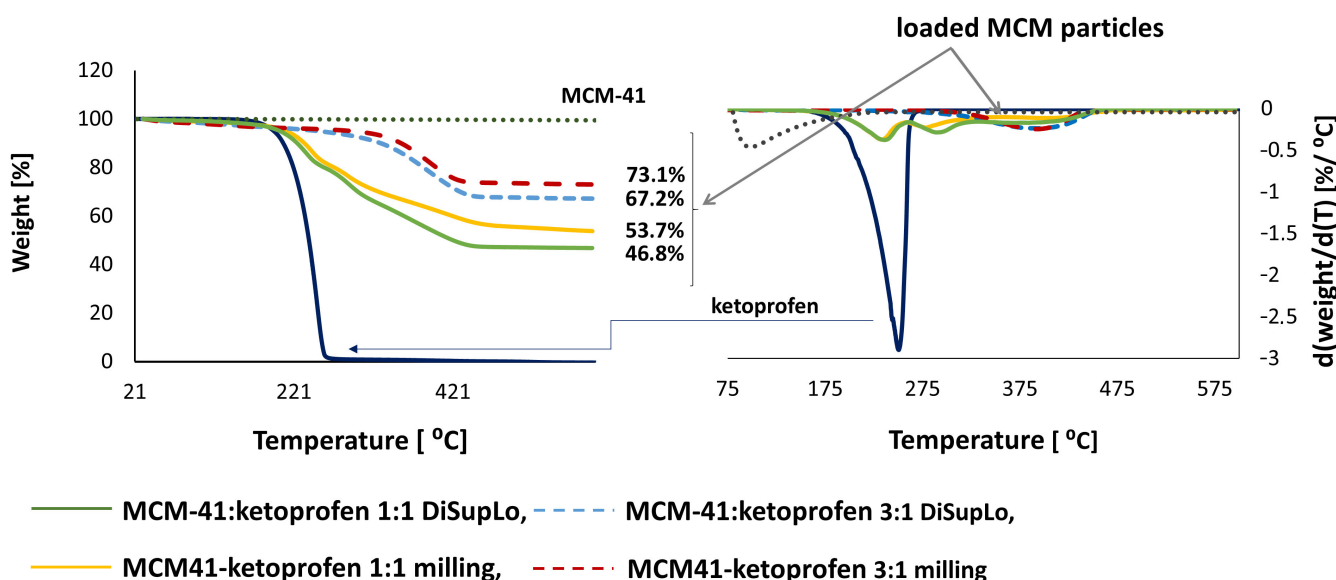


Figure 7. Illustration of TGA thermogram of native ketoprofen and ketoprofen loaded into MCM-41; ketoprofen presented a single mass loss step, with no residue at the end of the experiment, the sample does not decompose, but evaporated after melting; TGA weight% ver. temperature and 1st derivative curves show that in the samples loaded in a ratio of 1:1 there is a multi-step decomposition of ketoprofen, and in a 3:1 one-step decomposition. Data provided courtesy of Katarzyna Trzeciak.

3.2. Gas Sorption

Physical gas sorption is a well-established technique of the first choice for characterizing the textural properties of solid surfaces and their changes after various types of actions. The technique precisely determines the amount of gas adsorbed on the material, which is a direct measure of the porous properties and structure. The isotherm obtained from the adsorption measurements provides information on the surface area (SA), pore volume (PV), and pore size distribution (PSD). The measured isotherms are assessed according to the generally accepted and currently used IUPAC isothermal classification and conventional models [131–133]. Data on gas sorption have been collected, analyzed, and presented in numerous reports, therefore the results of the experiments can be easily compared with those previously published. In the case of mesoporous silica, changes in the native porous structure and drug-loaded adsorbents can be estimated based on the course of nitrogen adsorption-desorption isotherms of type IV at 77K and a wide range of relative pressures (p/p_0) (Figure 8).

Pore size controls of MSN can be achieved on both the adsorption branch and the desorption branch of the isotherm. For mesoporous materials, capillary condensation follows through adsorption, next by a metastable fluid state. Capillary evaporation takes place by desorption and forming a hemispherical meniscus, separating vapor and condensed capillary phase. This creates hysteresis as pores of definite size are filled at a higher pressure and evacuated at lower pressures. If the test material is fully mesoporous and encloses only non-intersecting mesoporous of a cylindrical geometry and similar size, the N_2 isotherm type IV occurs with a hysteresis loop of type H1 according to the IUPAC

classification [132,133]. Thermodynamically, the desorption branch is frequently preferred in these cases for isotherm-based mesoporous size distribution. In more realistic cases where pores are randomly distributed and interconnected, the hysteresis loop will be of the H2 or H3 type and pore size distribution from the desorption branch is often more subjective by the pore network effects than the adsorption branch (Figure 8). Among the conventional models, the Brunauer–Emmett–Teller (BET) theory is used to assess the surface area of mesoporous silica; however, it is recommended to support this procedure by the repeatability of measurement when the sample also contains micropores [19]. On the other hand, the analysis of the distribution of mesoporous sizes can be performed using the Barrett–Joyner–Halenda (BJH) models based on the Kelvin equation, although recent reports indicate low reliability of this method. Computational techniques based on the density functional theory (DFT) are recommended for further validation of experimental results [133,134].

The mesoporous silica with the defined diameter (MCM-41, SBA-15 and MCM-48, and others) act as selective sieves. Additionally, they can be easily functionalized, which influences the possibility of designing the models with the tailoring ability to penetrate the pore channels by drugs and control the release mechanism. An important point is the complementarity of pore and APIs sizes. For example, due to its small size, ibuprofen can be loaded into any mesoporous system. For other larger sized drugs, such as vancomycin or glycopeptide, or others of similar size, it is better to use SBA-15 as the first option to make sure these drugs are able to end up inside the pores. When the drug to be loaded has a size much smaller than the pore size silica, most drug molecules are not adsorbed on the pore surface because only a few of them can directly interact with the matrix surface. This essential fact investigated by Vallet-Regi et al. in an alendronate model with MCM-41 and SBA-15 matrices [135] indicates that MCM-41 can load more alendronate than SBA-15 (area = 719 m²/g) because in MCM-41 (area = 1157 m²/g) the alendronate contact area is higher than SBA-15. Molecules are trapped in the pores through interactions with the inner walls of the mesopores. Additionally, considering the reverse process of drug release will depend on the surface area of the material. Various experiments have shown that when the silica surface is very large, there is high molecular retention and as a result, a slower release of the drug compared to materials with smaller surfaces. The pore volume is also an important parameter for large particle sizes. The larger the space available for loading drug molecules, the greater the load will be [136], which also affects the release of the drug. If the pore volume is low, the matrix channel may become clogged with drug particles. Concluding, all properties of native, functionalized, or doped mesoporous silicas due to their textural properties, i.e., large surface area and internal pore volume, favor the adsorption of drugs, even of large sizes. Exemplary structure parameters of selected APIs loaded into MCM-41 and SBA-15 are presented in Table 2.

3.3. Microscopy

Electron microscopy offers insight into the nanoparticle's key parameters such as morphology, external diameter, surface area, and pore architecture. Because of its ability to provide detailed structural characterization in the nanometer scale, it has emerged as a powerful tool for the investigation of various nanostructured materials, including MSNs. Despite the undeniable advantages in imaging the structure and morphology of the API/MSNs systems, microscopic techniques have also several limitations. Its main disadvantage is the destructiveness and presence of undesirable artifacts from sample preparation such as drying or vacuum conditions. Additionally, large numbers of individual particles must be characterized to estimate the properties of the entire sample. Few recent reviews related to the application of novel microscopic tools for imaging of different nanomaterials are currently available [141–143], but none of them focuses specifically on the silica particles.

Transmission electron microscopy (TEM) and scanning electron microscopy (SEM) are the most popular microscopic tools for the characterization of nanomaterials. TEM,

based on an electron beam sent through a very thin slice of the sample, is capable of imaging with much higher resolution than light microscopes, thus allowing observation of much finer details. SEM creates images of the sample by scanning the surface with a focused electron beam and visualizes details on the surface of the samples, providing a 3D view. Both methods are widely utilized for MSNs characterization and can be used separately or might be combined to visualize the internal structure of particles as well as their morphologies. In recent years, more sophisticated electron microscopy techniques have been applied for MNPs imaging. High-resolution transmission electron microscopy (HR-TEM) is an imaging mode of specialized transmission electron microscopes that allows for direct imaging of the atomic structure of samples. It can be used to accurately determine the nanopore size. High resolution methods have been applied to check the pore size and morphology, as well as its stability after modification and guest incorporation [15]. High-angle annular dark-field scanning transmission electron microscopy (HAADF-STEM) is a TEM method that receives inelastically scattered electrons or thermal diffuse scattering (TDS) at high angles using an annular dark-field (ADF) detector. Its resolution is nearly determined by the incident probe diameter on the sample. A HAADF-STEM instrument provides an exceptional resolution, higher than 0.05 nm, and is highly sensitive to variations in the atomic number of atoms in the sample. A combination of HRTEM and HAADF-STEM can be used for in-depth characterization of nanoparticles that have a high pore volume while having a low outer surface area, as was shown by Huand et al. (Figure 9). Moreover, the application of the fast Fourier transform (FFT) of the high-resolution images, combined with the statistical analysis of images, revealed details regarding the pore sizes, their ordered structure, and integrity. The results were confirmed by applying the HAADF-STEM imaging over an extended tilt range acquiring images for every 2° of tilt. The contrast of obtained images depends solely on the projected mass-thickness, making it an ideal tool for visualizing the structure of the internal pore channels, and finally confirmed that individual pores run through the length of the particle and are arranged in an ordered structure [144].

HAADF-STEM was also used in several other recent works for detailed characterization of MSNs, especially to observe the specific morphology and to identify the position of loaded cargo [145–147]. For the determination of the structural characteristics and the localization of deposited phase within the mesoporous matrix, the incoherent HAADF-STEM imaging mode was applied on a few specimen fragments. It visualized the high organization of the mesopores, their long-range ordering, and preservation [148]. In the same work, the TEM-EDX and STEM-EELS/EDX have been performed for the chemical analysis of samples to further prove the presence of Mo in the bright areas and of S in the MoS₂ structures. Electron microscopy (TEM or SEM) combined with the energy-dispersive X-ray spectroscopy (EDX or EDS) or electron energy loss spectroscopy (EELS) is a tool used to identify the elemental and compositional analysis of the samples, regarding both, the compositional information of the whole sample, as well as the location of individual elements. The dark-field TEM imaging and corresponding EDS elemental mapping were applied as well to follow the distributions of various elements and loading of gold nanorods into dual-mesoporous silica spheres (DMSSs) [149]. TEM immunogold labeling (IGS-TEM) of ultrathin sections was developed to study the binding of human lysozyme on SBA-15 mesoporous silica, showing their adsorption on both the external and the internal pore surface. Additionally, a three-dimensional reconstruction of the particle from TEM micrographs was also implemented to improve the visualization of lysozyme distribution [150]. In the following studies, the technique was improved by the silver enhancement procedure, allowing the increase in the size of ultrasmall gold nanoparticles (GNPs), which enables the direct imaging of the absorbed conjugates [151,152]. Visualization and quantification of enzyme immobilized in MSNs have been facilitated by the combination of nitrogen sorption analysis and IGS-TEM, allowing direct imaging of guest distribution inside the particles [153].

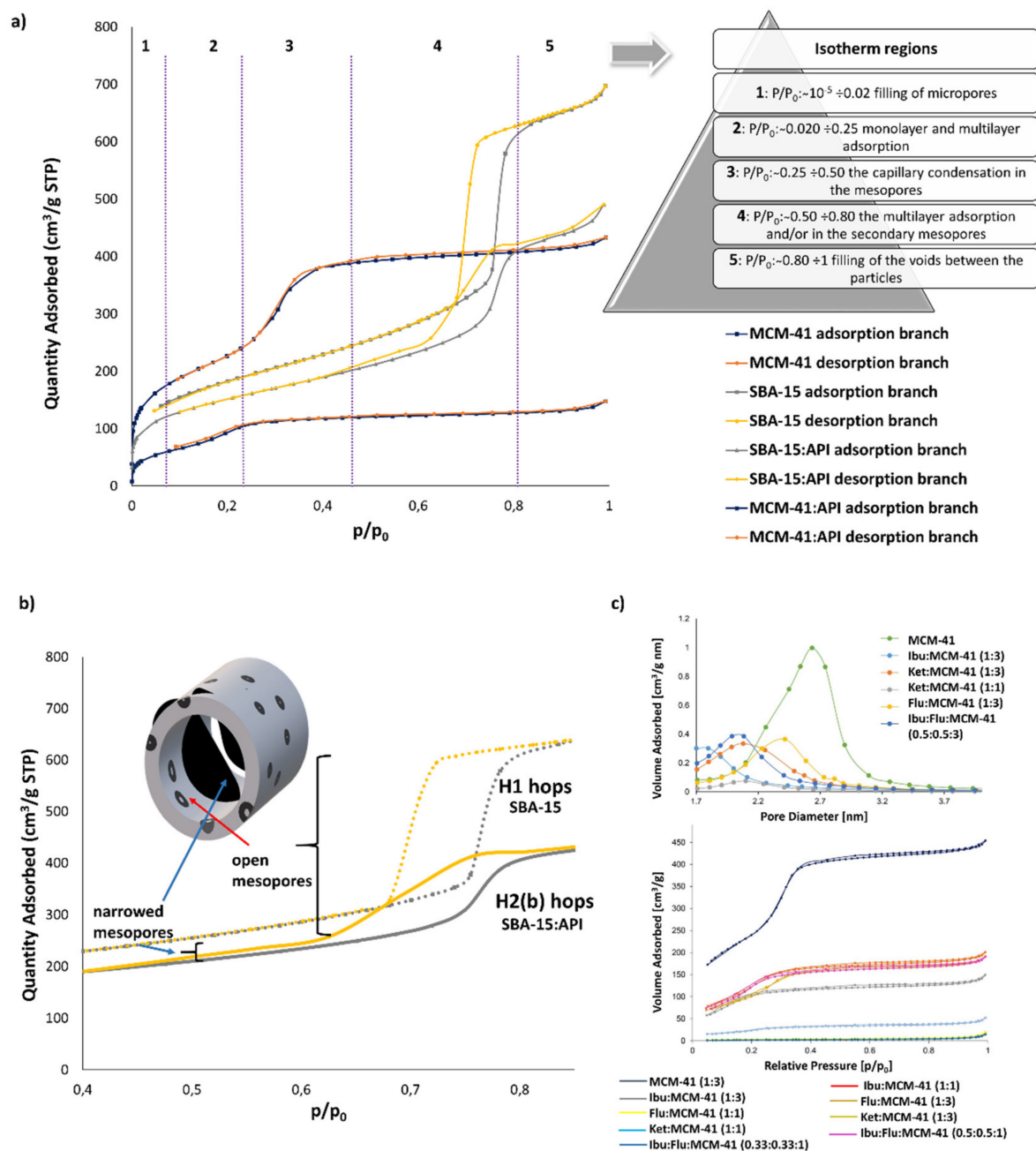


Figure 8. (a) The illustration of nitrogen adsorption/desorption isotherms, and (b) hysteresis loop results of SBA-15 and samples of SBA-15 with API. Data provided courtesy of Katarzyna Trzeciak. (c) Pore diameter distributions of MCM-41 and drug-loaded samples (up pictures) and nitrogen adsorption-desorption isotherms MSM-41 and drug-loaded samples (down pictures) in various weight ratios prepared by DiSupLo method. Adapted with permission from [47], Copyright 2020 Elsevier.

An optical microscope uses visible light and a system of lenses to generate magnified images of the sample. The basic microscope is a very simple instrument, but many complex designs have been developed over the years to improve resolution and contrast. In the characterization of nanoparticles, particularly those carrying fluorescent cargos, confocal microscopy is especially applicable. Super-resolution (SR) fluorescence microscopy is a class of optical microscopy techniques at a spatial resolution below the diffraction limit. Stochastic optical reconstruction microscopy (STORM) is a widely used type of SR technique, able to reconstruct a super-resolution image by combining the high-accuracy localization information of individual fluorophores in 3D and multiple colors. It is based

on a stochastic switching of a single fluorescent molecule using very low-intensity light, which by repetition through numerous cycles allows the fluorophores mapping with high precision. Although STORM has been used mostly in biological studies, it is also a great tool for experiments at the intersection of biology and materials science, and it was applied to study the penetration of proteins within the porous silica nanoparticles [154]. In comparison to the standard wide-field methods with a diffraction limit of 250 nm, STORM offers impressive improvement of performance (Figure 10).

Table 2. Structure parameters of the selected API loaded in MSN.

Material [Reference]	H Type	S _{BET} (m ² /g)		Pore Volume (cm ³ /g)		Pore Diameter (nm)	
		MSN	MSN-API	MSN	MSN-API	MSN	MSN-API
MCM41-lomefloxacin [137]	IV/I	1020	866	1.04	1.02	4.1	4.7
MCM41-hydroxyatite [138]	IV	895	649	0.7	0.64	3.1	3.95
MCM41-Ibuprofen _(25.5%) [139]	IV	1028	536	0.86	0.25	2.71	1.89
MCM41-Ibuprofen _(31.2%) [47]	IV	1072	361	0.69	0.22	2.6	1.8
SBA15-cisplatin [140]	IV	810	561	0.83	0.59	4.88	4.41
SBA15-Ibuprofen [136]	IV	787	254	1.06	0.37	8.8	7.1

Recently, STORM was employed for direct observation of nanoparticles within cells with high spatial resolution [155]. In order to characterize processes in situ, confocal laser scanning microscopy (CLSM) combined with microfluidics (MFs) was applied for monitoring of protein adsorption onto silica microparticles. The technique is based on monitoring the increase in fluorescence intensity from the adsorption of fluorescently labeled proteins onto the particles. It offers valuable information about formation kinetics and protein stability. The combination of MFs with high-speed camera imaging allowed detailed insights into very small time scales (~0.5 s) of protein corona formation [156].

Heating optical microscopy is used for the characterization of the drying behavior of droplets containing solids or solutes. The understanding of the dynamic process of drying is usually difficult but important for various nanotechnological applications, including the preparation of nanostructures. The optical microscope with a heating and vacuum stage has been used for the investigation of controlled drying of monodisperse emulsion droplets containing colloidal silica nanoparticles and their subsequent assembly into mesoporous silica microspheres (MSMs) [157].

Atomic force microscopy (AFM) is a type of scanning probe microscopy that uses a fine tip to probe surfaces and has a very high resolution. It is one of the most popular techniques for surface topography determination and nanostructures investigation. AFM can be applied to visualize almost any type of surface, constituting it as one of the most powerful microscopy tools for analyzing samples at the nanoscale. Moreover, AFM does not only provide screening of surface topography but may contribute significantly to the understanding of materials' properties in terms of mechanical, physical, thermal, and chemical features, by application of advanced tools such as phase image AFM, conductive AFM, or thermal analyses [158]. In general, three different AFM modes are used: contact mode, non-contact mode, and tapping mode. In contact mode, the tip makes direct contact with the surface of the sample. It is robust, but quite invasive and may lead to the displacement of objects on a surface, and even cause damages to the sample and the tip. In non-contact mode, an oscillating probe is moved close to the surface, and the tip never makes direct contact with the sample. This mode is usually used in (ultra) high vacuum

and can achieve very high resolutions, down to the atomic level. The tip never touches the sample and therefore cannot disturb or destroy it. Tapping mode (or intermittent contact mode) is similar to non-contact mode and uses an oscillating cantilever as well, but the tip “taps” on the surface during the oscillations. This mode is much less invasive than contact mode and can be used under atmospheric conditions. It was recently shown that the AFM technique can be applied to visualize protein aggregation at the single-molecule level [159]. Based on that, AFM images have been applied as a criterion to determine the aggregation state of xylanase before and after immobilization on organically modified MSNs, by following the heights of molecules in topographical imaging [160]. AFM imaging in the liquid phase was applied to investigate the MSNs templated self-supported HSA nanocapsules loaded with doxorubicin, revealing their shape, size, aggregation, and homogeneity [161].

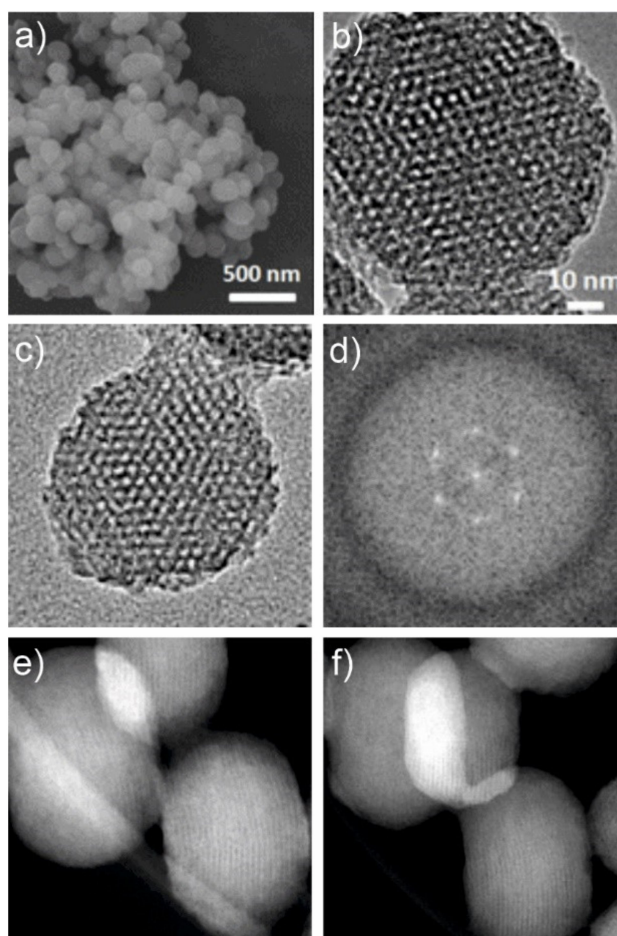


Figure 9. Characterization of hexagonal-symmetry MSNs (HMSNPs) by electron microscopy (a) SEM, (b) TEM, (c) HRTEM image, and (d) associated fast Fourier transform (FFT), (e), and (f) HAADF-STEM images obtained from different specimen orientations. Adapted from [144], Copyright 2014 SAGE Publishing.

Photoacoustic microscopy (PA) is an imaging method based on the photoacoustic effect and uses the rise of local temperature occurring as a result of light absorption in tissue. It has a wide range of applications in the biomedical field and recently has been used to follow the trafficking of nanoscale materials inside cells. The encapsulation of PA imaging agents inside functionalized MSNs has been studied to obtain the most efficient PA imaging performance [162,163]. Thus, there is a potential to use PA methodology in the future to study drug release *in vivo* relying on its co-delivery with PA imaging molecules.

Most of the microscopic techniques discussed above have also found applications in the study of the interaction of low molecular weight drugs with mesoporous silicon matrices. The literature cited here is proof of this [74,152,164].

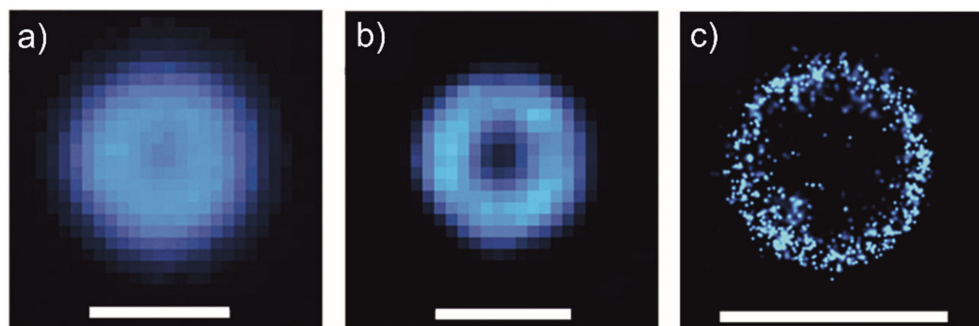


Figure 10. Microscopic analysis of protein adsorption onto 900 nm MSNs. (a) Wide-field, as acquired; (b) wide-field, deconvolved; (c) STORM. Scale bar = 1000 nm. Adapted with permission from [154], Copyright 2017 American Chemical Society.

3.4. Spectroscopy

3.4.1. Solid-State NMR

In the treatment process, most drugs are administered in the form of oral solid tablets. The action of such substances in the body, the biological activity, and bioavailability depends on the physical state of APIs (polymorphic forms, solubility) and accompanying substances (preservatives or auxiliary substances). Certainly, the study of molecular and physicochemical properties should be carried out with the use of tools that provide the broadest possible spectrum of structural information on condensed matter. Solid-state NMR (SS NMR) spectroscopy fulfills these conditions [165].

Taking into account that over 40% of drugs on the market are poorly water-soluble, which significantly limits their bioavailability, improving this parameter is extremely significant [166]. It is no wonder then that the use of mesoporous silica particles as solubilizers is of increasing importance [167–169]. From the pharmaceutical standpoint, drug-carrier interactions, amount (degree of loading), location, local molecular dynamics, and physical state of the loaded drug are important. SS NMR is a non-destructive, highly flexible technique which allows the determination of various parameters. By carrying out different experiments structural information and dynamic parameters can be obtained during one measurement session. Contrary to other techniques, SS NMR can be applied to any solid physical state (both crystalline and amorphous) and materials of different complexity, from pure APIs or excipients to solid dispersions (including commercial preparations) [165]. Moreover, the development of NMR methodology and the use of new experiments, especially fast magic angle spinning (MAS) [170–173], dynamical nuclear polarization (DNP), and surface-enhanced NMR spectroscopy (SENS) [174–176], makes the SS NMR the premier method in the study of mesoporous materials, drugs confined in nanocarriers and API-MSN interactions [170,177,178].

Since the pioneering work published by Vallett-Regi et al. [1], a lot of papers on drug encapsulation in mesoporous silicas, mainly MCM-41, SBA-15, and their various modifications appear regularly, where SS NMR is used [136,179–190]. In many of them, ibuprofen is often employed as a model molecule for the study of host-guest interactions. Ibuprofen is a common nonsteroidal anti-inflammatory drug (NSAID) that has a well-defined structure and physical properties (melting point, polymorphism, etc.). For example, Babonneau et al., presented studies of ibuprofen encapsulated into MCM-41 and MCM-41 functionalized by amino groups [179]. Using single pulse (SP) and cross-polarization (CP) ^{13}C MAS NMR techniques, as well as ^1H MAS NMR experiments, they showed extremely high mobility of ibuprofen molecules when the silica was not functionalized. In contrast, when the MCM-41- NH_2 silica matrix was used, the ^{13}C NMR experiment indicated more limited mobility

of ibuprofen, which confirmed interactions between silica amine groups and carboxyl groups from drug molecules. A more advanced and complete SS NMR study of ibuprofen encapsulated in MCM-41 silica with different pore diameters (35 Å and 116 Å) was presented by Azais et al. [180]. Its behavior was investigated using ^1H , ^{13}C , ^{29}Si multinuclear SS NMR experiments at ambient and low temperatures. They demonstrated that ibuprofen was extremely mobile and behaved like a liquid inside the pores at ambient temperature. This unexpected physical state of the encapsulated molecules in mesoporous silica was explained by the existence of the confinement effect [128,183,191–193], which was often studied on simple liquids such as water [194,195], methanol [196,197], or benzene [198–200]. The ^1H – ^{13}C and ^1H – ^{29}Si heteronuclear correlation (HETCOR) experiments proved that there was a weak interaction between the drug and the silica, which favors fast drug release from this material in simulated biological fluids. Moreover, the SS NMR study showed that the carboxylic proton of the ibuprofen was in a chemical exchange at room temperature with other protons, possibly from silica walls (SiOH) and/or water [180]. In the latter paper, the same group demonstrated examining ibuprofen and benzoic acid encapsulated in MCM-41 through incipient wetness impregnation method using variable temperature ^1H MAS NMR experiments [181]. The authors confirmed the presence of water molecules inside the pores of silica and their participation in the fast chemical exchange with protons of the COOH group of organic molecules at room temperature. Additionally, a study by Tielens et al., combining SS NMR with molecular dynamics calculations, proved that the presence of a monolayer of water surface molecules on silica plays the role of a “glue” permitting high mobility of ibuprofen and benzoic acid molecules [201]. In another study conducted for the ibuprofen/MCM-41 system, comparing the effectiveness of incipient wetness impregnation and melting methods by analysis of the filling factors, it has been shown that the affinity of ethanol used in the impregnation process for mesoporous silica significantly decreased this parameter [83]. The percentage of filled mesopores was determined by analysis of ^1H Very Fast (VF) MAS NMR spectra recorded at a spinning rate of 60 kHz. The obtained results presented on the performance profiles of both procedures showed that the filling factor for the melting method was much higher compared to incipient wetness impregnation and obtained at 60% and 20%, respectively (Figure 11). Moreover, the stability of the ibuprofen/MCM-41 sample prepared by the melting method in the environment of ethanol and water vapor was investigated. Using advanced SS NMR experiments it has been confirmed that ethanol vapor can remove ibuprofen from MCM-41 pores. When the sample was stored in a closed vessel filled with ethanol vapor for several hours, the ibuprofen was transported to the external walls of the silica. The action of water vapor was very similar, but the penetration of water into the pores and the exchange of ibuprofen were slower compared to the analogous procedure using ethanol. This study demonstrated that both solvents acted like “molecular pistons” pushing ibuprofen from the pores [83].

The structural and dynamic properties of indomethacin molecules embedded within the mesopores of SBA-15 and SBA-15 functionalized with 3-aminopropyltriethoxysilane (APTES) using ^1H , ^{13}C , ^{29}Si MAS NMR spectroscopy, and ^1H NMR spin-lattice relaxation measurements were investigated by Ukmar et al. [182]. The conducted studies showed that only when the concentration of indomethacin within the mesopores was high the hydrogen bonds between drug molecules were responsible for dimer formation, while at low concentrations indomethacin formed a layer on the silicate walls. Moreover, 2D NMR correlations revealed that the interaction between the indomethacin molecules and the silicate surface was moderate to weak. When indomethacin was incorporated into the functionalized SBA-15 matrix, drug-matrix interactions were enhanced. Skorupska et al. used advanced SS MAS experiments to analyze other systems of pharmaceutical co-crystal loaded into mesoporous silica [202,203]. The authors used very fast MAS NMR, ^1H detected ^1H – ^{13}C HETCOR and ^1H – ^{15}N HETCOR 2D correlations measurements, in combination with 2D ^1H – ^1H BaBa to characterize the loading process of naproxen/picolinamide and ibuprofen/nicotinamide co-crystals to SBA-15 and/or MCM-41 mesopores and their interactions.

Lately, co-crystals have become very popular among scientists and the pharmaceutical industry [204–206], and the issue of co-crystal embedded in MSN has not been described in the literature until 2015.

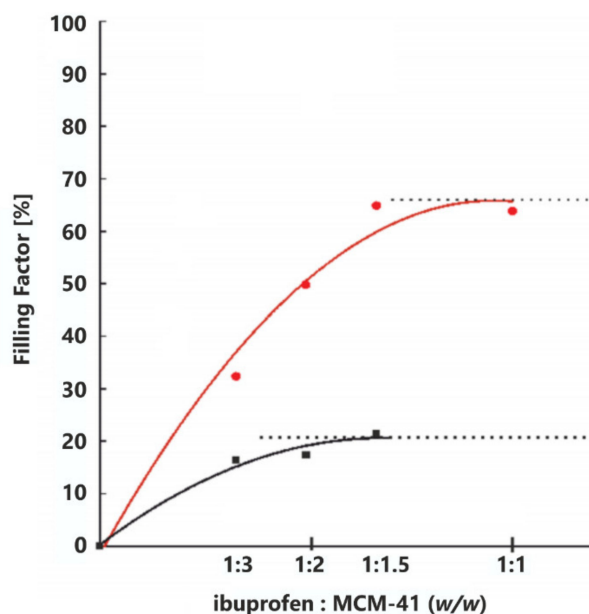


Figure 11. Comparison of the filling factors for the incipient wetness impregnation (black squares) and melting (red circles) methods. Values on the horizontal axes represent the weight ratio of ibuprofen: MCM-41 used for impregnation and melting. Adapted with permission from [83], Copyright 2014 American Chemical Society.

Very recently, the applicability of the new DiSupLo loading method employing selected APIs—ibuprofen, ketoprofen, flurbiprofen, and MCM-41 mesoporous silica, was confirmed by Potrzebowski et al. using advanced SS NMR experiments [47]. The ^1H NMR spectra recorded with sample spinning of 60 kHz, ^{13}C CP-MAS, ^{13}C single pulse experiment (SPE) and 2D correlations ^1H – ^1H RFDR (Frequency Driven Dipolar Recoupling) MAS, ^1H – ^{13}C invHETCOR, ^1H – ^{13}C HSQC High Resolution (HR) MAS were applied to analyze the loading process and APIs interactions inside the pores. The ^{13}C MAS spectra showed that APIs were located inside the MCM-41 pores when the weight ratio of API to MCM-41 was 1:3 and 1:2. The efficiency of CP significantly decreased due to the high mobility of drug molecules entrapped in the silica matrix, therefore SPE was appropriate. When the API/MCM-41 ratio was changed to 1:1, the CP-MAS spectra showed additional signals indicating the position of the API both inside and outside the MCM-41 pores. The ^{13}C NMR and ^1H VF MAS spectra were compatible. The peak of the acidic proton of API was not visible in the ^1H VF NMR spectra when the whole drug was in the pores. The acid hydrogen of API located in the pores is involved in the interaction with oxygen and MCM-41 hydroxyl groups, forming new C–O–H ... O–Si hydrogen bonds. The transfer of API carboxylic proton on the MCM-41 walls was confirmed by comparing the chemical shifts of ^{13}C and ^1H for the crystalline and loaded ibuprofen taken from the 2D ^1H – ^{13}C invHETCOR (Figure 12). The comparison showed that the downfield shift of the methine proton signal was the effect of carboxyl proton transfer and can be considered a measure of the efficiency of the API loading process. Moreover, it has been proven that the DiSupLo method allows quantitatively loading a mixture of two or three APIs into the pores of MCM-41 [47].

Progress in solid-state NMR studies of drugs confined within different drug delivery systems has been presented by Skorupska et al. [207]. Recently, Potrzebowski et al. have presented the use of SS NMR to study pharmaceuticals also API loaded into mesoporous DDS, extensively discussed modern NMR techniques that are used in structural research

of pharmaceutical products, including techniques using fast and very fast magical angle spinning with sample rotation over 40 kHz [208]. Li et al. reviewed the advancement and application of SS NMR in pharmaceutical sciences to overcome challenges in material characterizations [209].

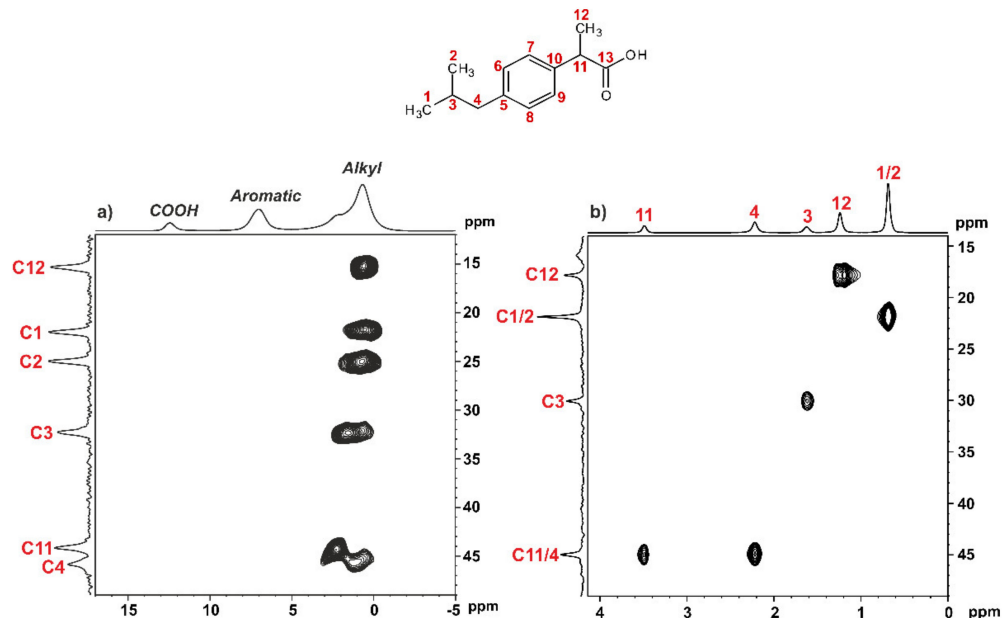


Figure 12. (a) ^1H - ^{13}C Inv-HETCOR NMR spectrum of Ibu recorded with a spinning rate of 60 kHz with contact time 2 ms; (b) ^1H - ^{13}C HSQC HR-MAS NMR spectrum of physical mixture of Ibu/MCM-41 in a weight ratio of 1:3 after DiSupLo and after removed ethanol. Adapted with permission from [47], Copyright 2020 Elsevier.

3.4.2. Vibrational Spectroscopy

Vibration spectroscopy techniques such as infrared and Raman spectroscopy compared to other methods discussed in previous sections offer specific advantages in a variety of applications. Even though both techniques are completely different from each other, they work in a complementary way. It is worth emphasizing that these two spectroscopies do not probe the same vibrational information of the molecule. Raman spectroscopy is based on an inelastic scattering process and detects vibrations related to a change in polarizability, while infrared spectroscopy is based on an absorption process and detects vibrations related to a change in dipole moment. As a result, the two spectroscopies have different selection rules and it is possible that a strong vibration mode in the Raman spectrum may be weak in the IR spectrum or not be visible, and vice versa. Moreover, in Raman spectroscopy, a compound can be tested in an aqueous solution, while in infrared spectroscopy it is a serious limitation due to the excessive adsorption of water. Infrared and Raman spectrometers are divided into two categories: dispersion and Fourier transform.

Infrared (IR) spectroscopy is a non-destructive, easy-to-use universal research tool for examining the chemical status of porous silica surfaces. The convenience of this method is due to the transparency of silicon for infrared light. The basis of the IR analysis of mesoporous silica is the knowledge of the position of the absorption bands of Si-O bonds. The silica matrix is reflected in the IR spectra by (a) bands of stretching vibrations in the range of $3700\text{--}3400\text{ cm}^{-1}$ isolated hydroxyl groups (sharp band shape) and/or derived of absorbed water (broadly absorbing band, confirmed by a strain band at 1620 cm^{-1}), (b) most strongly absorbing bands of Si-O-Si stretching vibrations observed at $1200\text{--}1000\text{ cm}^{-1}$ (asymmetric Si-O-Si stretch), (c) multiple absorption bands below 1000 cm^{-1} characterizing, for example, symmetrical Si-O-Si stretching vibrations (at 790 cm^{-1}), Si-O-Si bending vibrations (at 460 cm^{-1}) [210–212]. In recent years, infrared spectroscopy has become an

indispensable technique for pharmaceutical analysis. The infrared spectrum represents absorption and molecular transmission, creating a molecular fingerprint. The material is a unique combination of atoms, and no two compounds produce the same infrared spectrum. Changes in the frequency and shape of the drug bands in the IR spectrum can be used to analyze the electron density redistribution in the structure of the molecule to evaluate interactions [213]. The dynamic development of instruments and the use of the Fourier transform in the analysis of the recorded signal allowed for a significant reduction in the measurement time of a single IR spectrum and the development of FT-IR spectroscopy (infrared spectroscopy with Fourier transform spectroscopy). This technique is currently the most widely used to characterize the surface chemistry of mesoporous silica, both with surface modified [214,215] and drug-loaded. Changes in the appearance of functional groups on the FT-IR spectrum of mesoporous silica and drugs illustrate the structural changes that occur during the loading process and the interactions that occur between the studied systems. If the drug interacts with mesoporous silica, the drug band becomes smaller or less sharp compared to the pure drug spectrum. In other words, a reduction in the intensity of the drug functional group bands loaded into the mesoporous system indicates a strong molecular interaction between the drug and silica. In the case of physical interaction, distinct drug and silica bands appearing in the spectrum indicate that the drug has been adsorbed on the outer surface [7]. Most used in research study model drug—ibuprofen in the FT-IR spectrum shows a characteristic intense band at 1711 cm^{-1} for the stretching vibrations of the carbonyl group (C=O) and three bands in the range of $3300\text{--}2800\text{ cm}^{-1}$ corresponding to the stretching vibrations of the benzene ring (C–H), Figure 13 [47,216].

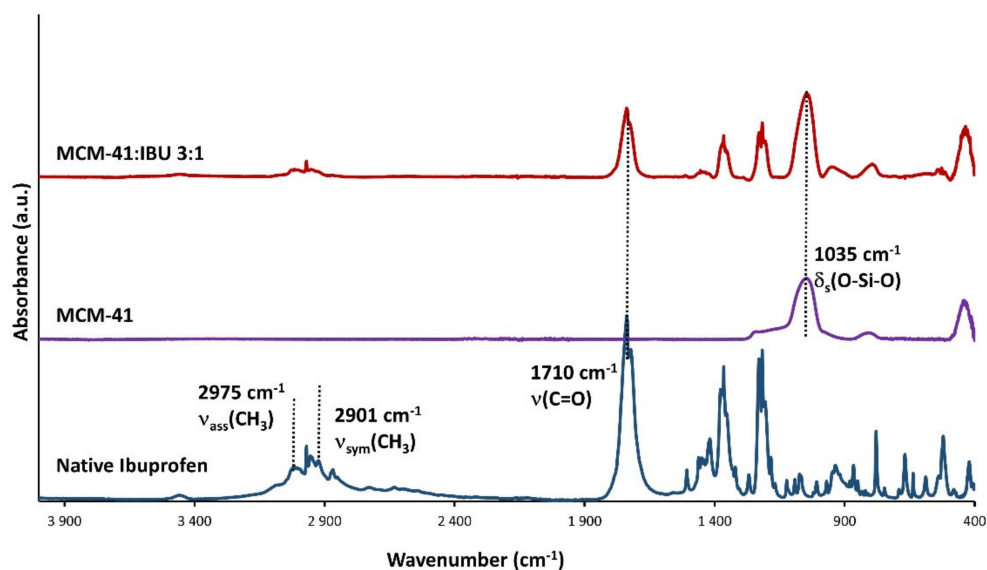


Figure 13. FTIR spectra for unloaded MCM-41, composite MCM-41:IBU 3:1, and native ibuprofen. Data provided courtesy of Katarzyna Trzeciak.

Li et al. investigated the effect of ibuprofen at various concentrations on the surface of two disordered mesoporous materials: Syloid 244FP and Neusilin NS2. In the FT-IR S244FP and ibuprofen spectra, all tested drug to silica ratios show bands characteristic of pure substances, which proves the physical adsorption of ibuprofen on the outer surface of mesoporous silica. In turn, in the samples of ibuprofen loaded into NS2, the carbonyl group was reduced to 1591 cm^{-1} , which indicates strong intermolecular interactions of IBU: NS2 [217]. In the discussed case, the carbonyl group reacted with the OH group of MgO and Al₂O₃ groups located on the surface of the pores of NS2, forming salts. On the other hand, SiO₂ groups of silica did not participate in the reaction, so the bands characteristic for this group at $1300\text{--}900\text{ cm}^{-1}$ and $3700\text{--}3000\text{ cm}^{-1}$ did not change in the

FTIR spectrum. Tzankov and co-workers presented the encapsulation of pramipexol in MCM-41 mesoporous silica particles. The FTIR spectrum of empty MCM-41 showed a band at 1047 cm^{-1} corresponding to the Si–O–Si stretch vibration. The spectrum of the pure drug showed absorption bands at 3410 cm^{-1} (N–H stretching vibration), 2945 cm^{-1} (C–H stretching vibration), 1586 cm^{-1} (C=C stretching vibration), 1309 cm^{-1} (C–N stretching vibration), and 760 cm^{-1} (C–H bending vibration). On the other hand, the FTIR spectrum of particles loaded with pramipexol revealed bands at 1520 cm^{-1} characteristic of secondary amines and bands of 1585 and 1633 cm^{-1} for primary amines. The spectrum also shows the 2972 cm^{-1} band, indicating the presence of the NH_3^+ group and indicating interaction with silanol groups of the silica [218].

Raman spectroscopy of porous silica can provide valuable information on the properties of silicon nanostructures, which are strongly dependent on symmetry, structural geometry, morphology, pore diameter, backbone size, etc. The first-order phonon entrapment model of optical phonons at 521 cm^{-1} (calibration of spectrometer) is often used for shape analysis. Raman scattering of the porous silicon bands, thereby determining the size of the crystallites embedded in the porous layer. The nano-sized particles also exhibit low-frequency acoustic vibrations, which can be observed by Raman spectroscopy. Pure MCM-41 on the Raman spectrum has characteristic bands at about 918 , 542 , and 126 cm^{-1} assigned to Si–OH, six or four-membered ring vibration, and bending mode of Si–O–Si vibrations, respectively [219]. Using UV resonance Raman spectroscopy, it was estimated that sample MCM-41 showed four weak bands at 499 , 595 , 798 , and 982 cm^{-1} . The 499 and 595 cm^{-1} bands are assigned to the asymmetric and symmetrical ascending vibrations of the Si–O–Si bond, respectively, and the 798 cm^{-1} bands are assigned to the vibrational mode of the siloxane bond. The 982 cm^{-1} band is related to the Si–O–Si bond which is directly related to the skeleton defects. In the case of surface modification of MCM-41 with sulfated zirconium, an increase in the intensity of this band was found [220]. Similar relationships were shown in the study of the mesoporous SBA-15 surface loaded with vanadium [221]. The much higher sensitivity of Raman spectroscopy compared to IR for groups such as the thiol group made this spectroscopy the basis for determining the cisplatin loading of mesoporous silica modified with SH groups [222]. Bouyer et al. observed vibration bands of tetracyclosiloxane rings— 486 cm^{-1} , symmetric stretching bands from the Si–O–Si group— 800 cm^{-1} , and vibrations related to the stretching mode of Si–OH hydroxyl surfaces— 978 cm^{-1} for both MSN–SH and MSN. In addition, the band assigned to the S–H binding at 2581 cm^{-1} was identified in the MSN–SH spectrum. In turn, pure cisplatin on the Raman spectrum shows four characteristic bands attributed to the deformation of the skeleton in the bond plane: a. Cl–Pt–Cl (162 cm^{-1}), b. N–Pt–N (255 cm^{-1}), c. Pt–Cl (322 cm^{-1}) and a band in the Pt–N stretching mode (524 cm^{-1}). In the mesoporous silica-drug system, pure cisplatin bands are not revealed, which confirms the presence of the drug in the pores of the silica. On the other hand, a wide band of vibrations was observed at 310 cm^{-1} , which corresponds to the Pt–S stretching mode and confirms the coordination of cisplatin by thiol groups, Figure 14.

The introduction of the poorly soluble drug indomethacin into mesoporous silica MCM-41 and SBA-15 first using imaging by Raman spectroscopy was discussed by Hellstem et al. [223]. Raman imaging is particularly useful in the pharmaceutical industry because determines the spatial distribution of compounds in a sample and is sensitive to the crystallinity and polymorphism of compounds. The study of polymorphism is especially important because it relates directly to the stability and safety of the drugs [224]. The Raman spectra of solid indomethacin forms present in the silica particles are shown in Figure 15. The characteristic band for α -indomethacin loaded silica occurs at the wavenumber of 1650 cm^{-1} and for γ -polymorph at 1699 cm^{-1} . The spectrum of amorphous indomethacin has a broad band around 1681 cm^{-1} . As shown in Figure 15, the bands of these three forms partially overlap, which makes the spectra interpretation more demanding. The authors used a partial least-squares analysis of the Raman spectra, thus determining the solid form of the loaded drug. Figure 15 presents the uniform distribution of the two indomethacin

alpha and gamma polymorphs in the carriers, while the increase in temperature and humidity leads to the formation of clusters with higher crystallinity.

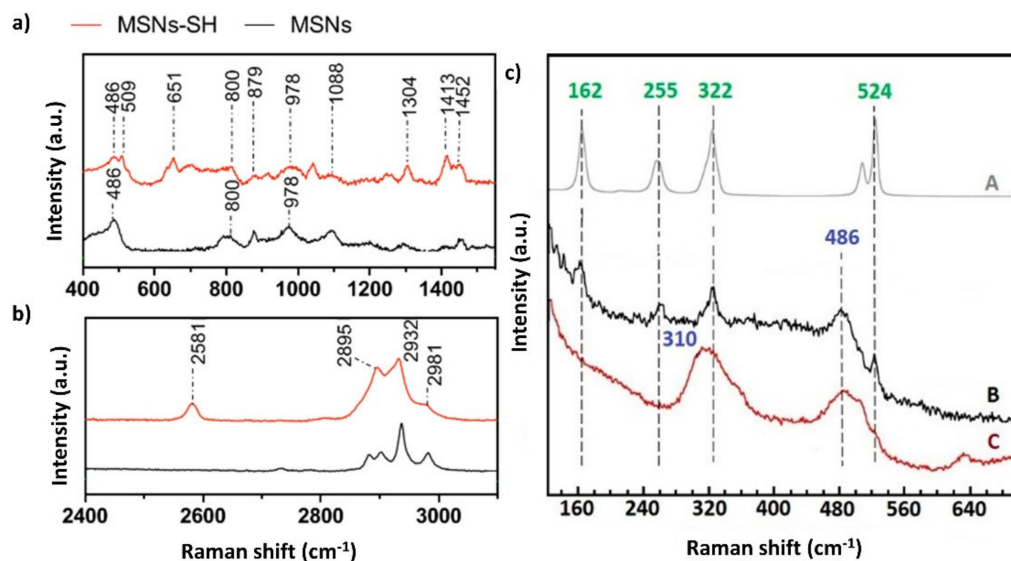


Figure 14. (a) Raman spectra of mesoporous silica pristine MSN (black line), mesoporous silica modified with SH group MSN-SH (red line) in the range 400–1500 cm⁻¹, (b) Raman spectra of mesoporous silica pristine MSN (black line), mesoporous silica modified with SH group MSN-SH (red line) in the range 2400–3100 cm⁻¹, (c) Raman spectra cisplatin A (grey line), cisplatin:MSN B (black line), cisplatin:MSN-SH C (red line). Adapted with permission from [222], Copyright 2019 American Chemical Society.

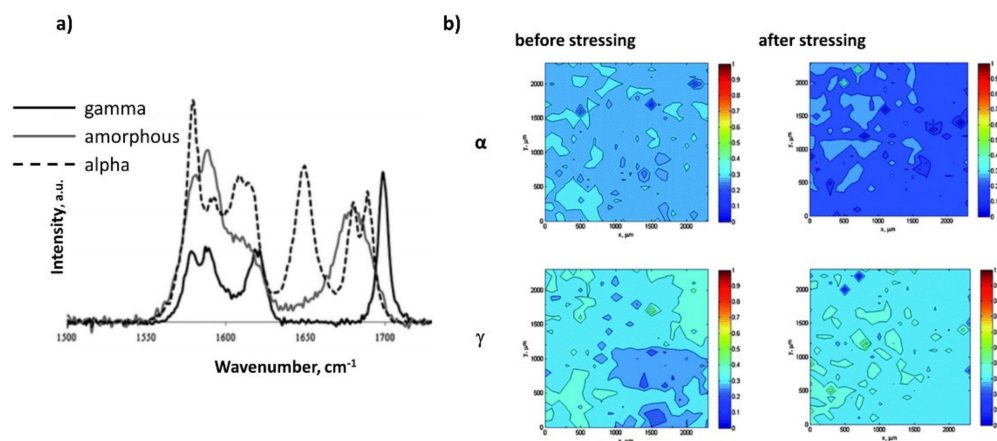


Figure 15. (a) Raman spectra of alpha and gamma and amorphous indomethacin; (b) distribution of crystalline indomethacin alpha and beta loaded in SBA-15 and the effect of stressing it at high temperature and humidity as the results of PLS analysis at each measurement point of the Raman mapping. Adapted with permission from [223], Copyright 2011 Elsevier.

Despite the problems encountered during the analysis: fluorescence and combustion of the samples, this study provided useful information on drug distribution and the presence of unexpected solids such as solvates or rare polymorphs of the model drug.

The combination of Raman scattering anti-Stokes microscopy (CARS) with CARS hyperspectral analysis is a powerful tool capable of selectively imaging drugs incorporated into mesoporous silica-based materials. The CARS variant microscopy was used for the first time by Offerhaus et al. [223–225] to observe differences in the distribution of drugs

(itraconazole and griseofulvin) and the physicochemical structure of ordered mesoporous silica particles.

3.5. Powder X-ray Diffraction (PXRD) and Small-Angle X-ray Scattering (SAXS)

In order to understand the structural characterization of nanocarriers different X-ray scattering techniques might be applied revealing information about their crystal structure, chemical composition, and physical properties. It is especially important for the development of drug delivery systems, where there is a strong structure-function correlation.

In powder X-ray diffraction (PXRD) the pattern is obtained from a bulk matter, rather than an individual crystal as happens in the case of single-crystal X-ray diffraction. Not only each API will produce a specific pattern depending on the structure of its crystal lattice but even each polymorph, salt, or co-crystalline material will have its characteristic diffractogram. PXRD can be used to determine if any change in drug form has occurred during the loading process [226]. The absence of crystalline peaks with sufficient quantity indicates that the material is amorphous. For example, it was shown by a combination of DSC and PXRD that mesopores change the insoluble crystalline form of angiotensin II receptor blocker called valsartan to a soluble amorphous state [227]. Similarly, the PXRD patterns of untreated drugs: ibuprofen, ketoprofen, and flurbiprofen have shown their crystalline structure, while the absence of APIs peaks in the drug-loaded MCM-41 diffractograms indicates that the drugs are loaded inside the pores of the carriers and that they are amorphous (Figure 16) [47].

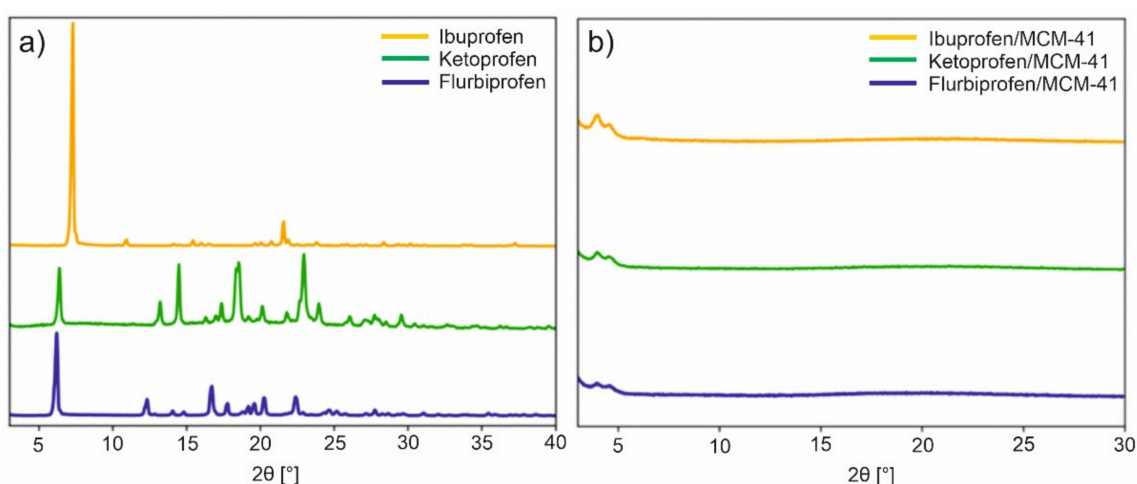


Figure 16. PXRD diffractograms of (a) untreated ibuprofen, ketoprofen, and flurbiprofen, and (b) 1:3 drug-loaded MCM-41. Adapted with permission from [47], Copyright 2020 Elsevier.

PXRD is widely used for the MSNs characterization and there are many recent literature examples for its application. For example, to determine the crystalline structure of the magnetic nanoparticles before and after silica coating [228], or to confirm the presence of iron oxide and identify the relative crystalline phases formed in the synthesis of polymer grafted MSNs [229]. Further cases show the loading of indomethacin in an amorphous phase [230], and characterization of the mercapto-functionalized MCM-41 proving their stability after the modification process [222]. Importantly, one has to realize that the data provided by XRD experiments arises from the structural properties of crystal domains and not necessarily from the entire particle. Thus, when analyzing particle sizes, the use of different methods, such as microscopy, is necessary to obtain reliable information.

Small-angle X-ray scattering (SAXS) provides information about the structural characteristics of nanomaterials. It determines nanoparticle size distributions, resolves the size and shape of macromolecules, verifies pore sizes, etc. For successful application of SAXS, the prior study of the sample preparation method, particle morphology, size distribution,

aging stability, etc., is required via other approaches, such as electron microscopy, dynamic light scattering, and zeta potential. SAXS has been applied, for example, in the characterization of the amino-functionalized mesoporous silica nanoparticles that display the typical pattern of hexagonal mesoporous structures, with an intense peak, due to the reflection of 1 0 plane, and two weak peaks due to the reflection of 1 1 and 2 0 planes, respectively. The value of lattice parameter, a , has been obtained as well [231]. SAXS analysis supported characterization of modified and unmodified silica nanoparticles, before and after loading with naproxen. Three resolved reflections were attributed to the well-defined mesoporous structure with two-dimensional hexagonal $p6mm$ symmetry, while the samples with larger heterogeneity of the surface exhibited lower scattering power [15]. It was applied also in some other recent drug loading studies [184,232], and to characterize in detail the inner structures of MSNs, providing information about their homogeneity, average mass density of spheres, and the volume fraction of silica [233]. It is worth mentioning that SAXS is also a widely used method for MSNs preparation. For the first time, the growth and kinetics of MSNs were investigated by time-resolved SAXS with synchrotron irradiation [234]. Nucleation and growth of SBA-15 silica particles have also been studied by SAXS and USAXS (ultras-small-angle X-ray scattering). In comparison to SAXS that measures sizes related to the micelles and mesoscopic ordering, USAXS probes length scales up to a few micrometers. Thus, the combination of both methods gives information on all length scales associated with the system [235]. Moreover, wide-angle X-ray scattering (WAXS) might be occasionally applied to characterize the amorphous structure of synthesized MSNs [236].

3.6. Chromatography

High performance liquid chromatography (HPLC) is used to separate, identify, and quantify different mixture components, and it is applied to confirm the chemical stability of the molecules loaded into nanoparticles [237,238], entrapment efficiency [239,240], and to obtain the drug release curves, as demonstrated in the release studies of naproxen [15], paclitaxel [87], resveratrol [241], felodipine and furosemide [17], and many others. For the determination of drug loading efficiency, after the completion of the loading process, samples undergo centrifugation and the unloaded molecules present in the supernatant are analyzed by HPLC, as was shown in the case of rifampin [242].

3.7. Mass Spectrometry

Secondary ion mass spectrometry with a time-of-flight analyzer (ToF-SIMS) is a destructive and extremely sensitive technique for analyzing the surface composition and depth profiling of organic and inorganic materials. The test method consists of etching the surface of the sample by bombarding with a beam of primary ions (Cs or micro-focused Ga), and then by carrying out a mass analysis of the ionized matter, information on the elemental composition of the tested sample is obtained [243]. Along with the etching of successive layers of the material, information is obtained regarding the change in the composition of the sample as a function of depth (the so-called deep profile). TOF-SIMS analysis provides information in the sample about 1–1.5 μm area, with high mass resolution up to 10,000 $m/\Delta m$ and spatial resolution for 1-micron imaging. Thanks to it, it is possible to determine the levels of admixtures, assess the stability of layers, determine diffusion parameters and describe other phenomena occurring during the production and processing of samples [244]. Kempson et al. [245] used TOF-SIMS to map the distribution of methylene blue and papain in silicon layers. Methylene blue was used as a small molecule drug simulant. The mass of the dye—284 g/mol is within the range of primary masses of the Ga TOF SIMS ion beam and can be easily and unambiguously identified. Papain represented the larger molecules of pharmaceutical importance. It contains 212 amino acid units and forms two domains. Due to its high molecular weight of 23,406 g/mol, only fragmentation products can be detected in TOF-SIMS. Smaller organic papain fragments were compared to the methylene blue decomposition to investigate similarities and differences in loading. Secondary ion mass spectrometry revealed evidence of Si–O, Si–C bonding, it also showed decomposition

of organic matter after deposition and loading behavior, literally observing where the organic molecules were. Porous structures are a good medium for loading small and large organic molecules. Load dynamics can be studied as a function of time, concentration, and pore structure. Additionally, detecting organic, inorganic, and molecular fragments from TOF-SIMS, together with complementary data obtained from other spectroscopy, can help better understand the chemical mechanisms of adsorption (Figure 17).

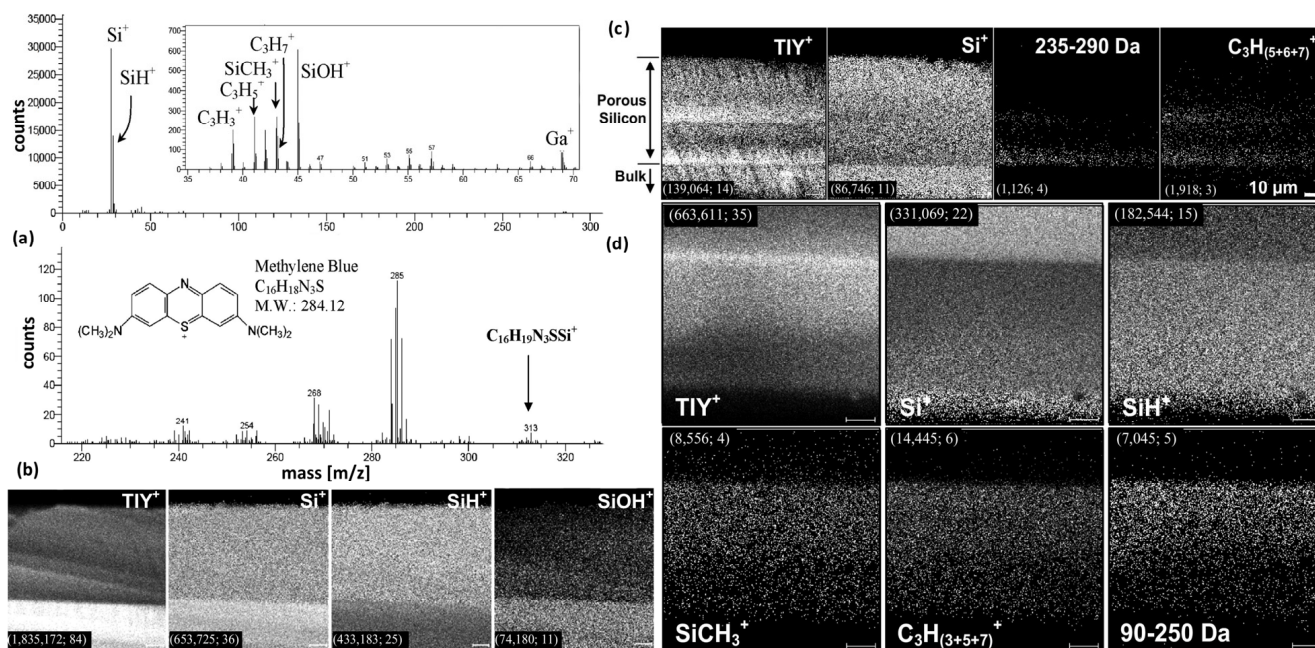


Figure 17. (a) and (b) Positive TOF-SIMS images of the porous region of a “blank” porous silicon, (a) and (c) methylene blue, and (d) papain loaded wafer. Adapted with permission from [245], Copyright 2009 Elsevier.

3.8. Other Methods

Dynamic Light Scattering (DLS) provides information about the size distribution of particles and populations of particles and gives insights into the system’s agglomeration. The main weakness of the method lies in its low resolution and inability to handle highly concentrated samples. Moreover, DLS works only on optically clear particle suspension based on the known or well characterized kinematic viscosity of the solvent. In few MSNs studies, hydrodynamic diameters of the nanoparticles were determined by DLS to show both frequency distribution and cumulative particle-size distribution [228] and mean hydrodynamic diameter [246]. DLS together with static light scattering (SLS) has been applied to characterize size, stability, and porosity of porous silicon and silica nanoparticles [247].

Zeta-potential (ZP) measures the electrostatic or charge repulsion or attraction between nanoparticles and can be applied to study the colloid stability and surface charge. The electrophoretic mobility of the particles in drug delivery studies is mostly measured by electrophoretic light scattering. The literature often states NP-dispersions with ZP values of ± 0 –10 mV, ± 10 –20 mV and ± 20 –30 mV and $> \pm 30$ mV as highly unstable, relatively stable, moderately stable and highly stable, respectively [248]. However, the results are not straightforward, and it is possible to have stable colloids with low ZP and vice versa. Moreover, it is important to report all the information about the measurement conditions including the medium ionic strength, composition, and pH, since they considerably influence the zeta potential. The surface charge measurements are determined by identifying which electrode the particles are moving towards during electrophoresis [249]. The method is widely used in the preparation of MSNs to ensure stability, the success of modification, and lack of aggregation [228,246,250].

Contact angle measurement gives the angle between a solid surface and a droplet of liquid on the surface, providing information about the wettability of a solid by a liquid. In the case of complete wetting, the contact angle is 0° . The solid is wettable in the range between 0° and 90° , and not wettable above 90° . In the case of ultra-hydrophobic materials, the contact angle approaches the theoretical limit of 180° . Hence, it provides information about the wettability of silica. Contact angles of the silica particle samples were determined from capillary penetration [251]. The method was used for example in the research about the impact of surface hydrophilicity and pore size on water uptake by mesoporous silica [252], to study superhydrophobic MSNs for doxorubicin delivery [253], and to measure the wettability of ciprofloxacin-loaded MCM-based solid films [254].

Elemental analysis (CHNS analysis) provides information about the elemental and sometimes isotopic composition of the sample and is applicable to study the chemical modification of surfaces, thus allowing insights into verification of the functionalization process [255].

Gas pycnometry is used for measuring the density of the sample, obtained by calculation of the ratio of mass to volume. The method has been applied to determine the amorphous densities of the model drugs and used to calculate the loading capacities of mesoporous silica [129].

Isothermal titration calorimetry (ITC) is a technique commonly used to determine the binding affinity and thermodynamics of biomolecules interactions. ITC measures directly the heat released or absorbed during a binding, simultaneously providing information about a range of binding parameters such as entropy, enthalpy, the equilibrium constants, etc. It is relevant in some studies, involving nucleic acid incorporation into MSNs, to determine the nature of DNA or RNA interaction with the silica [256,257].

Vibration Sample Magnetometry (VSM) is applied to test the magnetic properties of samples. It is occasionally used in MSNs studies, in the cases of nanoparticles with magnetic properties. It has been applied to obtain the magnetization curves of mesoporous silica hybrid nanoparticles with superparamagnetic features [228].

4. Conclusions and Future Perspectives

The application of nanotechnology-enabled drug delivery systems has gained increasing interest over the past few decades and is emerging as one of the key areas for future developments in pharmaceuticals. MSNs are one of the most well-studied inorganic nanoparticles for biomedical applications, due to their high drug-loading capacity, tunable size, and high pore volume. They have a great potential to enhance important drug properties, such as solubility, stability, bio-availability, and controlled release. Moreover, they can be easily functionalized, opening an even wider range of potential applications.

In comparison to the MSNs, non-ordered porous silicas, do not have a uniform and narrow pore size distribution, but disordered pore structures. Different types of them have been explored previously, due to the simpler and inexpensive preparation methods [258]. Lately, the interest in the non-ordered silica materials has re-emerged and there are some recent examples of their application in the DDS, for example, different types of Syloid[®] particles were used as API carriers [7,62,259,260]. Studies focusing on the other silica materials, such as silica xerogels [261,262], silica aerogels [263–266], silica nanocomposites [267–269], etc. have also been published. Non-ordered silicas seem to be an attractive alternative as drug carrier candidates, nonetheless due to the lack of precise control of their critical parameters, they are less favorable for pharmaceutical applications.

Many methods to load drugs onto mesoporous silica have been developed over the years. The choice of the loading process is one of the most crucial steps in the design of the drug delivery platform since it influences the amount of incorporated drugs, their physicochemical properties, distribution, and availability. Even though there are several excellent techniques available, they all display some disadvantages. Solvent-free methods are relatively fast and enable a quite high drug loading, but on the other hand, they exhibit limited penetration of cargo inside the pores, negatively impacting the amount

of drug present. In comparison, the organic solvent methods provide much better drug penetration but are very time-consuming and contribute to the loss of a significant part of the drug due to the filtration step [18]. The solubility of API in a pharmaceutically appropriate solvent also limits the efficiency of ‘wet’ methods. Worthy of mention are novel procedures combining the benefits of both groups, such as DiSupLo, based on the API embodiment into mesopores by organic solvent vapors. It is easy, efficient, environmentally friendly, and does not require any special equipment and/or demanding experimental conditions [47]. Another interesting example is co-spray drying, based on the two-step process: the creation of the initial suspension, followed by the diffusion of the drug into the pores. The method is relatively fast and allows easy separation of the loaded product from the solvent [184]. The sol-gel approach allows a simultaneous synthesis of MSNs and their loading with an amphiphilic biologically active compound that works as a template. It was developed for miramistin but might be easily extended by using micelles or vesicles of other active compounds, providing a very effective one-stage production of loaded particles [270]. Unfortunately, even though the above mentioned loading methods are sufficient for laboratory purposes, there is a need to focus on the development of the scale-up processes for simplified and cost-effective commercial manufacturing. It is also important to remember that for future clinical success the loading method needs to provide a homogeneous distribution of incorporated APIs with very high reproducibility.

Advancement in the production of novel specialized MSNs, particularly for drug delivery purposes, demands progress in analytical techniques suited for their characterization. Such methods require extreme sensitivity, precision, and often resolution on the atomic level. There is no one technique sufficient for the complete characterization of particles-based systems and a combination of methods needs to be applied to obtain satisfactory information. Thus, the development of new analytical instruments combining different instrumental techniques into one piece of equipment may provide reliable results in a shorter time resulting in faster and more efficient work. Accurate and non-destructive methods for the quantification of embodied drugs are still in need of further improvement.

The translation of MSNs laboratory results to human clinical trials is still limited, mostly due to the issues with a precise characterization of nanosystems *in vivo*. Therefore, one of the most important future trends will be novel developments toward nanomaterial characterization in physiological conditions, in order to follow the fate of both carriers and drugs upon their administration into the body. There are many established analytical tools sufficient for the stage of discovery and development, but for the following phases of preclinical and clinical research, they are often uninformative, too invasive, and require laborious and complex data analysis. The product development needs to address those limitations and find methodologies to predict the clinical outcomes of nanoparticle therapy with reliability and accuracy. Some of the other remaining challenges in this area include the design of new cell and animal models of human diseases, labeling and detection methods, mathematical modeling, and computational simulations.

Despite various obstacles, the progress in the field in the last decade demonstrates growing hope for new silica-based drug delivery methods with considerable market potential. Some of the most promising examples come from the currently ongoing or just concluded clinical trials. Mesoporous silica was shown to be safe in a dose up to 9 g/day in male humans according to completed Phase I and Phase II trials [271]. Cornell dots, ultrasmall inorganic optical-PET imaging nanoparticles [272–274] were approved for three different human clinical trials for diagnostic purposes that are currently active or recruiting. Above all, we believe that the outstanding potential of MSNs can soon be explored further, taking into account the possibility to load or functionalize them with combinations of molecules to design multifunctional stimuli-responsive drug delivery platforms enabling simultaneous diagnosis and targeted treatment.

Author Contributions: Conceptualization, writing—original draft preparation, writing—review and editing, visualization, K.T., A.C.-O., I.I.B.-S. and M.J.P.; supervision, M.J.P. All authors have read and agreed to the published version of the manuscript.

Funding: This research was funded by the NATIONAL SCIENCE CENTRE OF POLAND, grant number 2018/31B/ST4/01973, Regional Operational Program of the Lodz Region RPLD.01.01.00-10-0008/18.

Institutional Review Board Statement: Not applicable.

Informed Consent Statement: Not applicable.

Data Availability Statement: No new data were created or analyzed in this study. Data sharing is not applicable to this article.

Conflicts of Interest: The authors declare no conflict of interest.

References

1. Vallet-Regi, M.; Ramila, A.; del Real, R.P.; Perez-Pariente, J. A new property of MCM-41: Drug delivery system. *Chem. Mater.* **2001**, *13*, 308–311. [[CrossRef](#)]
2. Garcia-Bennett, A.E. Synthesis, toxicology and potential of ordered mesoporous materials in nanomedicine. *Nanomedicine* **2011**, *6*, 867–877. [[CrossRef](#)]
3. Liu, T.L.; Li, L.L.; Teng, X.; Huang, X.L.; Liu, H.Y.; Chen, D.; Ren, J.; He, J.Q.; Tang, F.Q. Single and repeated dose toxicity of mesoporous hollow silica nanoparticles in intravenously exposed mice. *Biomaterials* **2011**, *32*, 1657–1668. [[CrossRef](#)]
4. He, Q.J.; Shi, J.L.; Zhu, M.; Chen, Y.; Chen, F. The three-stage in vitro degradation behavior of mesoporous silica in simulated body fluid. *Micropor. Mesopor. Mater.* **2010**, *131*, 314–320. [[CrossRef](#)]
5. Fu, C.H.; Liu, T.L.; Li, L.L.; Liu, H.Y.; Chen, D.; Tang, F.Q. The absorption, distribution, excretion and toxicity of mesoporous silica nanoparticles in mice following different exposure routes. *Biomaterials* **2013**, *34*, 2565–2575. [[CrossRef](#)] [[PubMed](#)]
6. Tang, F.Q.; Li, L.L.; Chen, D. Mesoporous Silica Nanoparticles: Synthesis, Biocompatibility and Drug Delivery. *Adv. Mater.* **2012**, *24*, 1504–1534. [[CrossRef](#)]
7. Kinnari, P.; Makila, E.; Heikkila, T.; Salonen, J.; Hirvonen, J.; Santos, H.A. Comparison of mesoporous silicon and non-ordered mesoporous silica materials as drug carriers for itraconazole. *Int. J. Pharm.* **2011**, *414*, 148–156. [[CrossRef](#)]
8. Buyuktimkin, T.; Wurster, D.E. The influence of the adsorption of metoclopramide on the surface ionization of fumed silica. *Int. J. Pharm.* **2015**, *478*, 164–171. [[CrossRef](#)] [[PubMed](#)]
9. McCarthy, C.A.; Ahern, R.J.; Dontireddy, R.; Ryan, K.B.; Crean, A.M. Mesoporous silica formulation strategies for drug dissolution enhancement: A review. *Expert Opin. Drug Deliv.* **2016**, *13*, 93–108. [[CrossRef](#)]
10. Bharti, C.; Nagaich, U.; Pal, A.K.; Gulati, N. Mesoporous silica nanoparticles in target drug delivery system: A review. *Int. J. Pharm. Investig.* **2015**, *5*, 124–133. [[CrossRef](#)] [[PubMed](#)]
11. Jeelani, P.G.; Mulay, P.; Venkat, R.; Ramalingam, C. Multifaceted Application of Silica Nanoparticles. A Review. *Silicon* **2020**, *12*, 1337–1354. [[CrossRef](#)]
12. Miura, H.; Kanebako, M.; Shirai, H.; Nakao, H.; Inagi, T.; Terada, K. Enhancement of dissolution rate and oral absorption of a poorly water-soluble drug, K-832, by adsorption onto porous silica using supercritical carbon dioxide. *Eur. J. Pharm. Biopharm.* **2010**, *76*, 215–221. [[CrossRef](#)]
13. Carvalho, G.C.; Sábio, R.M.; de Cássia Ribeiro, T.; Monteiro, A.S.; Pereira, D.V.; Ribeiro, S.J.L.; Chorilli, M. Highlights in Mesoporous Silica Nanoparticles as a Multifunctional Controlled Drug Delivery Nanoplatfor for Infectious Diseases Treatment. *Pharm. Res.* **2020**, *37*, 191. [[CrossRef](#)]
14. Chircov, C.; Spoiala, A.; Paun, C.; Craciun, L.; Fikai, D.; Fikai, A.; Andronescu, E.; Turculet, S.C. Mesoporous Silica Platforms with Potential Applications in Release and Adsorption of Active Agents. *Molecules* **2020**, *25*, 3814. [[CrossRef](#)]
15. Zid, L.; Zelenak, V.; Almasi, M.; Zelenakova, A.; Szucsova, J.; Bednarcik, J.; Sulekova, M.; Hudak, A.; Vahovska, L. Mesoporous Silica as a Drug Delivery System for Naproxen: Influence of Surface Functionalization. *Molecules* **2020**, *25*, 4722. [[CrossRef](#)]
16. Natarajan, S.K.; Selvaraj, S. Mesoporous silica nanoparticles: Importance of surface modifications and its role in drug delivery. *RSC Adv.* **2014**, *4*, 14328–14334. [[CrossRef](#)]
17. Le, T.T.; Elyafi, A.K.E.; Mohammed, A.R.; Al-Khattawi, A. Delivery of Poorly Soluble Drugs via Mesoporous Silica: Impact of Drug Overloading on Release and Thermal Profiles. *Pharmaceutics* **2019**, *11*, 269. [[CrossRef](#)]
18. Seljak, K.B.; Kocbek, P.; Gašperlin, M. Mesoporous silica nanoparticles as delivery carriers: An overview of drug loading techniques. *J. Drug Deliv. Sci. Technol.* **2020**, *59*, 101906. [[CrossRef](#)]
19. Li, Z.; Zhang, Y.T.; Feng, N.P. Mesoporous silica nanoparticles: Synthesis, classification, drug loading, pharmacokinetics, biocompatibility, and application in drug delivery. *Expert Opin. Drug Deliv.* **2019**, *16*, 219–237. [[CrossRef](#)] [[PubMed](#)]
20. Maleki, A.; Kettiger, H.; Schoubben, A.; Rosenholm, J.M.; Ambroggi, V.; Hamidi, M. Mesoporous silica materials: From physico-chemical properties to enhanced dissolution of poorly water-soluble drugs. *J. Control. Release* **2017**, *262*, 329–347. [[CrossRef](#)]
21. Andersson, J.; Rosenholm, J.; Areva, S.; Lindén, M. Influences of Material Characteristics on Ibuprofen Drug Loading and Release Profiles from Ordered Micro- and Mesoporous Silica Matrices. *Chem. Mater.* **2004**, *16*, 4160–4167. [[CrossRef](#)]
22. Singh, A.; Worku, Z.A.; Van den Mooter, G. Oral formulation strategies to improve solubility of poorly water-soluble drugs. *Expert Opin. Drug Deliv.* **2011**, *8*, 1361–1378. [[CrossRef](#)]
23. Prestidge, C.A.; Barnes, T.J.; Lau, C.-H.; Barnett, C.; Loni, A.; Canham, L. Mesoporous silicon: A platform for the delivery of therapeutics. *Expert Opin. Drug Deliv.* **2007**, *4*, 101–110. [[CrossRef](#)] [[PubMed](#)]

24. Kumar, D.; Sailaja Chirravuri, S.V.; Shastri, N.R. Impact of surface area of silica particles on dissolution rate and oral bioavailability of poorly water soluble drugs: A case study with aceclofenac. *Int. J. Pharm.* **2014**, *461*, 459–468. [[CrossRef](#)]
25. Andrade, G.F.; Soares, D.C.F.; Almeida, R.K.d.S.; Sousa, E.M.B. Mesoporous Silica SBA-16 Functionalized with Alkoxysilane Groups: Preparation, Characterization, and Release Profile Study. *J. Nanomater.* **2012**, *2012*, 1687–4110. [[CrossRef](#)]
26. Maleki, A.; Hamidi, M. Dissolution enhancement of a model poorly water-soluble drug, atorvastatin, with ordered mesoporous silica: Comparison of MSF with SBA-15 as drug carriers. *Expert Opin. Drug Deliv.* **2016**, *13*, 171–181. [[CrossRef](#)] [[PubMed](#)]
27. Thomas, M.J.K.; Slipper, I.; Walunj, A.; Jain, A.; Favretto, M.E.; Kallinteri, P.; Douroumis, D. Inclusion of poorly soluble drugs in highly ordered mesoporous silica nanoparticles. *Int. J. Pharm.* **2010**, *387*, 272–277. [[CrossRef](#)]
28. Ambrogi, V.; Perioli, L.; Marmottini, F.; Accorsi, O.; Pagano, C.; Ricci, M.; Rossi, C. Role of mesoporous silicates on carbamazepine dissolution rate enhancement. *Micropor. Mesopor. Mater.* **2008**, *113*, 445–452. [[CrossRef](#)]
29. Speybroeck, M.V.; Barillaro, V.; Thi, T.D.; Mellaerts, R.; Martens, J.; Humbeeck, J.V.; Vermant, J.; Annaert, P.; Den Mooter, G.V.; Augustijns, P. Ordered Mesoporous Silica Material SBA-15: A Broad-Spectrum Formulation Platform for Poorly Soluble Drugs. *J. Pharm. Sci.* **2009**, *98*, 2648–2658. [[CrossRef](#)] [[PubMed](#)]
30. Ambrogi, V.; Marmottini, F.; Pagano, C. Amorphous carbamazepine stabilization by the mesoporous silicate SBA-15. *Micropor. Mesopor. Mater.* **2013**, *177*, 1–7. [[CrossRef](#)]
31. Chen, B.; Wang, Z.; Quan, G.; Peng, X.; Pan, X.; Wang, R.; Xu, Y.; Li, G.; Wu, C. In vitro and in vivo evaluation of ordered mesoporous silica as a novel adsorbent in liquisolid formulation. *Int. J. Nanomed.* **2012**, *7*, 1176–9114. [[CrossRef](#)]
32. Hu, Y.; Zhi, Z.; Zhao, Q.; Wu, C.; Zhao, P.; Jiang, H.; Jiang, T.; Wang, S. 3D cubic mesoporous silica microsphere as a carrier for poorly soluble drug carvedilol. *Micropor. Mesopor. Mater.* **2012**, *147*, 94–101. [[CrossRef](#)]
33. Gunaydin, S.; Yilmaz, A. Improvement of solubility of celecoxib by inclusion in MCM-41 mesoporous silica: Drug loading and release. *Turk. J. Chem.* **2015**, *39*, 317–333. [[CrossRef](#)]
34. Eren, Z.S.; Tunçer, S.; Gezer, G.; Yildirim, L.T.; Banerjee, S.; Yilmaz, A. Improved solubility of celecoxib by inclusion in SBA-15 mesoporous silica: Drug loading in different solvents and release. *Micropor. Mesopor. Mater.* **2016**, *235*, 211–223. [[CrossRef](#)]
35. Li, J.; Wang, Y.; Zheng, X.; Zhang, Y.; Sun, C.; Gao, Y.; Jiang, T.; Wang, S. The synthesis and application involving regulation of the insoluble drug release from mesoporous silica nanotubes. *Appl. Surf. Sci.* **2015**, *330*, 374–382. [[CrossRef](#)]
36. Chen, W.; Cheng, C.-A.; Lee, B.-Y.; Clemens, D.L.; Huang, W.-Y.; Horwitz, M.A.; Zink, J.I. Facile Strategy Enabling Both High Loading and High Release Amounts of the Water-Insoluble Drug Clofazimine Using Mesoporous Silica Nanoparticles. *ACS Appl. Mater. Interfaces* **2018**, *10*, 31870–31881. [[CrossRef](#)] [[PubMed](#)]
37. Kjellman, T.; Xia, X.; Alfredsson, V.; Garcia-Bennett, A.E. Influence of microporosity in SBA-15 on the release properties of anticancer drug dasatinib. *J. Mater. Chem. B* **2014**, *2*, 5265–5271. [[CrossRef](#)] [[PubMed](#)]
38. Ambrogi, V.; Perioli, L.; Pagano, C.; Marmottini, F.; Moretti, M.; Mizzi, F.; Rossi, C. Econazole Nitrate-Loaded MCM-41 for an Antifungal Topical Powder Formulation. *J. Pharm. Sci.* **2010**, *99*, 4738–4745. [[CrossRef](#)] [[PubMed](#)]
39. Kiekens, F.; Eelen, S.; Verheyden, L.; Daems, T.; Martens, J.; Den Mooter, G.V. Use of Ordered Mesoporous Silica to Enhance the Oral Bioavailability of Ezetimibe in Dogs. *J. Pharm. Sci.* **2012**, *101*, 1136–1144. [[CrossRef](#)]
40. Wu, C.; Zhao, Z.; Zhao, Y.; Hao, Y.; Liu, Y.; Liu, C. Preparation of a push–pull osmotic pump of felodipine solubilized by mesoporous silica nanoparticles with a core–shell structure. *Int. J. Pharm.* **2014**, *475*, 298–305. [[CrossRef](#)]
41. Ahern, R.J.; Crean, A.M.; Ryan, K.B. The influence of supercritical carbon dioxide (SC-CO₂) processing conditions on drug loading and physicochemical properties. *Int. J. Pharm.* **2012**, *439*, 92–99. [[CrossRef](#)]
42. Van Speybroeck, M.; Mellaerts, R.; Mols, R.; Thi, T.D.; Martens, J.A.; Van Humbeeck, J.; Annaert, P.; Van den Mooter, G.; Augustijns, P. Enhanced absorption of the poorly soluble drug fenofibrate by tuning its release rate from ordered mesoporous silica. *Eur. J. Pharm. Sci.* **2010**, *41*, 623–630. [[CrossRef](#)] [[PubMed](#)]
43. Ahern, R.J.; Hanrahan, J.P.; Tobin, J.M.; Ryan, K.B.; Crean, A.M. Comparison of fenofibrate–mesoporous silica drug-loading processes for enhanced drug delivery. *Eur. J. Pharm. Sci.* **2013**, *50*, 400–409. [[CrossRef](#)] [[PubMed](#)]
44. Hong, S.; Shen, S.; Tan, D.C.T.; Ng, W.K.; Liu, X.; Chia, L.S.O.; Irwan, A.W.; Tan, R.; Nowak, S.A.; Marsh, K.; et al. High drug load, stable, manufacturable and bioavailable fenofibrate formulations in mesoporous silica: A comparison of spray drying versus solvent impregnation methods. *Drug Deliv.* **2016**, *23*, 316–327. [[CrossRef](#)]
45. Bouledjoudja, A.; Masmoudi, Y.; Van Speybroeck, M.; Schueller, L.; Badens, E. Impregnation of Fenofibrate on mesoporous silica using supercritical carbon dioxide. *Int. J. Pharm.* **2016**, *499*, 1–9. [[CrossRef](#)]
46. Kerkhofs, S.; Saïdi, F.; Vandervoort, N.; Van den Mooter, G.; Martineau, C.; Taulelle, F.; Martens, J.A. Silica capsules enclosing P123 triblock copolymer micelles for flurbiprofen storage and release. *J. Mater. Chem. B* **2015**, *3*, 3054–3061. [[CrossRef](#)] [[PubMed](#)]
47. Trzeciak, K.; Kaźmierski, S.; Wielgus, E.; Potrzebowski, M.J. DiSupLo—New extremely easy and efficient method for loading of active pharmaceutical ingredients into the pores of MCM-41 mesoporous silica particles. *Micropor. Mesopor. Mater.* **2020**, *308*, 110506. [[CrossRef](#)]
48. Ambrogi, V.; Perioli, L.; Pagano, C.; Latterini, L.; Marmottini, F.; Ricci, M.; Rossi, C. MCM-41 for furosemide dissolution improvement. *Micropor. Mesopor. Mater.* **2012**, *147*, 343–349. [[CrossRef](#)]
49. Ambrogi, V.; Perioli, L.; Pagano, C.; Marmottini, F.; Ricci, M.; Sagnella, A.; Rossi, C. Use of SBA-15 for furosemide oral delivery enhancement. *Eur. J. Pharm. Sci.* **2012**, *46*, 43–48. [[CrossRef](#)]

50. Van Speybroeck, M.; Mellaerts, R.; Thi, T.D.; Martens, J.A.; Van Humbeeck, J.; Annaert, P.; Van den Mooter, G.; Augustijns, P. Preventing release in the acidic environment of the stomach via occlusion in ordered mesoporous silica enhances the absorption of poorly soluble weakly acidic drugs. *J. Pharm. Sci.* **2011**, *100*, 4864–4876. [[CrossRef](#)] [[PubMed](#)]
51. Jambhrunkar, S.; Qu, Z.; Popat, A.; Karmakar, S.; Xu, C.; Yu, C. Modulating in vitro release and solubility of griseofulvin using functionalized mesoporous silica nanoparticles. *J. Colloid Interface Sci.* **2014**, *434*, 218–225. [[CrossRef](#)] [[PubMed](#)]
52. Hillerström, A.; van Stam, J.; Andersson, M. Ibuprofen loading into mesostructured silica using liquid carbon dioxide as a solvent. *Green Chem.* **2009**, *11*, 662–667. [[CrossRef](#)]
53. Shen, S.-C.; Ng, W.K.; Chia, L.; Hu, J.; Tan, R.B.H. Physical state and dissolution of ibuprofen formulated by co-spray drying with mesoporous silica: Effect of pore and particle size. *Int. J. Pharm.* **2011**, *410*, 188–195. [[CrossRef](#)]
54. Charnay, C.; Bégu, S.; Tourné-Péteilh, C.; Nicole, L.; Lerner, D.A.; Devoisselle, J.M. Inclusion of ibuprofen in mesoporous templated silica: Drug loading and release property. *Eur. J. Pharm. Biopharm.* **2004**, *57*, 533–540. [[CrossRef](#)] [[PubMed](#)]
55. Tourné-Péteilh, C.; Brunel, D.; Bégu, S.; Chiche, B.; Fajula, F.; Lerner, D.A.; Devoisselle, J.-M. Synthesis and characterisation of ibuprofen-anchored MCM-41 silica and silica gel. *New J. Chem.* **2003**, *27*, 1415–1418. [[CrossRef](#)]
56. Heikkilä, T.; Salonen, J.; Tuura, J.; Kumar, N.; Salmi, T.; Murzin, D.Y.; Hamdy, M.S.; Mul, G.; Laitinen, L.; Kaukonen, A.M.; et al. Evaluation of mesoporous TCPSi, MCM-41, SBA-15, and TUD-1 materials as API carriers for oral drug delivery. *Drug Deliv.* **2007**, *14*, 337–347. [[CrossRef](#)] [[PubMed](#)]
57. Mellaerts, R.; Jammaer, J.A.G.; Van Speybroeck, M.; Chen, H.; Humbeeck, J.V.; Augustijns, P.; Van den Mooter, G.; Martens, J.A. Physical State of Poorly Soluble Therapeutic Molecules Loaded into SBA-15 Ordered Mesoporous Silica Carriers: A Case Study with Itraconazole and Ibuprofen. *Langmuir* **2008**, *24*, 8651–8659. [[CrossRef](#)]
58. Shen, S.C.; Ng, W.K.; Chia, L.; Dong, Y.C.; Tan, R.B.H. Stabilized Amorphous State of Ibuprofen by Co-Spray Drying With Mesoporous SBA-15 to Enhance Dissolution Properties. *J. Pharm. Sci.* **2010**, *99*, 1997–2007. [[CrossRef](#)] [[PubMed](#)]
59. Malfait, B.; Correia, N.T.; Mussi, A.; Paccou, L.; Guinet, Y.; Hédoux, A. Solid-state loading of organic molecular materials within mesoporous silica matrix: Application to ibuprofen. *Micropor. Mesopor. Mater.* **2019**, *277*, 203–207. [[CrossRef](#)]
60. Hu, Y.; Wang, J.; Zhi, Z.; Jiang, T.; Wang, S. Facile synthesis of 3D cubic mesoporous silica microspheres with a controllable pore size and their application for improved delivery of a water-insoluble drug. *J. Colloid Interface Sci.* **2011**, *363*, 410–417. [[CrossRef](#)]
61. Wang, Y.; Zhao, Q.; Hu, Y.; Sun, L.; Bai, L.; Jiang, T.; Wang, S. Ordered nanoporous silica as carriers for improved delivery of water insoluble drugs: A comparative study between three dimensional and two dimensional macroporous silica. *Int. J. Nanomed.* **2013**, *8*, 4015–4031. [[CrossRef](#)]
62. Linnell, T.; Santos, H.A.; Mäkilä, E.; Heikkilä, T.; Salonen, J.; Murzin, D.Y.; Kumar, N.; Laaksonen, T.; Peltonen, L.; Hirvonen, J. Drug Delivery Formulations of Ordered and Nonordered Mesoporous Silica: Comparison of Three Drug Loading Methods. *J. Pharm. Sci.* **2011**, *100*, 3294–3306. [[CrossRef](#)]
63. Liu, X.; Che, S. Enhanced release of the poorly soluble drug itraconazole loaded in ordered mesoporous silica. *Sci. China Chem.* **2015**, *58*, 400–410. [[CrossRef](#)]
64. Vialpando, M.; Aerts, A.; Persoons, J.; Martens, J.; Van Den Mooter, G. Evaluation of ordered mesoporous silica as a carrier for poorly soluble drugs: Influence of pressure on the structure and drug release. *J. Pharm. Sci.* **2011**, *100*, 3411–3420. [[CrossRef](#)]
65. Abd-elbary, A.; El Nabarawi, M.A.; Hassen, D.H.; Taha, A.A. Inclusion and characterization of ketoprofen into different mesoporous silica nanoparticles using three loading methods. *Int. J. Pharm. Pharm. Sci.* **2014**, *6*, 183–191.
66. Vadia, N.; Rajput, S. Study on formulation variables of methotrexate loaded mesoporous MCM-41 nanoparticles for dissolution enhancement. *Eur. J. Pharm. Sci.* **2012**, *45*, 8–18. [[CrossRef](#)] [[PubMed](#)]
67. Guo, Z.; Liu, X.-M.; Ma, L.; Li, J.; Zhang, H.; Gao, Y.-P.; Yuan, Y. Effects of particle morphology, pore size and surface coating of mesoporous silica on Naproxen dissolution rate enhancement. *Colloids Surf. B* **2013**, *101*, 228–235. [[CrossRef](#)] [[PubMed](#)]
68. Jia, L.; Shen, J.; Li, Z.; Zhang, D.; Zhang, Q.; Duan, C.; Liu, G.; Zheng, D.; Liu, Y.; Tian, X. Successfully tailoring the pore size of mesoporous silica nanoparticles: Exploitation of delivery systems for poorly water-soluble drugs. *Int. J. Pharm.* **2012**, *439*, 81–91. [[CrossRef](#)]
69. Yuan, L.; Chen, W.; Hu, J.; Zhang, J.Z.; Yang, D. Mechanistic Study of the Covalent Loading of Paclitaxel via Disulfide Linkers for Controlled Drug Release. *Langmuir* **2013**, *29*, 734–743. [[CrossRef](#)]
70. Tingming, F.; Liwei, G.; Kang, L.; Tianyao, W.; Jin, L. Template occluded SBA-15: An effective dissolution enhancer for poorly water-soluble drug. *Appl. Surf. Sci.* **2010**, *256*, 6963–6968. [[CrossRef](#)]
71. Ambrogi, V.; Perioli, L.; Marmottini, F.; Giovagnoli, S.; Esposito, M.; Rossi, C. Improvement of dissolution rate of piroxicam by inclusion into MCM-41 mesoporous silicate. *Eur. J. Pharm. Sci.* **2007**, *32*, 216–222. [[CrossRef](#)]
72. Martín, A.; García, R.A.; Karaman, D.S.; Rosenholm, J.M. Polyethyleneimine-functionalized large pore ordered silica materials for poorly water-soluble drug delivery. *J. Mater. Sci.* **2014**, *49*, 1437–1447. [[CrossRef](#)]
73. Bi, Y.; Wu, C.; Xin, M.; Bi, S.; Yan, C.; Hao, J.; Li, F.; Li, S. Facile large-scale preparation of mesoporous silica microspheres with the assistance of sucrose and their drug loading and releasing properties. *Int. J. Pharm.* **2016**, *500*, 77–84. [[CrossRef](#)]
74. Zhang, Y.; Zhi, Z.; Jiang, T.; Zhang, J.; Wang, Z.; Wang, S. Spherical mesoporous silica nanoparticles for loading and release of the poorly water-soluble drug telmisartan. *J. Controll. Release* **2010**, *145*, 257–263. [[CrossRef](#)] [[PubMed](#)]
75. ICH Guideline Q3C (R6). Available online: <https://www.ema.europa.eu/en/ich-q3c-r6-residual-solvents> (accessed on 27 April 2021).
76. Belhadj-Ahmed, F.; Badens, E.; Llewellyn, P.; Denoyel, R.; Charbit, G. Impregnation of vitamin E acetate on silica mesoporous phases using supercritical carbon dioxide. *J. Supercrit. Fluids* **2009**, *51*, 278–286. [[CrossRef](#)]

77. Lehto, V.P.; Riikonen, J. Drug loading and characterization of porous silicon materials. In *Porous Silicon for Biomedical Applications*; Santos, H.A., Ed.; Woodhead Publishing: Cambridge, UK, 2014; pp. 337–355.
78. Xie, X.; Li, F.; Zhang, H.; Lu, Y.; Lian, S.; Lin, H.; Gao, Y.; Jia, L. EpCAM aptamer-functionalized mesoporous silica nanoparticles for efficient colon cancer cell-targeted drug delivery. *Eur. J. Pharm. Sci.* **2016**, *83*, 28–35. [[CrossRef](#)]
79. Sarkar, A.; Ghosh, S.; Chowdhury, S.; Pandey, B.; Sil, P.C. Targeted delivery of quercetin loaded mesoporous silica nanoparticles to the breast cancer cells. *Biochim. Biophys. Acta* **2016**, *1860*, 2065–2075. [[CrossRef](#)]
80. Brás, A.R.; Fonseca, I.M.; Dionísio, M.; Schönhals, A.; Affouard, F.; Correia, N.T. Influence of Nanoscale Confinement on the Molecular Mobility of Ibuprofen. *J. Phys. Chem. C* **2014**, *118*, 13857–13868. [[CrossRef](#)]
81. Zheng, X.; Feng, S.; Wang, X.; Shi, Z.; Mao, Y.; Zhao, Q.; Wang, S. MSNCs and MgO-MSNCs as drug delivery systems to control the adsorption kinetics and release rate of indometacin. *Asian J. Pharm. Sci.* **2019**, *14*, 275–286. [[CrossRef](#)]
82. Šoltys, M.; Kovačik, P.; Dammer, O.; Beránek, J.; Štěpánek, F. Effect of solvent selection on drug loading and amorphisation in mesoporous silica particles. *Int. J. Pharm.* **2019**, *555*, 19–27. [[CrossRef](#)] [[PubMed](#)]
83. Skorupska, E.; Jeziorna, A.; Paluch, P.; Potrzebowski, M.J. Ibuprofen in Mesopores of Mobil Crystalline Material 41 (MCM-41): A Deeper Understanding. *Mol. Pharm.* **2014**, *11*, 1512–1519. [[CrossRef](#)] [[PubMed](#)]
84. Deraz, N. The comparative jurisprudence of catalysts preparation methods: I. Precipitation and impregnation methods. *J. Ind. Environ. Chem.* **2017**, *2*, 19–21.
85. Campanati, M.; Fornasari, G.; Vaccari, A. Fundamentals in the preparation of heterogeneous catalysts. *Catal. Today* **2003**, *77*, 299–314. [[CrossRef](#)]
86. Wang, Y.; Zhao, Q.; Han, N.; Bai, L.; Li, J.; Liu, J.; Che, E.; Hu, L.; Zhang, Q.; Jiang, T.; et al. Mesoporous silica nanoparticles in drug delivery and biomedical applications. *Nanomed. NBM* **2015**, *11*, 313–327. [[CrossRef](#)]
87. He, Y.; Liang, S.; Long, M.; Xu, H. Mesoporous silica nanoparticles as potential carriers for enhanced drug solubility of paclitaxel. *Mater. Sci. Eng. C* **2017**, *78*, 12–17. [[CrossRef](#)]
88. Liu, Q.; Zhang, J.; Sun, W.; Xie, Q.R.; Xia, W.; Gu, H. Delivering hydrophilic and hydrophobic chemotherapeutics simultaneously by magnetic mesoporous silica nanoparticles to inhibit cancer cells. *Int. J. Nanomed.* **2012**, *7*, 999–1013. [[CrossRef](#)]
89. Rosenholm, J.M.; Peuhu, E.; Eriksson, J.E.; Sahlgren, C.; Lindén, M. Targeted Intracellular Delivery of Hydrophobic Agents using Mesoporous Hybrid Silica Nanoparticles as Carrier Systems. *Nano Lett.* **2009**, *9*, 3308–3311. [[CrossRef](#)] [[PubMed](#)]
90. Kompella, U.B.; Koushik, K. Preparation of drug delivery systems using supercritical fluid technology. *Crit. Rev. Ther. Drug Carr. Syst.* **2001**, *18*, 173–199. [[CrossRef](#)]
91. Pasquali, I.; Bettini, R. Are pharmaceuticals really going supercritical? *Int. J. Pharm.* **2008**, *364*, 176–187. [[CrossRef](#)]
92. Bush, J.R.; Akgerman, A.; Hall, K.R. Synthesis of controlled release device with supercritical CO₂ and co-solvent. *J. Supercrit. Fluids* **2007**, *41*, 311–316. [[CrossRef](#)]
93. Li-Hong, W.; Xin, C.; Hui, X.; Li-Li, Z.; Jing, H.; Mei-Juan, Z.; Jie, L.; Yi, L.; Jin-Wen, L.; Wei, Z.; et al. A novel strategy to design sustained-release poorly water-soluble drug mesoporous silica microparticles based on supercritical fluid technique. *Int. J. Pharm.* **2013**, *454*, 135–142. [[CrossRef](#)]
94. Hillerström, A.; Andersson, M.; Samuelsson, J.; van Stam, J. Solvent strategies for loading and release in mesoporous silica. *Colloid Interface Sci. Commun.* **2014**, *3*, 5–8. [[CrossRef](#)]
95. Gurikov, P.; Smirnova, I. Amorphization of drugs by adsorptive precipitation from supercritical solutions: A review. *J. Supercrit. Fluids* **2018**, *132*, 105–125. [[CrossRef](#)]
96. Nuchuchua, O.; Nejadnik, M.R.; Goulooze, S.C.; Lješević, N.J.; Every, H.A.; Jiskoot, W. Characterization of drug delivery particles produced by supercritical carbon dioxide technologies. *J. Supercrit. Fluids* **2017**, *128*, 244–262. [[CrossRef](#)]
97. Padrela, L.; Rodrigues, M.A.; Duarte, A.; Dias, A.M.A.; Braga, M.E.M.; de Sousa, H.C. Supercritical carbon dioxide-based technologies for the production of drug nanoparticles/nanocrystals—A comprehensive review. *Adv. Drug Deliv. Rev.* **2018**, *131*, 22–78. [[CrossRef](#)]
98. Dohrn, R.; Bertakis, E.; Behrend, O.; Voutsas, E.; Tassios, D. Melting point depression by using supercritical CO₂ for a novel melt dispersion micronization process. *J. Mol. Liq.* **2007**, *131–132*, 53–59. [[CrossRef](#)]
99. Dementeva, O.V.; Rudoy, V.M.; Zhigletsova, S.K. One-pot synthesis and loading of silica nanocontainers using surface active drugs as templating agents. *Int. J. Drug Dev. Res.* **2018**, *10*, C1–C002.
100. Dementeva, O.V.; Rudoy, V.M. One-pot synthesis and loading of mesoporous SiO₂ nanocontainers using micellar drugs as a template. *RSC Adv.* **2016**, *6*, 36207–36210. [[CrossRef](#)]
101. Dementeva, O.V.; Roumyantseva, T.B.; Rudoy, V.M. The first example of silica nanoshell synthesis on vesicles of a cationic glycerolipid—Potential antitumor drug. *Colloid J.* **2016**, *78*, 281–284. [[CrossRef](#)]
102. Davis, B.; Richens, J.; O’Shea, P. Label-free critical micelle concentration determination of bacterial quorum sensing molecules. *Biophys. J.* **2011**, *101*, 245–254. [[CrossRef](#)]
103. Zhou, C.; Weir, M.D.; Zhang, K.; Deng, D.; Cheng, L.; Xu, H.H.K. Synthesis of new antibacterial quaternary ammonium monomer for incorporation into CaP nanocomposite. *Dent. Mater.* **2013**, *29*, 859–870. [[CrossRef](#)]
104. Wan, M.M.; Li, Y.Y.; Yang, T.; Zhang, T.; Sun, X.D.; Zhu, J.H. In Situ Loading of Drugs into Mesoporous Silica SBA-15. *Chem. Eur. J.* **2016**, *22*, 6294–6301. [[CrossRef](#)]
105. Tourne-Peteilh, C.; Begu, S.; Lerner, D.A.; Galarneau, A.; Lafont, U.; Devoisselle, J.-M. Sol-gel one-pot synthesis in soft conditions of mesoporous silica materials ready for drug delivery system. *J. Sol. Gel Sci. Technol.* **2012**, *61*, 455–462. [[CrossRef](#)]

106. Wang, N.; Cheng, X.; Li, N.; Wang, H.; Chen, H. Nanocarriers and Their Loading Strategies. *Adv. Healthcare Mater.* **2019**, *8*, [CrossRef] [PubMed]
107. Fasiku, V.; Amuhaya, E.K.; Rajab, K.M.; Omolo, C.A. Nano/Microparticles Encapsulation Via Covalent Drug Conjugation. In *Nano- and Micro-Encapsulation—Techniques and Applications*; Abu-Thabit, N., Ed.; IntechOpen: London, UK, 2019; Volume 86, pp. 230–251.
108. Giret, S.; Wong Chi Man, M.; Carcel, C. Mesoporous-Silica-Functionalized Nanoparticles for Drug Delivery. *Chem. Eur. J.* **2015**, *21*, 13850–13865. [CrossRef] [PubMed]
109. Wong, P.T.; Choi, S.K. Mechanisms of Drug Release in Nanotherapeutic Delivery Systems. *Chem. Rev.* **2015**, *115*, 3388–3432. [CrossRef] [PubMed]
110. Ding, C.; Li, Z. A review of drug release mechanisms from nanocarrier systems. *Mater. Sci. Eng. C* **2017**, *76*, 1440–1453. [CrossRef]
111. Manzano, M.; Vallet-Regí, M. New developments in ordered mesoporous materials for drug delivery. *J. Mater. Chem.* **2010**, *20*, 5593–5604. [CrossRef]
112. Mortera, R.; Vivero-Escoto, J.; Slowing, I.I.; Garrone, E.; Onida, B.; Lin, V.S.-Y. Cell-induced intracellular controlled release of membrane impermeable cysteine from a mesoporous silica nanoparticle-based drug delivery system. *Chem. Commun.* **2009**, 3219–3221. [CrossRef]
113. Popat, A.; Ross, B.P.; Liu, J.; Jambhrunkar, S.; Kleitz, F.; Qiao, S. Enzyme-responsive controlled release of covalently bound prodrug from functional mesoporous silica nanospheres. *Angew. Chem. Int. Ed. Engl.* **2012**, *51*, 12486–12489. [CrossRef]
114. Rosenholm, J.M.; Peuhu, E.; Bate-Eya, L.T.; Eriksson, J.E.; Sahlgren, C.; Lindén, M. Cancer-cell-specific induction of apoptosis using mesoporous silica nanoparticles as drug-delivery vectors. *Small* **2010**, *6*, 1234–1241. [CrossRef]
115. Carino, I.S.; Pasqua, L.; Testa, F.; Aiello, R.; Puoci, F.; Iemma, F.; Picci, N. Silica-Based Mesoporous Materials as Drug Delivery System for Methotrexate Release. *Drug Deliv.* **2007**, *14*, 491–495. [CrossRef]
116. Uejo, F.; Limwikrant, W.; Moribe, K.; Yamamoto, K. Dissolution improvement of fenofibrate by melting inclusion in mesoporous silica. *Asian J. Pharm. Sci.* **2013**, *8*, 329–335. [CrossRef]
117. Niu, X.; Wan, L.; Hou, Z.; Wang, T.; Sun, C.; Sun, J.; Zhao, P.; Jiang, T.; Wang, S. Mesoporous carbon as a novel drug carrier of fenofibrate for enhancement of the dissolution and oral bioavailability. *Int. J. Pharm.* **2013**, *452*, 382–389. [CrossRef] [PubMed]
118. Waters, L.J.; Bedford, S.; Parkes, G.M.B. Controlled Microwave Processing Applied to the Pharmaceutical Formulation of Ibuprofen. *AAPS PharmSciTech* **2011**, *12*, 1038–1043. [CrossRef] [PubMed]
119. Waters, L.J.; Hussain, T.; Parkes, G.; Hanrahan, J.P.; Tobin, J.M. Inclusion of fenofibrate in a series of mesoporous silicas using microwave irradiation. *Eur. J. Pharm. Biopharm.* **2013**, *85*, 936–941. [CrossRef]
120. Hampsey, J.E.; Castro, C.M.; McCaughey, B.; Wang, D.; Mitchell, B.; Lu, Y. Preparation of Micrometer- to Sub-micrometer-Sized Nanostructured Silica Particles Using High-Energy Ball Milling. *J. Am. Ceram. Soc.* **2004**, *87*, 1280–1286. [CrossRef]
121. Willart, J.F.; Descamps, M. Solid State Amorphization of Pharmaceuticals. *Mol. Pharm.* **2008**, *5*, 905–920. [CrossRef] [PubMed]
122. Trzeciak, K.; Kaźmierski, S.; Druzbicki, K.; Potrzebowski, M.J. Mapping of Guest Localization in Mesoporous Silica Particles by Solid-State NMR and Ab Initio Modeling: New Insights into Benzoic Acid and p-Fluorobenzoic Acid Embedded in MCM-41 via Ball Milling. *J. Phys. Chem. C* **2021**, *125*, 10096–10109. [CrossRef]
123. Abu-Zied, B.M.; Schwieger, W.; Asiri, A.M. Effect of ball milling on the structural and textural features of MCM-41 mesoporous material. *Micropor. Mesopor. Mater.* **2015**, *218*, 153–159. [CrossRef]
124. Torres-Barthelemy, V.; Pérez-Hernández, N.; Shenderovich, I.G.; Tolstoy, P.M.; Denisov, G.S.; Limbach, H.-H. NMR-Detected Host-Guest Proton Exchange as a Tool to Explore Surface/Volume Ratios and Fluid Filling of Internal and External Spaces of Porous Solids Containing Surface OH Groups. *J. Phys. Chem. C* **2020**, *124*, 22082–22095. [CrossRef]
125. Höhne, G.W.H.; Hemminger, W.F.; Flammersheim, H.J. Theoretical Fundamentals of Differential Scanning Calorimeters. In *Differential Scanning Calorimetry*, 2nd ed.; Messerschmidt, C., Ed.; Springer: Berlin/Heidelberg, Germany, 2003; pp. 21–40.
126. Shilyaeva, Y.; Volovlikova, O.; Poyarkov, K.; Yuditskaya, S.; Gavrilov, S. Characterization of Mesoporous Silicon Using DSC Thermoporometry. *Int. J. Nanosci.* **2019**, *18*, 1940073–1940077. [CrossRef]
127. Hempel, N.J.; Brede, K.; Olesen, N.E.; Genina, N.; Knopp, M.M.; Lobmann, K. A fast and reliable DSC-based method to determine the monomolecular loading capacity of drugs with good glass-forming ability in mesoporous silica. *Int. J. Pharm.* **2018**, *544*, 153–157. [CrossRef]
128. Lehto, V.P.; Vaha-Heikkilä, K.; Paski, J.; Salonen, J. Use of thermoanalytical methods in quantification of drug load in mesoporous silicon microparticles. *J. Therm. Anal. Calorim.* **2005**, *80*, 393–397. [CrossRef]
129. Bavnhøj, C.G.; Knopp, M.M.; Madsen, C.M.; Lobmann, K. The role interplay between mesoporous silica pore volume and surface area and their effect on drug loading capacity. *Int. J. Pharm. X* **2019**, *1*, 1000082–1000087. [CrossRef]
130. Nassimbeni, L.R.; Ba’thori, N.B.; Atwood, J.L. (Eds.) Thermal Analysis. In *Comprehensive Supramolecular Chemistry II*, Molecular Sciences and Chemical Engineering, 2nd ed.; Elsevier: Burlington, MA, USA, 2017; pp. 3–21.
131. Sing, K.S.W.; Everett, D.H.; Haul, R.A.W.; Moscou, L.; Pierotti, R.A.; Rouquerol, J.; Siemieniewska, T. Reporting physisorption data for gas solid systems with special reference to the determination of surface-area and porosity (recommendations 1984). *Pure Appl. Chem.* **1985**, *57*, 603–619. [CrossRef]
132. Thommes, M.; Kaneko, K.; Neimark, A.V.; Olivier, J.P.; Rodriguez-Reinoso, F.; Rouquerol, J.; Sing, K.S.W. Physisorption of gases, with special reference to the evaluation of surface area and pore size distribution (IUPAC Technical Report). *Pure Appl. Chem.* **2015**, *87*, 1051–1069. [CrossRef]

133. Rouquerol, J.; Avnir, D.; Everett, D.H.; Fairbridge, C.; Haynes, M.; Pernicone, N.; Ramsay, J.D.F.; Sing, K.S.W.; Unger, K.K. Guidelines for the characterization of porous solids. Characterization of Porous Solids. *Stud. Surf. Sci. Catal.* **1994**, *87*, 1–9.
134. Huang, B.Y.; Bartholomew, C.H.; Woodfield, B.F. Improved calculations of pore size distribution for relatively large, irregular slit-shaped mesopore structure. *Micropor. Mesopor. Mater.* **2014**, *184*, 112–121. [[CrossRef](#)]
135. Vallet-Regi, M.; Balas, F.; Colilla, M.; Manzano, M. Bone-regenerative bioceramic implants with drug and protein controlled delivery capability. *Prog. Solid. State Chem.* **2008**, *36*, 163–191. [[CrossRef](#)]
136. Izquierdo-Barba, I.; Sousa, E.; Doadrio, J.C.; Doadrio, A.L.; Pariente, J.P.; Martinez, A.; Babonneau, F.; Vallet-Regi, M. Influence of mesoporous structure type on the controlled delivery of drugs: Release of ibuprofen from MCM-48, SBA-15 and functionalized SBA-15. *J. Solgel. Sci. Technol.* **2009**, *50*, 421–429. [[CrossRef](#)]
137. Tzankova, V.; Aluani, D.; Yordanov, Y.; Valoti, M.; Frosini, M.; Spassova, I.; Kovacheva, D.; Tzankov, B. In vitro toxicity evaluation of lomefloxacin-loaded MCM-41 mesoporous silica nanoparticles. *Drug Chem. Toxicol.* **2021**, *44*, 238–249. [[CrossRef](#)]
138. Jani, A.T.; Haghghi, N.B.; Pour, M.S.H.; Aminian, M.; Molzemi, S. Hydroxyapatite incorporation into MCM-41 and study of ibuprofen drug release. *J. Aust. Ceram. Soc.* **2020**, *56*, 653–661. [[CrossRef](#)]
139. Burguete, P.; Beltran, A.; Guillem, C.; Latorre, J.; Perez-Pla, F.; Beltran, D.; Amoros, P. Pore Length Effect on Drug Uptake and Delivery by Mesoporous Silicas. *ChemPlusChem* **2012**, *77*, 817–831. [[CrossRef](#)]
140. Edeler, D.; Kaluderovic, M.R.; Dojcinovic, B.; Schmidt, H.; Kaluderovic, G.N. SBA-15 mesoporous silica particles loaded with cisplatin induce senescence in B16F10 cells. *RSC Adv.* **2016**, *6*, 111031–111040. [[CrossRef](#)]
141. Jin, D.; Xi, P.; Wang, B.; Zhang, L.; Enderlein, J.; van Oijen, A.M. Nanoparticles for super-resolution microscopy and single-molecule tracking. *Nat. Methods* **2018**, *15*, 415–423. [[CrossRef](#)]
142. Wang, W. Imaging the chemical activity of single nanoparticles with optical microscopy. *Chem. Soc. Rev.* **2018**, *47*, 2485–2508. [[CrossRef](#)] [[PubMed](#)]
143. Stewart, P.L. Cryo-electron microscopy and cryo-electron tomography of nanoparticles. *WIREs Nanomed. Nanobiotechnol.* **2017**, *9*, e1417. [[CrossRef](#)]
144. Huang, X.; Young, N.P.; Townley, H.E. Characterization and Comparison of Mesoporous Silica Particles for Optimized Drug Delivery. *Nanomater. Nanotechnol.* **2014**, *4*, 2. [[CrossRef](#)]
145. Fu, L.; Zhao, S.; Chen, Y.; Liu, Z. One-pot synthesis of mesoporous silica hollow spheres with Mn–N–C integrated into the framework for ethylbenzene oxidation. *Chem. Commun.* **2016**, *52*, 5577–5580. [[CrossRef](#)]
146. Lin, X.; Fu, L.; Chen, Y.; Zhu, R.; Wang, S.; Liu, Z. Mn–N–C Nanoreactor Prepared through Heating Metalloporphyrin Supported in Mesoporous Hollow Silica Spheres. *ACS Appl. Mater. Interfaces* **2016**, *8*, 26809–26816. [[CrossRef](#)]
147. Li, K.; Wei, J.; Yu, H.; Xu, P.; Wang, J.; Yin, H.; Cohen Stuart, M.A.; Wang, J.; Zhou, S. A Generic Method for Preparing Hollow Mesoporous Silica Catalytic Nanoreactors with Metal Oxide Nanoparticles inside Their Cavities. *Angew. Chem. Int. Ed.* **2018**, *57*, 16458–16463. [[CrossRef](#)] [[PubMed](#)]
148. Girleanu, M.; Lopes Silva, S.; Ihiawakrim, D.; Chaumonnot, A.; Bonduelle-Skrzypczak, A.; Lefebvre, F.; Dufaud, V.; Gay, A.-S.; Ersen, O. HAADF-STEM high-resolution study of nanometric MoS₂ inside mesoporous SBA-15. *Micropor. Mesopor. Mater.* **2015**, *217*, 190–195. [[CrossRef](#)]
149. Qin, L.; Niu, D.; Jiang, Y.; He, J.; Jia, X.; Zhao, W.; Li, P.; Li, Y. Confined growth of multiple gold nanorices in dual-mesoporous silica nanospheres for improved computed tomography imaging and photothermal therapy. *Int. J. Nanomed.* **2019**, *14*, 1519–1532. [[CrossRef](#)] [[PubMed](#)]
150. Piras, M.; Salis, A.; Piludu, M.; Steri, D.; Monduzzi, M. 3D vision of human lysozyme adsorbed onto a SBA-15 nanostructured matrix. *Chem. Commun.* **2011**, *47*, 7338–7340. [[CrossRef](#)] [[PubMed](#)]
151. Piludu, M.; Medda, L.; Cugia, F.; Monduzzi, M.; Salis, A. Silver Enhancement for Transmission Electron Microscopy Imaging of Antibody Fragment–Gold Nanoparticles Conjugates Immobilized on Ordered Mesoporous Silica. *Langmuir* **2015**, *31*, 9458–9463. [[CrossRef](#)]
152. Piludu, M.; Medda, L.; Monduzzi, M.; Salis, A. Gold Nanoparticles: A Powerful Tool to Visualize Proteins on Ordered Mesoporous Silica and for the Realization of Theranostic Nanobioconjugates. *Int. J. Mol. Sci.* **2018**, *19*, 1991. [[CrossRef](#)] [[PubMed](#)]
153. Zezzi do Valle Gomes, M.; Nabavi Zadeh, P.S.; Palmqvist, A.E.C.; Åkerman, B. Spatial Distribution of Enzymes Immobilized in Mesoporous Silicas for Biocatalysis. *ACS Appl. Nano Mater.* **2019**, *2*, 7245–7254. [[CrossRef](#)]
154. Clemments, A.M.; Botella, P.; Landry, C.C. Spatial Mapping of Protein Adsorption on Mesoporous Silica Nanoparticles by Stochastic Optical Reconstruction Microscopy. *J. Am. Chem. Soc.* **2017**, *139*, 3978–3981. [[CrossRef](#)]
155. Chen, S.; Wang, J.; Xin, B.; Yang, Y.; Ma, Y.; Zhou, Y.; Yuan, L.; Huang, Z.; Yuan, Q. Direct Observation of Nanoparticles within Cells at Subcellular Levels by Super-Resolution Fluorescence Imaging. *Anal. Chem.* **2019**, *91*, 5747–5752. [[CrossRef](#)]
156. Weiss, A.C.G.; Krüger, K.; Besford, Q.A.; Schlenk, M.; Kempe, K.; Förster, S.; Caruso, F. In Situ Characterization of Protein Corona Formation on Silica Microparticles Using Confocal Laser Scanning Microscopy Combined with Microfluidics. *ACS Appl. Mater. Interfaces* **2019**, *11*, 2459–2469. [[CrossRef](#)] [[PubMed](#)]
157. Fijneman, A.J.; Heinrichs, J.M.J.J.; van Leuken, S.H.M.; de With, G.; Friedrich, H. Time-resolved investigation of mesoporous silica microsphere formation using in situ heating optical microscopy. *J. Colloid Interface Sci.* **2021**, *585*, 118–125. [[CrossRef](#)]
158. Marrese, M.; Guarino, V.; Ambrosio, L. Atomic Force Microscopy: A Powerful Tool to Address Scaffold Design in Tissue Engineering. *J. Funct. Biomater.* **2017**, *8*, 7. [[CrossRef](#)]

159. Ivanov, Y.D.; Pleshakova, T.O.; Shumov, I.D.; Kozlov, A.F.; Ivanova, I.A.; Valueva, A.A.; Tatur, V.Y.; Smelov, M.V.; Ivanova, N.D.; Ziborov, V.S. AFM Imaging of Protein Aggregation in Studying the Impact of Knotted Electromagnetic Field on A Peroxidase. *Sci. Rep.* **2020**, *10*, 9022. [[CrossRef](#)] [[PubMed](#)]
160. Ariaeenejad, S.; Jokar, F.; Hadian, P.; Ma'mani, L.; Gharaghani, S.; Fereidoonzhad, M.; Salekdeh, G.H. An efficient nanobiocatalyst for lignocellulosic biomass hydrolysis: Xylanase immobilization on organically modified biogenic mesoporous silica nanoparticles. *Int. J. Biol. Macromol.* **2020**, *164*, 3462–3473. [[CrossRef](#)]
161. Ménard, M.; Meyer, F.; Parkhomenko, K.; Leuvre, C.; Francius, G.; Bégin-Colin, S.; Mertz, D. Mesoporous silica templated-albumin nanoparticles with high doxorubicin payload for drug delivery assessed with a 3-D tumor cell model. *Biochim. Biophys. Acta* **2019**, *1863*, 332–341. [[CrossRef](#)]
162. Chaudhary, Z.; Khan, G.M.; Abeer, M.M.; Pujara, N.; Wan-Chi Tse, B.; McGuckin, M.A.; Papat, A.; Kumeria, T. Efficient photoacoustic imaging using indocyanine green (ICG) loaded functionalized mesoporous silica nanoparticles. *Biomater. Sci.* **2019**, *7*, 5002–5015. [[CrossRef](#)] [[PubMed](#)]
163. Kang, J.; Kim, D.; Wang, J.; Han, Y.; Zuidema, J.M.; Hariri, A.; Park, J.H.; Jokerst, J.V.; Sailor, M.J. Enhanced Performance of a Molecular Photoacoustic Imaging Agent by Encapsulation in Mesoporous Silicon Nanoparticles. *Adv. Mater.* **2018**, *30*, e1800512. [[CrossRef](#)]
164. Prokopowicz, M.; Żegliński, J.; Gandhi, A.; Sawicki, W.; Tofail, S.A.M. Bioactive silica-based drug delivery systems containing doxorubicin hydrochloride: In vitro studies. *Colloids Surf. B Biointerfaces* **2012**, *93*, 249–259. [[CrossRef](#)] [[PubMed](#)]
165. Geppi, M.; Mollica, G.; Borsacchi, S.; Veracini, C.A. Solid-State NMR Studies of Pharmaceutical Systems. *Appl. Spectrosc. Rev.* **2008**, *43*, 202–302. [[CrossRef](#)]
166. Merisko-Liversidge, E.M.; Liversidge, G.G. Drug Nanoparticles: Formulating Poorly Water-Soluble Compounds. *Toxicol. Pathol.* **2008**, *36*, 43–48. [[CrossRef](#)] [[PubMed](#)]
167. Kalepu, S.; Nekkanti, V. Insoluble drug delivery strategies: Review of recent advances and business prospects. *Acta Pharm. Sin. B* **2015**, *5*, 442–453. [[CrossRef](#)] [[PubMed](#)]
168. Mirzaei, M.; Zarch, M.B.; Darroudi, M.; Sayyadi, K.; Keshavarz, S.T.; Sayyadi, J.; Fallah, A.; Maleki, H. Silica Mesoporous Structures: Effective Nanocarriers in Drug Delivery and Nanocatalysts. *Appl. Sci.* **2020**, *10*, 7533. [[CrossRef](#)]
169. Vallet-Regí, M.; Balas, F.; Arcos, D. Mesoporous Materials for Drug Delivery. *Angew. Chem. Int. Ed.* **2007**, *46*, 7548–7558. [[CrossRef](#)]
170. Trébosc, J.; Wiench, J.W.; Huh, S.; Lin, V.S.-Y.; Pruski, M. Solid-State NMR Study of MCM-41-type Mesoporous Silica Nanoparticles. *J. Am. Chem. Soc.* **2005**, *127*, 3057–3068. [[CrossRef](#)] [[PubMed](#)]
171. Trébosc, J.; Wiench, J.W.; Huh, S.; Lin, V.S.-Y.; Pruski, M. Studies of Organically Functionalized Mesoporous Silicas Using Heteronuclear Solid-State Correlation NMR Spectroscopy under Fast Magic Angle Spinning. *J. Am. Chem. Soc.* **2005**, *127*, 7587–7593. [[CrossRef](#)] [[PubMed](#)]
172. Mao, K.; Kobayashi, T.; Wiench, J.W.; Chen, H.-T.; Tsai, C.-H.; Lin, V.S.-Y.; Pruski, M. Conformations of Silica-Bound (Pentafluorophenyl)propyl Groups Determined by Solid-State NMR Spectroscopy and Theoretical Calculations. *J. Am. Chem. Soc.* **2010**, *132*, 12452–12457. [[CrossRef](#)]
173. Wiench, J.W.; Avadhut, Y.S.; Maity, N.; Bhaduri, S.; Lahiri, G.K.; Pruski, M.; Ganapathy, S. Characterization of Covalent Linkages in Organically Functionalized MCM-41 Mesoporous Materials by Solid-State NMR and Theoretical Calculations. *J. Phys. Chem. B* **2007**, *111*, 3877–3885. [[CrossRef](#)]
174. Kobayashi, T.; Pruski, M. Spatial Distribution of Silica-Bound Catalytic Organic Functional Groups Can Now Be Revealed by Conventional and DNP-Enhanced Solid-State NMR Methods. *ACS Catal.* **2019**, *9*, 7238–7249. [[CrossRef](#)]
175. Perras, F.A.; Kobayashi, T.; Pruski, M. Natural Abundance 17O DNP Two-Dimensional and Surface-Enhanced NMR Spectroscopy. *J. Am. Chem. Soc.* **2015**, *137*, 8336–8339. [[CrossRef](#)]
176. Perras, F.A.; Chaudhary, U.; Slowing, I.I.; Pruski, M. Probing Surface Hydrogen Bonding and Dynamics by Natural Abundance, Multidimensional, 17O DNP-NMR Spectroscopy. *J. Phys. Chem. C* **2016**, *120*, 11535–11544. [[CrossRef](#)]
177. Baccile, N. Application of Advanced Solid-State NMR Techniques to the Characterization of Nanomaterials: A Focus on Interfaces and Structure. In *Ideas in Chemistry and Molecular Sciences: Advances in Nanotechnology, Part II*; Pignataro, B., Ed.; WILEY-VCH Verlag GmbH: Weinheim, Germany, 2010; pp. 139–182.
178. Shenderovich, I.G.; Limbach, H.-H. Solid State NMR for Nonexperts: An Overview of Simple but General Practical Methods. *Solids* **2021**, *2*, 139–154. [[CrossRef](#)]
179. Babonneau, F.; Yeung, L.; Steunou, N.; Gervais, C. Solid State NMR Characterisation of Encapsulated Molecules in Mesoporous Silica. *J. Sol. Gel Sci. Technol.* **2004**, *31*, 219–223. [[CrossRef](#)]
180. Azaïs, T.; Tourné-Péteilh, C.; Aussenac, F.; Baccile, N.; Coelho, C.; Devoisselle, J.-M.; Babonneau, F. Solid-State NMR Study of Ibuprofen Confined in MCM-41 Material. *Chem. Mater.* **2006**, *18*, 6382–6390. [[CrossRef](#)]
181. Azaïs, T.; Laurent, G.; Panesar, K.; Nossou, A.; Guenneau, F.; Sanfeliu Cano, C.; Tourné-Péteilh, C.; Devoisselle, J.-M.; Babonneau, F. Implication of Water Molecules at the Silica–Ibuprofen Interface in Silica-Based Drug Delivery Systems Obtained through Incipient Wetness Impregnation. *J. Phys. Chem. C* **2017**, *121*, 26833–26839. [[CrossRef](#)]
182. Ukmar, T.; Čendak, T.; Mazaj, M.; Kaučič, V.; Mali, G. Structural and Dynamical Properties of Indomethacin Molecules Embedded within the Mesopores of SBA-15: A Solid-State NMR View. *J. Phys. Chem. C* **2012**, *116*, 2662–2671. [[CrossRef](#)]
183. Azaïs, T.; Hartmeyer, G.; Quignard, S.; Laurent, G.; Tourné-Péteilh, C.; Devoisselle, J.-M.; Babonneau, F. Solid-state NMR characterization of drug-model molecules encapsulated in MCM-41 silica. *Pure Appl. Chem.* **2009**, *81*, 1345–1355. [[CrossRef](#)]

184. Ruffel, L.; Soulié, J.; Coppel, Y.; Roblin, P.; Brouillet, F.; Frances, C.; Tourbin, M. Ibuprofen loading into mesoporous silica nanoparticles using Co-Spray drying: A multi-scale study. *Micropor. Mesopor. Mater.* **2020**, *291*, 109689. [\[CrossRef\]](#)
185. Vogt, F.G.; Roberts-Skilton, K.; Kennedy-Gabb, S.A. A solid-state NMR study of amorphous ezetimibe dispersions in mesoporous silica. *Pharm. Res.* **2013**, *30*, 2315–2331. [\[CrossRef\]](#)
186. Fatnassi, M.; Tourne-Peteilh, C.; Mineva, T.; Devoisselle, J.-M.; Gaveau, P.; Fayon, F.; Alonso, B. Drug nano-domains in spray-dried ibuprofen-silica microspheres. *Phys. Chem. Chem. Phys.* **2012**, *14*, 1463–9076. [\[CrossRef\]](#) [\[PubMed\]](#)
187. Ukmar, T.; Godec, A.; Planinšek, O.; Kaučič, V.; Mali, G.; Gaberšček, M. The phase (trans)formation and physical state of a model drug in mesoscopic confinement. *Phys. Chem. Chem. Phys.* **2011**, *13*, 16046–16054. [\[CrossRef\]](#)
188. Aiello, D.; Folliet, N.; Laurent, G.; Testa, F.; Gervais, C.; Babonneau, F.; Azais, T. Solid state NMR characterization of phenylphosphonic acid encapsulated in SBA-15 and aminopropyl-modified SBA-15. *Micropor. Mesopor. Mater.* **2013**, *166*, 109–116. [\[CrossRef\]](#)
189. Datt, A.; El-Maazawi, I.; Larsen, S.C. Aspirin Loading and Release from MCM-41 Functionalized with Aminopropyl Groups via Co-condensation or Postsynthesis Modification Methods. *J. Phys. Chem. C* **2012**, *116*, 18358–18366. [\[CrossRef\]](#)
190. Brodrecht, M.; Kumari, B.; Breitzke, H.; Gutmann, T.; Buntkowsky, G. Chemically Modified Silica Materials as Model Systems for the Characterization of Water-Surface Interactions. *Z. Phys. Chem.* **2018**, *232*, 1127–1146. [\[CrossRef\]](#)
191. Juère, E.; Caillard, R.; Kleitz, F. Pore confinement and surface charge effects in protein-mesoporous silica nanoparticles formulation for oral drug delivery. *Micropor. Mesopor. Mater.* **2020**, *306*, 110482. [\[CrossRef\]](#)
192. Juère, E.; Kleitz, F. On the nanopore confinement of therapeutic drugs into mesoporous silica materials and its implications. *Micropor. Mesopor. Mater.* **2018**, *270*, 109–119. [\[CrossRef\]](#)
193. Riikonen, J.; Mäkilä, E.; Salonen, J.; Lehto, V.-P. Determination of the Physical State of Drug Molecules in Mesoporous Silicon with Different Surface Chemistries. *Langmuir* **2009**, *25*, 6137–6142. [\[CrossRef\]](#) [\[PubMed\]](#)
194. Patrick, W.A.; Kemper, W.A. Melting temperatures of compounds adsorbed on silica gel1. *J. Phys. Chem.* **1938**, *42*, 369–380. [\[CrossRef\]](#)
195. Rennie, G.K.; Clifford, J. Melting of ice in porous solids. *J. Chem. Soc. Faraday Trans. 1* **1977**, *73*, 680–689. [\[CrossRef\]](#)
196. Morineau, D.; Guegan, R.; Xia, Y.; Alba-Simionesco, C. Structure of liquid and glassy methanol confined in cylindrical pores. *J. Chem. Phys.* **2004**, *121*, 1466–1473. [\[CrossRef\]](#) [\[PubMed\]](#)
197. Morishige, K.; Kawano, K. Freezing and melting of methanol in a single cylindrical pore: Dynamical supercooling and vitrification of methanol. *J. Chem. Phys.* **2000**, *112*, 11023–11029. [\[CrossRef\]](#)
198. Takei, T.; Konishi, T.; Fuji, M.; Watanabe, T.; Chikazawa, M. Phase transition of capillary condensed liquids in porous silica: Effect of surface hydroxyl groups. *Thermochimica Acta* **1995**, *267*, 159–167. [\[CrossRef\]](#)
199. Gedat, E.; Schreiber, A.; Albrecht, J.; Emmler, T.; Shenderovich, I.; Findenegg, G.H.; Limbach, H.-H.; Buntkowsky, G. 2H-Solid-State NMR Study of Benzene-d₆ Confined in Mesoporous Silica SBA-15. *J. Phys. Chem. B* **2002**, *106*, 1977–1984. [\[CrossRef\]](#)
200. Aksnes, D.W.; Kintys, L. 1H and 2H NMR studies of benzene confined in porous solids: Melting point depression and pore size distribution. *Solid State Nucl. Magn. Reson.* **2004**, *25*, 146–152. [\[CrossRef\]](#)
201. Tielens, F.; Folliet, N.; Bondaz, L.; Etemovic, S.; Babonneau, F.; Gervais, C.; Azais, T. Molecular Picture of the Adsorption of Ibuprofen and Benzoic Acid on Hydrated Amorphous Silica through DFT-D Calculations Combined with Solid-State NMR Experiments. *J. Phys. Chem. C* **2017**, *121*, 17339–17347. [\[CrossRef\]](#)
202. Skorupska, E.; Jeziorna, A.; Potrzebowski, M.J. Thermal Solvent-Free Method of Loading of Pharmaceutical Cocrystals into the Pores of Silica Particles: A Case of Naproxen/Picolinamide Cocrystal. *J. Phys. Chem. C* **2016**, *120*, 13169–13180. [\[CrossRef\]](#)
203. Skorupska, E.; Kaźmierski, S.; Potrzebowski, M.J. Solid State NMR Characterization of Ibuprofen:Nicotinamide Cocrystals and New Idea for Controlling Release of Drugs Embedded into Mesoporous Silica Particles. *Mol. Pharm.* **2017**, *14*, 1800–1810. [\[CrossRef\]](#)
204. Karagianni, A.; Malamataris, M.; Kachrimanis, K. Pharmaceutical Cocrystals: New Solid Phase Modification Approaches for the Formulation of APIs. *Pharmaceutics* **2018**, *10*, 18. [\[CrossRef\]](#)
205. Douroumis, D.; Ross, S.A.; Nokhodchi, A. Advanced methodologies for cocrystal synthesis. *Adv. Drug Deliv. Rev.* **2017**, *117*, 178–195. [\[CrossRef\]](#)
206. Pindelska, E.; Sokal, A.; Kolodziejewski, W. Pharmaceutical cocrystals, salts and polymorphs: Advanced characterization techniques. *Adv. Drug Deliv. Rev.* **2017**, *117*, 111–146. [\[CrossRef\]](#)
207. Skorupska, E.; Jeziorna, A.; Kazmierski, S.; Potrzebowski, M.J. Recent progress in solid-state NMR studies of drugs confined within drug delivery systems. *Solid State Nucl. Magn. Reson.* **2014**, *57–58*, 2–16. [\[CrossRef\]](#) [\[PubMed\]](#)
208. Dudek, M.K.; Kaźmierski, S.; Potrzebowski, M.J. Fast and very fast MAS solid state NMR studies of pharmaceuticals. *Annu. Rep. NMR Spectrosc.* **2021**. [\[CrossRef\]](#)
209. Li, M.Y.; Xu, W.; Su, Y.C. Solid-state NMR spectroscopy in pharmaceutical sciences. *TRAC Trend Anal. Chem.* **2021**, *135*. [\[CrossRef\]](#)
210. Wu, H.M.; Xiao, Y.; Guo, Y.; Miao, S.J.; Chen, Q.Q.; Chen, Z. Functionalization of SBA-15 mesoporous materials with 2-acetylthiophene for adsorption of Cr(III) ions. *Micropor. Mesopor. Mater.* **2020**, *292*, 109754–109765. [\[CrossRef\]](#)
211. Melnyk, I.V.; Nazarchuk, G.I.; Vaclavikova, M.; Zub, Y.L. IR spectroscopy study of SBA-15 silicas functionalized with the ethylthiocarbamidepropyl groups and their interactions with Ag(I) and Hg(II) ions. *Appl. Nanosci.* **2019**, *9*, 683–694. [\[CrossRef\]](#)
212. Tomozawa, M.; Hong, J.W.; Ryu, S.R. Infrared (IR) investigation of the structural changes of silica glasses with fictive temperature. *J. Non. Cryst. Solids* **2005**, *351*, 1054–1060. [\[CrossRef\]](#)

213. Acharya, M.; Mishra, S.; Sahoo, R.N.; Mallick, S. Infrared Spectroscopy for Analysis of Co-processed Ibuprofen and Magnesium Trisilicate at Milling and Freeze Drying. *Acta Chim. Slov.* **2017**, *64*, 45–54. [[CrossRef](#)]
214. Daneluti, A.L.M.; Neto, F.M.; Velasco, M.V.R.; Baby, A.R.; Matos, J.D. Evaluation and characterization of the encapsulation/entrapping process of octyl methoxycinnamate in ordered mesoporous silica type SBA-15. *J. Therm. Anal. Calorim.* **2018**, *131*, 789–798. [[CrossRef](#)]
215. Albayati, T.M.; Salih, I.K.; Alazzawi, H.F. Synthesis and characterization of a modified surface of SBA-15 mesoporous silica for a chloramphenicol drug delivery system. *Heliyon* **2019**, *5*, e02539–e02547. [[CrossRef](#)] [[PubMed](#)]
216. Liu, L.K.; Gao, H.W. Molecular structure and vibrational spectra of ibuprofen using density function theory calculations. *Spectrochim. Acta A Mol. Biomol. Spectrosc.* **2012**, *89*, 201–209. [[CrossRef](#)]
217. Lai, J.M.; Lin, W.; Scholes, P.; Li, M.Z. Investigating the Effects of Loading Factors on the In Vitro Pharmaceutical Performance of Mesoporous Materials as Drug Carriers for Ibuprofen. *Materials* **2017**, *10*, 150. [[CrossRef](#)]
218. Tzankov, B.; Tzankova, V.; Aluani, D.; Yordanov, Y.; Spassova, I.; Kovacheva, D.; Avramova, K.; Valoti, M.; Yoncheva, K. Development of MCM-41 mesoporous silica nanoparticles as a platform for pramipexole delivery. *J. Drug Deliv. Sci. Technol.* **2019**, *51*, 26–35. [[CrossRef](#)]
219. Rahman, M.M.; Aznan, M.; Yusof, A.M.; Ansary, H.; Siddiqi, M.J.; Yusan, S. Synthesis and Characterization of Functionalized Se-MCM-41 a New Drug Carrier Mesopore Composite. *Orient. J. Chem.* **2017**, *33*, 611–621. [[CrossRef](#)]
220. Salam, M.S.A.; Betiha, M.A.; Shaban, S.A.; Elsabagh, A.M.; Abd El-Aal, R.M.; El Kady, F.Y. Synthesis and characterization of MCM-41-supported nano zirconia catalysts. *Egypt. J. Pet.* **2015**, *24*, 49–57. [[CrossRef](#)]
221. Liu, Y.M.; Cao, Y.; Yi, N.; Feng, W.L.; Dai, W.L.; Yan, S.R.; He, H.Y.; Fan, K.N. Vanadium oxide supported on mesoporous SBA-15 as highly selective catalysts in the oxidative dehydrogenation of propane. *J. Catal.* **2004**, *224*, 417–428. [[CrossRef](#)]
222. Varache, M.; Bezverkhyy, I.; Weber, G.; Saviot, L.; Chassagnon, R.; Baras, F.; Bouyer, F. Loading of Cisplatin into Mesoporous Silica Nanoparticles: Effect of Surface Functionalization. *Langmuir* **2019**, *35*, 8984–8995. [[CrossRef](#)]
223. Hellstaen, S.; Qu, H.Y.; Heikkila, T.; Kohonen, J.; Reinikainen, S.P.; Louhi-Kultanen, M. Raman spectroscopic imaging of indomethacin loaded in porous silica. *Cryst. Eng. Comm.* **2012**, *14*, 1582–1587. [[CrossRef](#)]
224. Paudel, A.; Rajjada, D.; Rantanen, J. Raman spectroscopy in pharmaceutical product design. *Adv. Drug Deliv. Rev.* **2015**, *89*, 3–20. [[CrossRef](#)] [[PubMed](#)]
225. Fussell, A.L.; Mah, P.T.; Offerhaus, H.; Niemi, S.M.; Salonen, J.; Santos, H.A.; Strachan, C. Coherent anti-Stokes Raman scattering microscopy driving the future of loaded mesoporous silica imaging. *Acta Biomater.* **2014**, *10*, 4870–4877. [[CrossRef](#)]
226. Scrivens, G.; Ticehurst, M.; Swanson, J.T. Strategies for improving the reliability of accelerated predictive stability (APS) studies. In *Accelerated Predictive Stability*; Qiu, F., Scrivens, G., Eds.; Academic Press: Cambridge, MA, USA, 2018; pp. 175–206. [[CrossRef](#)]
227. Biswas, N. Modified mesoporous silica nanoparticles for enhancing oral bioavailability and antihypertensive activity of poorly water soluble valsartan. *Eur. J. Pharm. Sci.* **2017**, *99*, 152–160. [[CrossRef](#)]
228. Abedi, M.; Abolmaali, S.S.; Abedanzadeh, M.; Farjadian, F.; Mohammadi Samani, S.; Tamaddon, A.M. Core-Shell Imidazoline-Functionalized Mesoporous Silica Superparamagnetic Hybrid Nanoparticles as a Potential Theranostic Agent for Controlled Delivery of Platinum(II) Compound. *Int. J. Nanomed.* **2020**, *15*, 2617–2631. [[CrossRef](#)]
229. Peralta, M.E.; Jadhav, S.A.; Magnacca, G.; Scalarone, D.; Mártire, D.O.; Parolo, M.E.; Carlos, L. Synthesis and in vitro testing of thermoresponsive polymer-grafted core-shell magnetic mesoporous silica nanoparticles for efficient controlled and targeted drug delivery. *J. Colloid Interface Sci.* **2019**, *544*, 198–205. [[CrossRef](#)]
230. Zhang, W.; Zheng, N.; Chen, L.; Xie, L.; Cui, M.; Li, S.; Xu, L. Effect of Shape on Mesoporous Silica Nanoparticles for Oral Delivery of Indomethacin. *Pharmaceutics* **2019**, *11*, 4. [[CrossRef](#)] [[PubMed](#)]
231. Delpiano, G.R.; Casula, M.F.; Piludu, M.; Corpino, R.; Ricci, P.C.; Vallet-Regí, M.; Sanjust, E.; Monduzzi, M.; Salis, A. Assembly of Multicomponent Nano-Bioconjugates Composed of Mesoporous Silica Nanoparticles, Proteins, and Gold Nanoparticles. *ACS Omega* **2019**, *4*, 11044–11052. [[CrossRef](#)]
232. Gounani, Z.; Asadollahi, M.A.; Pedersen, J.N.; Lyngsø, J.; Skov Pedersen, J.; Arpanaei, A.; Meyer, R.L. Mesoporous silica nanoparticles carrying multiple antibiotics provide enhanced synergistic effect and improved biocompatibility. *Colloids Surf. B* **2019**, *175*, 498–508. [[CrossRef](#)] [[PubMed](#)]
233. Harada, M.; Nakamura, T.; Yano, K. Evaluating the internal structure of monodispersed mesoporous silica spheres by small-angle X-ray scattering. *Colloid Interface Sci. Commun.* **2019**, *33*, 100203. [[CrossRef](#)]
234. Yi, Z.; Dumée, L.F.; Garvey, C.J.; Feng, C.; She, F.; Rookes, J.E.; Mudie, S.; Cahill, D.M.; Kong, L. A New Insight into Growth Mechanism and Kinetics of Mesoporous Silica Nanoparticles by in Situ Small Angle X-ray Scattering. *Langmuir* **2015**, *31*, 8478–8487. [[CrossRef](#)] [[PubMed](#)]
235. Schmitt, J.; Kjellman, T.; Kwaśniewski, P.; Meneau, F.; Pedersen, J.S.; Edler, K.J.; Rennie, A.R.; Alfredsson, V.; Impéror-Clerc, M. Outset of the Morphology of Nanostructured Silica Particles during Nucleation Followed by Ultrasmall-Angle X-ray Scattering. *Langmuir* **2016**, *32*, 5162–5172. [[CrossRef](#)]
236. Bhavsar, D.; Gajjar, J.; Sawant, K. Formulation and development of smart pH responsive mesoporous silica nanoparticles for breast cancer targeted delivery of anastrozole: In vitro and in vivo characterizations. *Micropor. Mesopor. Mater.* **2019**, *279*, 107–116. [[CrossRef](#)]

237. Limnell, T.; Heikkilä, T.; Santos, H.A.; Sistonen, S.; Hellstén, S.; Laaksonen, T.; Peltonen, L.; Kumar, N.; Murzin, D.Y.; Louhi-Kultanen, M.; et al. Physicochemical stability of high indomethacin payload ordered mesoporous silica MCM-41 and SBA-15 microparticles. *Int. J. Pharm.* **2011**, *416*, 242–251. [[CrossRef](#)] [[PubMed](#)]
238. Hooshyar, S.; Nafisi, S.; Mohseni, M.; Mehravi, B. Design and synthesis of potential nano-carrier for delivery of diphencyprone to hair follicle. *J. Pharm. Investig.* **2021**, *51*, 173–181. [[CrossRef](#)]
239. Christoforidou, T.; Giasafaki, D.; Andriotis, E.G.; Bouropoulos, N.; Theodoroula, N.F.; Vizirianakis, I.S.; Steriotis, T.; Charalambopoulou, G.; Fatouros, D.G. Oral Drug Delivery Systems Based on Ordered Mesoporous Silica Nanoparticles for Modulating the Release of Aprepitant. *Int. J. Mol. Sci.* **2021**, *22*, 1896. [[CrossRef](#)]
240. Masood, A.; Maheen, S.; Khan, H.U.; Shafqat, S.S.; Irshad, M.; Aslam, I.; Rasul, A.; Bashir, S.; Zafar, M.N. Pharmaco-Technical Evaluation of Statistically Formulated and Optimized Dual Drug-Loaded Silica Nanoparticles for Improved Antifungal Efficacy and Wound Healing. *ACS Omega* **2021**, *6*, 8210–8225. [[CrossRef](#)] [[PubMed](#)]
241. Chaudhary, Z.; Subramaniam, S.; Khan, G.M.; Abeer, M.M.; Qu, Z.; Janjua, T.; Kumeria, T.; Batra, J.; Papat, A. Encapsulation and Controlled Release of Resveratrol Within Functionalized Mesoporous Silica Nanoparticles for Prostate Cancer Therapy. *Front. Bioeng. Biotechnol.* **2019**, *7*, 225. [[CrossRef](#)]
242. Mohseni, M.; Gilani, K.; Mortazavi, S.A. Preparation and characterization of rifampin loaded mesoporous silica nanoparticles as a potential system for pulmonary drug delivery. *Iran. J. Pharm. Res.* **2015**, *14*, 27–34. [[PubMed](#)]
243. Baer, D.R.; Shutthanandan, V. Nano-objects as biomaterials: Immense opportunities, significant challenges and the important use of surface analytical methods. In *Comprehensive Biomaterials II*; Elsevier: Amsterdam, The Netherlands, 2017; Volume 3.6, pp. 86–107.
244. Barnes, T.J.; Kempson, I.M.; Prestidge, C.A. Surface analysis for compositional, chemical and structural imaging in pharmaceuticals with mass spectrometry: A ToF-SIMS perspective. *Int. J. Pharm.* **2011**, *417*, 61–69. [[CrossRef](#)]
245. Kempson, I.M.; Barnes, T.J.; Prestidge, C.A. Use of TOF-SIMS to Study Adsorption and Loading Behavior of Methylene Blue and Papain in a Nano-Porous Silicon Layer. *J. Am. Soc. Mass Spectrom.* **2010**, *21*, 254–260. [[CrossRef](#)]
246. Clemens, D.; Lee, B.-Y.; Plamthottam, S.; Tullius, M.V.; Wang, R.; Yu, C.-J.; Li, Z.; Dillon, B.J.; Zink, J.I.; Horwitz, M.A. Nanoparticle Formulation of Moxifloxacin and Intramuscular Route of Delivery Improve Antibiotic Pharmacokinetics and Treatment of Pneumonic Tularemia in a Mouse Model. *ACS Infect. Dis.* **2019**, *5*, 281–291. [[CrossRef](#)]
247. Kaasalainen, M.; Aseyev, V.; von Haartman, E.; Karaman, D.Ş.; Mäkilä, E.; Tenhu, H.; Rosenholm, J.; Salonen, J. Size, Stability, and Porosity of Mesoporous Nanoparticles Characterized with Light Scattering. *Nanoscale Res. Lett.* **2017**, *12*, 74. [[CrossRef](#)]
248. Patel, V.R.; Agrawal, Y.K. Nanosuspension: An approach to enhance solubility of drugs. *J. Adv. Pharm. Technol. Res.* **2011**, *2*, 81–87. [[CrossRef](#)]
249. Bhattacharjee, S. DLS and zeta potential—What they are and what they are not? *J. Controll. Release* **2016**, *235*, 337–351. [[CrossRef](#)]
250. You, Y.; He, L.; Ma, B.; Chen, T. High-Drug-Loading Mesoporous Silica Nanorods with Reduced Toxicity for Precise Cancer Therapy against Nasopharyngeal Carcinoma. *Adv. Funct. Mat.* **2017**, *27*, 1703313. [[CrossRef](#)]
251. Muster, T.H.; Prestidge, C.A.; Hayes, R.A. Water adsorption kinetics and contact angles of silica particles. *Colloids Surf. A* **2001**, *176*, 253–266. [[CrossRef](#)]
252. Rother, G.; Stack, A.G.; Gautam, S.; Liu, T.; Cole, D.R.; Busch, A. Water Uptake by Silica Nanopores: Impacts of Surface Hydrophilicity and Pore Size. *J. Phys. Chem. C* **2020**, *124*, 15188–15194. [[CrossRef](#)]
253. Ho, Y.-J.; Wu, C.-H.; Jin, Q.-F.; Lin, C.-Y.; Chiang, P.-H.; Wu, N.; Fan, C.-H.; Yang, C.-M.; Yeh, C.-K. Superhydrophobic drug-loaded mesoporous silica nanoparticles capped with β -cyclodextrin for ultrasound image-guided combined antivasculature and chemo-sonodynamic therapy. *Biomaterials* **2020**, *232*, 119723. [[CrossRef](#)]
254. Skwira, A.; Szewczyk, A.; Prokopowicz, M. The Effect of Polydimethylsiloxane-Ethylcellulose Coating Blends on the Surface Characterization and Drug Release of Ciprofloxacin-Loaded Mesoporous Silica. *Polymers* **2019**, *11*, 1450. [[CrossRef](#)]
255. Mäkilä, E.; Bimbo, L.M.; Kaasalainen, M.; Herranz, B.; Airaksinen, A.J.; Heinonen, M.; Kukk, E.; Hirvonen, J.; Santos, H.A.; Salonen, J. Amine Modification of Thermally Carbonized Porous Silicon with Silane Coupling Chemistry. *Langmuir* **2012**, *28*, 14045–14054. [[CrossRef](#)]
256. Chen, W.-Y.; Matulis, D.; Hu, W.-P.; Lai, Y.-F.; Wang, W.-H. Studies of the interactions mechanism between DNA and silica surfaces by Isothermal Titration Calorimetry. *J. Taiwan Inst. Chem. Eng.* **2020**, *116*, 62–66. [[CrossRef](#)]
257. Khan, M.A.; Kiser, M.R.; Moradipour, M.; Nadeau, E.A.; Ghanim, R.W.; Webb, B.A.; Rankin, S.E.; Knutson, B.L. Effect of Confinement in Nanopores on RNA Interactions with Functionalized Mesoporous Silica Nanoparticles. *J. Phys. Chem. B* **2020**, *124*, 8549–8561. [[CrossRef](#)]
258. Zhang, X.; Cresswell, M. Silica-Based Amorphous Drug Delivery Systems. In *Inorganic Controlled Release Technology*; Zhang, X., Cresswell, M., Eds.; Butterworth-Heinemann: Oxford, UK, 2016; pp. 93–137.
259. Waters, L.J.; Hanrahan, J.P.; Tobin, J.M.; Finch, C.V.; Parkes, G.M.B.; Ahmad, S.A.; Mohammad, F.; Saleem, M. Enhancing the dissolution of phenylbutazone using Syloid® based mesoporous silicas for oral equine applications. *J. Pharm. Anal.* **2018**, *8*, 181–186. [[CrossRef](#)] [[PubMed](#)]
260. Mura, P.; Valleri, M.; Fabianelli, E.; Maestrelli, F.; Cirri, M. Characterization and evaluation of different mesoporous silica kinds as carriers for the development of effective oral dosage forms of glibenclamide. *Int. J. Pharm.* **2019**, *563*, 43–52. [[CrossRef](#)] [[PubMed](#)]
261. Angelopoulou, A.; Efthimiadou, E.K.; Kordas, G. Dextran modified pH sensitive silica hydro-xerogels as promising drug delivery scaffolds. *Mater. Lett.* **2012**, *74*, 50–53. [[CrossRef](#)]

262. Zhang, P.; Jiang, Q.; Zheng, Y.; Li, J. Double-nano silica xerogel contributes to establish nifedipine delivery system with superior delivery effect. *Micropor. Mesopor. Mater.* **2020**, *296*, 109996. [[CrossRef](#)]
263. Rajanna, S.K.; Kumar, D.; Vinjamur, M.; Mukhopadhyay, M. Silica Aerogel Microparticles from Rice Husk Ash for Drug Delivery. *Ind. Eng. Chem. Res.* **2015**, *54*, 949–956. [[CrossRef](#)]
264. Smirnova, I.; Suttiruengwong, S.; Arlt, W. Feasibility study of hydrophilic and hydrophobic silica aerogels as drug delivery systems. *J. Non Cryst. Solids* **2004**, *350*, 54–60. [[CrossRef](#)]
265. Giray, S.; Bal, T.; Kartal, A.M.; Kızılel, S.; Erkey, C. Controlled drug delivery through a novel PEG hydrogel encapsulated silica aerogel system. *J. Biomed. Mater. Res. A* **2012**, *100A*, 1307–1315. [[CrossRef](#)]
266. Guenther, U.; Smirnova, I.; Neubert, R.H.H. Hydrophilic silica aerogels as dermal drug delivery systems—Dithranol as a model drug. *Eur. J. Pharm. Biopharm.* **2008**, *69*, 935–942. [[CrossRef](#)]
267. Luo, G.; Chen, W.; Jia, H.; Sun, Y.; Cheng, H.; Zhuo, R.; Zhang, X. An indicator-guided photo-controlled drug delivery system based on mesoporous silica/gold nanocomposites. *Nano Res.* **2015**, *8*, 1893–1905. [[CrossRef](#)]
268. Zou, H.; Wu, S.; Shen, J. Polymer/Silica Nanocomposites: Preparation, Characterization, Properties, and Applications. *Chem. Rev.* **2008**, *108*, 3893–3957. [[CrossRef](#)]
269. Rasouli, S.; Davaran, S.; Rasouli, F.; Mahkam, M.; Salehi, R. Synthesis, characterization and pH-controllable methotrexate release from biocompatible polymer/silica nanocomposite for anticancer drug delivery. *Drug Deliv.* **2014**, *21*, 155–163. [[CrossRef](#)] [[PubMed](#)]
270. Dementeva, O.V.; Senchikhin, I.N.; Kartseva, M.E.; Ogarev, V.A.; Zaitseva, A.V.; Matushkina, N.N.; Rudoy, V.M. A new method for loading mesoporous silica nanoparticles with drugs: Sol–gel synthesis using drug micelles as a template. *Colloid J.* **2016**, *78*, 586–595. [[CrossRef](#)]
271. Hagman, E.; Elimam, A.; Kupferschmidt, N.; Ekbom, K.; Rössner, S.; Iqbal, M.N.; Johnston, E.; Lindgren, M.; Bengtsson, T.; Danielsson, P. Oral intake of mesoporous silica is safe and well tolerated in male humans. *PLoS ONE* **2020**, *15*, e0240030. [[CrossRef](#)] [[PubMed](#)]
272. Phillips, E.; Penate-Medina, O.; Zanzonico, P.B.; Carvajal, R.D.; Mohan, P.; Ye, Y.; Humm, J.; Gönen, M.; Kalaigian, H.; Schöder, H.; et al. Clinical translation of an ultrasmall inorganic optical-PET imaging nanoparticle probe. *Sci. Transl. Med.* **2014**, *6*, 260ra149. [[CrossRef](#)] [[PubMed](#)]
273. Donaldson, L. ‘Cornell Dots’ receive approval for clinical trials: Nanotechnology. *Mater. Today* **2011**, *14*, 131. [[CrossRef](#)]
274. Chen, F.; Ma, K.; Madajewski, B.; Zhuang, L.; Zhang, L.; Rickert, K.; Marelli, M.; Yoo, B.; Turker, M.Z.; Overholtzer, M.; et al. Ultrasmall targeted nanoparticles with engineered antibody fragments for imaging detection of HER2-overexpressing breast cancer. *Nat. Commun.* **2018**, *9*, 4141. [[CrossRef](#)] [[PubMed](#)]